T2R2 東京科学大学 リサーチリポジトリ
Science Tokyo Research Repository

論文 / 著書情報
Article / Book Information

題目(和文)	
Title(English)	DEVELOPMENT AND EVALUATION OF A GAIT-ASSIST WEARABLE ROBOT USING INTERACTIVE RHYTHMIC STIMULATION TO THE UPPER AND LOWER LIMBS
著者(和文)	YAPMiaoSinRobin
Author(English)	Miaosinrobin Yap
出典(和文)	学位:博士(工学), 学位授与機関:東京工業大学, 報告番号:甲第11340号, 授与年月日:2019年12月31日, 学位の種別:課程博士, 審査員:三宅 美博,山村 雅幸,宮下 英三,瀧ノ上 正浩,小野 功
Citation(English)	Degree:Doctor (Engineering), Conferring organization: Tokyo Institute of Technology, Report number:甲第11340号, Conferred date:2019/12/31, Degree Type:Course doctor, Examiner:,,,,
学位種別(和文)	博士論文
Type(English)	Doctoral Thesis

Powered by T2R2 (Science Tokyo Research Repository)

DEVELOPMENT AND EVALUATION OF A GAIT-ASSIST WEARABLE ROBOT USING INTERACTIVE RHYTHMIC STIMULATION TO THE UPPER AND LOWER LIMBS

Submitted by

Yap Miao Sin, Robin

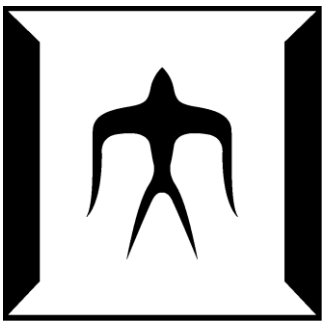

Department of Computational Intelligence and Systems Science

In fulfillment of the requirements
for the Doctoral of Engineering Degree
Tokyo Institute of Technology

Session 2019/2020

SUMMARY

Many power-assist wearable exoskeletons have been developed to provide walking support and gait rehabilitation for elderly subjects and gait disorder patients. Most designers have focused on a direct power-assist to the wearer's lower limbs. However, gait is a coordinated rhythmic movement of four limbs controlled intrinsically by central pattern generators, with the upper limbs playing an important role in walking. Maintaining a normal gait can become difficult as a person ages, because of decreases in limb coordination, stride length, and gait speed. It is known that coordination mechanisms can be governed by the principle of mutual entrainment, in which synchronization develops through the interaction between nonlinear phase oscillators in biological systems. This principle led us to hypothesize that interactive rhythmic stimulation to upper and lower limb movements might compensate for the age-related decline in coordination, thereby improving the gait in the elderly. To investigate this hypothesis, we developed a gait-assist wearable exoskeleton that employs interactive rhythmic stimulation to the upper and lower limbs based on the mutual entrainment principle to provide coordination to the upper and lower limbs.

In particular, we investigated the effect of stimulation to the upper and lower limbs on spatial gait parameters (i.e., shoulder- and hip-joint amplitude), their corresponding coefficient of variance (*CV*s), and upper–lower–limbs' coordination by conducting walking experiments with 5 healthy elderly subjects under a non-assist and assist condition, where the output motor torque was applied at a 15% lag time between the foot contact timing and upper-limb motors. The results showed a significant increase in the mean right shoulder- and hip-joint amplitude, with a mean increment of about 63% and 12.5%, respectively between the non-assist and assist conditions. In addition, the

results showed a symmetrical pattern in the right upper–lower–limbs' coordination between the non-assist and assist conditions. However, the results showed a significant increase in the *CV* of the right shoulder- and hip-joint amplitude with an elderly subject between the non-assist and assist conditions. Although the results indicate that interactive rhythmic stimulation to the upper and lower limbs significantly increases the shoulder- and hip-joint amplitude without adversely affecting the upper–lower–limbs' coordination, the results indicate an increase in the *CV* of the shoulder- and hip-joint amplitude for the elderly. We speculate that the increase in gait variability might be attributed to the heavy weight of the lower limb motors, and a direct stimulation to the wearer's lower limbs, which might cause gait instability for the elderly.

To overcome the aforementioned limitations, we next developed a gait-assist wearable exoskeleton using interactive rhythmic stimulation to the upper limbs based on the mutual entrainment principle in human-robot interaction, and upper–lower–limbs' neural coupling in human locomotion. We investigated the effect of stimulation to the upper limbs on a spatial (i.e., hip-swing amplitude) and temporal (i.e., hip-swing period) gait parameter, their corresponding *CV*s, and upper–lower–limbs' coordination by conducting walking experiments with 12 elderly subjects under one control condition and five upper-limb-assist conditions, where the output motor torque was applied at five different upper-limb swing positions. Here, the swing position corresponds to the arm position with respect to the rearmost position at 0%, 10%, 20%, 30%, and 40% lag times. The results showed a statistically significant increase in the mean hip-swing amplitude, with a mean increment of about 7% between the control and upper-limb-assist conditions at all lag times. They also showed a statistically significant decrease in the mean hip-swing period, with a mean decrement of about 2.3% between the control and the upper-limb-assist condition at 40% lag time. In addition, the results showed a

symmetrical pattern in the left and right upper–lower–limbs' coordination between the free and upper-limb-assist conditions at all lag times. Further, the results showed no statistically significant difference in the mean *CV*s of the hip-swing amplitude and period between the free and upper-limb-assist conditions at all lag times. Although no stimulations were applied to the lower limbs, the results indicate that stimulation to the upper limbs statistically significantly increases the hip-swing amplitude and gait speed, without adversely affecting the elderly's gait stability, and upper–lower–limbs' coordination. Hence, the results indicate that interactive rhythmic stimulation to the upper limbs at an optimal condition could offer a promising neurorehabilitation strategy for the elderly's gait.

ACKNOWLEDGEMENT

I would like to thank the following people for their helpful advice and support throughout the research and development phase of the gait-assist wearable exoskeletons, without their support this study would not have been possible.

First, Dr Masatoshi Seki, Dr Ken Ichiryu and Mr Masayuki Nakayama from Kikuchi Seisakusho Co. Ltd for their helpful support and advice on the hardware and software development of the gait-assist wearable exoskeleton (WalkMate).

Second, Dr Leo Ota, former doctoral student of the Tokyo Institute of Technology for his helpful advice in this research, Mr Hirobe Yuki, former researcher, and Mr Koyu Hori, former master student of the Tokyo Institute of Technology, Miyake laboratory for their support with the development of the gait analysis program, former master students, Mr Kono Daiki, Ms Yuriko Saruta, Mr Hironobu Matsui and Mr Terumasa Nagashima at the Tokyo Institute of Technology for their support on the experimental evaluation of the gait-assist wearable exoskeletons.

Third, Professor Yoshihiro Miyake and Assistant Professor Ken-ichiro Ogawa for their helpful advice on the preparation of the manuscript for journal submission to *Frontier in Robotics and AI* as well as the preparation of this thesis despite their busy schedule, and Assistant Professor Hiroki Ora for his kind word of advice on the statistical analysis and evaluation of the gait-assist wearable exoskeleton.

Fourth, my wife, Ms Nakamura Kumiko for her kind words of advice and moral support who has always been an avid listener for my research. Without her support, life as a doctoral candidate would have been more difficult.

Finally, I would like to thank all the students and staffs from the Tokyo Institute of Technology, Miyake laboratory who have provided me with support in one way or another, and who have not been mentioned above, from the bottom of my heart.

TABLE OF CONTENTS

List of Figures

List of Tables

List of Symbols

$\theta_{h,r}$	Right upper limb phase
$\theta_{h,l}$	Left upper limb phase
$\theta_{m,r}$	Right upper-limb motor phase
$\theta_{m,l}$	Left upper-limb motor phase
$\dot{\theta}_{m,r}$	Rate of change of right upper-limb motor phase
$\dot{\theta}_{m,l}$	Rate of change of left upper-limb motor phase
$\omega_{m,r}$	Intrinsic angular frequency of right upper-limb motor
$\omega_{m,l}$	Intrinsic angular frequency of left upper-limb motor
$\dot{\omega}_{m,r}$	Rate of change of intrinsic angular frequency of right upper-limb motor
$\dot{\omega}_{m,l}$	Rate of change of intrinsic angular frequency of left upper-limb motor
$\Delta\theta_{m,l}$	Phase difference between left upper limb and left upper-limb motor phase
$\Delta\theta_{m,r}$	Phase difference between right upper limb and right upper-limb motor phase
$\Delta\theta_d$	Target phase difference between human's foot contact timing/upper limb and robot's upper-limb motor
Δt	Sampling rate
K_m	Human-robot coupling constant
K_{lr}	Robot left-right coupling constant
E	Control gain (> 0)
N	Sample size
K	Constant of sigmoid function

CHAPTER 1. INTRODUCTION

1.1 Social Background

An aging population is a serious social problem in many advanced countries. According to the World Population Data (2018), Japan has the world's largest proportion of older people aged 65 years and above (28% of the total population in 2018), while the proportion of people aged 65 years and above in China and USA is 11% and 25% of the total population in 2018, respectively. As a result of an aging society, the elderly's health conditions especially weakened walking functions become important.

For instance, a high incidence of falls rate among the elderly in Japan (Haga et al., 1986), Amsterdam (Graafmans et al., 1996), Finland (Kannus et al., 1999), and other countries (Rubenstein et al., 2002) have been reported. Gait and balance disorders are common in older adults and is a major cause of falls in this population (Salzman, 2010) As a result of aging, functional decline in the elderly's arm-swing amplitude (Mirelman et al., 2015), gait speed (Winter et al., 1990; Ostrosky et al., 1994; Cromwell and Newton, 2004, McGibbon and Krebs, 2004; Laufer, 2005; Mirelman et al., 2015), hip flexion and extension (Crosbie et al., 1997), stride length (Winter et al., 1990; Ostrosky et al., 1994; DeVita and Hortobagyi, 2000; McGibbon and Krebs, 2004; Laufer, 2005; Mirelman et al., 2015), and upper–lower–limbs' coordination (Serrien et al., 2000; Fujiyama et al., 2009; Krasovsky et al., 2014) as well as an increase in elderly's gait variability (Kang and Dingwell, 2008, Callisaya et al., 2010) have been reported. This has meant that the basic activity of daily living for older people is severely affected. In this regard, programs or strategies targeting to improve physical performance, especially walking ability, among community-dwelling elderly is urgently needed (Shinkai et al., 2003).

1.2 Previous Works

In recent years, many power-assist wearable exoskeletons have been developed to provide walking support and gait rehabilitation for elderly subjects (Kawamoto et al., 2003; Choi et al., 2018), gait disorder patients (Reiner et al., 2005; Veneman et al., 2007; Kim et al., 2010; Strausser and Kazerooni, 2011; Esquenaszi et al., 2012; Alexander et al., 2012; Barbareschi et al., 2015; Bortole et al., 2015; Yi et al., 2016; Chen et al., 2017; Lerner et al., 2017), and healthy subjects in walking (Alan et al., 2014; Yi et al., 2017) and crossing obstacles (Deng et al., 2017). Most of these exoskeletons aimed to provide direct power-assist support to the wearer's lower limbs.

For example, the hybrid-assistive-leg (HAL) (Tsukuba, Japan) uses the patient's intention-based electromyography signals to provide power-assist support for the lower limbs of patients with gait disorder (Kawamoto et al., 2003). For patients with neurological disorders, the robotic-gait-orthosis (Lokomat) (Hacoma AG, Switzerland) provides task-oriented repetitive movement using a patient-cooperative strategy based on impedance, adaptive control, and visual biofeedback to control the hip and knee joint trajectories on a treadmill (Riener et al., 2005). The lower-extremity powered-exoskeleton (LOPES) (EA Enschede, The Netherlands) provides both patient- and robot-in-charge modes to control the patient's hip and knee trajectories on a treadmill (Veneman et al., 2007). The active-leg exoskeleton (ALEX) (Delaware, USA) uses a force-field controller and visual guidance on a treadmill to control the hip and knee joint trajectories (Kim et al., 2010). The medical exoskeleton, eLEGS (California, USA) applies inertial measurement unit to the upper limbs of patients with spinal cord injuries to assist the patient to stand up, walk and sit down independently, based on intention signals from the patient (Strausser and Kazerooni, 2011). The ReWalk powered

exoskeleton (Marlborough, USA) interprets a signal from the torso tilt sensor and generates alternating limb-coordinated motion to produce bipedal walking for people with paraplegia due to spinal cord injury (Esquenazi et al., 2012). Finally, the novel knee-extension assist (KEA) (Waterloo, Canada) uses passive components to provide a knee-extension moment to assist with stand-to-sit and sit-to-stand mobility tasks for individuals with quadriceps muscle weakness (Alexander et al., 2012).

More recently, the portable wearable robot "exosuit" (Cambridge, USA) (Alan et al., 2014), lower limb robotic exoskeletons, REX (Florida, USA) (Barbareschi et al., 2015), H2 (Technaid S.L., Spain) (Bortole et al., 2015), hybrid control mode-based wearable exoskeleton rehabilitation system (Yi. et al., 2016) (Harbin, China), active power-assist lower limb, APAL (Harbin, China) (Deng et al., 2017), CUHK-EXO (Hongkong, China) (Chen et al., 2017), novel powered lower-extremity exoskeleton (Maryland, USA) (Lerner et al., 2017), double compact elastic module-based lower extremity powered wearable exoskeleton (Yi et al., 2017) (Harbin, China), and gait-enhancing mechatronic system, GEMS (Samsung, Korea) (Choi et al., 2018) have been developed.

The pneumatically-powered and electromechanically-driven exosuit uses textiles to interface the body, and apply joint torques via tensile forces over the outside of the body in parallel with the muscles to assist the lower body during walking (Alan et al., 2014). The REX exoskeleton uses a touch panel graphical user interface to provide an output torque to the wearer's lower limbs to achieve a target performance (Barbareschi et al., 2015). The H2 robotic exoskeleton provides an output torque to the patient's lower limbs using a force-field controller that guides hemiplegia patients' limb in a correct pattern (Bortole et al., 2015). The hybrid control mode-based wearable exoskeleton uses both passive and active training to assist in the rehabilitation of patients with unilateral

lower limb disorders (Yi et al., 2016). The APAL exoskeleton provides output torque to the wearer's lower limbs from the torso posture and joint angles obtained from the inertial measurement unit (IMU) to enable the user to walk on rough ground, climb stairs and cross obstacles (Deng et al., 2017). The CUHK-EXO exoskeleton provides assistive torque to the patient's lower limbs using position control and was able to support the patient's stand up/sit down and walking motions (Chen et al., 2017). The novel powered lower-extremity exoskeleton provides output torque to the patient's knee joint using a proportional-integrative-derivative control algorithm and improvement in the hip and knee joint angle was reported (Lerner et al., 2017). The double compact elastic module-based lower extremity exoskeleton uses physical human-robot interaction measurement and the elastic actuation system with a closed-loop position control strategy to drive the robotic exoskeleton system to follow the human limb's movement (Yi et al., 2017). Finally, the GEMS exoskeleton assists elderly patients with walking difficulty by providing an output torque to the hip using particularly shaped adaptive oscillators (Choi et al., 2018).

On the other hand, mutual entrainment is a biological phenomenon in which two non-linear coupled oscillators are synchronized through appropriate couplings (Kuramoto, 1984). Such biological phenomena have been observed in many internal parts of living organisms, such as segmental oscillators in the lamprey spinal generator (Cohen et al., 1982), swimming patterns of aquatic animals (Yuasa and Ito, 1990), and the coordinated movements of bipedal human locomotion (Taga et al., 1991) and stable movement patterns have been reported. Based on these background studies, we have developed a gait-assist virtual robot (i.e., WalkMate) that provides subjects with auditory stimulation as an interactive rhythmic stimulation to establish synchronization between the stimulation and their walking footsteps. The stimulation is generated by the

interaction between the artificial nonlinear phase oscillators of the robot and the subject's walking footsteps and is based on the principle of mutual entrainment (Miyake, 2009).

Although many power-assist wearable exoskeletons have been developed, two problems remained with these exoskeletons. First, these previous exoskeletons aimed to control the wearer's lower limbs to reach a target trajectory based on a master-slave control principle. In these wearable exoskeletons, the robot (i.e., master) controls the human (i.e., slave) to reach a target trajectory (i.e., passive mode). Phase synchronization based on the mutual entrainment principle in human-robot interaction (i.e., active mode) (Miyake, 2009) has not been implemented in these wearable exoskeletons. Second, most of these exoskeletons aimed to provide a direct torque to the lower limbs to assist the wearer's gait without considering the global dynamics of upper–lower–limbs' coordination in human locomotion (Delwaide et al., 1977; Baldissera et al., 1982, 1998; Guadagnoli et al., 2000; Dietz et al., 2001; Zehr et al., 2004; Frigon et al., 2004; Huang et al., 2004, 2009; Kawashima et al., 2008).

1.3 Gait-assist Wearable Exoskeleton

Therefore, the objective of this research is two-folds. First, we aim to extend the previous WalkMate by developing a gait-assist wearable exoskeleton that provides interactive rhythmic stimulation to the upper and lower limbs based on the mutual entrainment principle in human-robot interaction. Second, we aim to develop a gait-assist wearable exoskeleton that provides coordination to the upper and lower limbs. We carried out our investigation using a four-step methodology. First, we developed a gait-assist wearable exoskeleton using interactive rhythmic stimulation to the upper and lower limbs. Second, we conducted a preliminary walking experiment with healthy

elderly adults and evaluated the remaining problems associated with the exoskeleton from the experimental results. Third, we developed a gait-assist wearable exoskeleton using interactive rhythmic stimulation to the upper limbs to overcome the remaining problems from the previous step. Finally, we conducted walking experiments with healthy elderly subjects and evaluated the effect of interactive rhythmic stimulation to the upper limbs for the elderly's gait.

1.4 Thesis Outline

The title of this thesis is "Development and evaluation of a gait-assist wearable exoskeleton using interactive rhythmic stimulation to the upper and lower limbs". This thesis presents an exploration of the effect of interactive rhythmic stimulation to the upper and lower limbs from the perspective of mutual entrainment in human-robot interaction, and upper–lower–limbs' coordination in human locomotion. It comprises of five chapters.

In Chapter 1: Introduction, the author summarized the recent development of the power-assist wearable exoskeletons to the lower limbs and pointed out that all the previous exoskeletons focused on a master-slave control principle, whereby the robot (i.e., master) controls the human (i.e., slave)'s gait to a target trajectory. In addition, these previous exoskeletons focused on a direct power-assist support to the wearer's lower limbs without considering upper–lower–limbs' coordination. Therefore, the author asserted the necessity for the development of a gait-assist wearable exoskeleton (i.e., WalkMate) that provides interactive rhythmic stimulation to the upper and lower limbs based on the mutual entrainment principle in human-robot interaction, and upper–lower–limbs' coordination.

In Chapter 2: Gait-assist wearable exoskeleton to the upper and lower limbs: A

preliminary investigation, the author presented the development and evaluation of a gait-assist wearable exoskeleton using interactive rhythmic stimulation to the upper and lower limbs, aiming to evaluate the remaining problems associated with the exoskeleton for the healthy elderly's gait. The author found that this stimulation significantly increases the shoulder- and hip-joint amplitude without adversely affecting the elderly's upper–lower–limbs' coordination. However, the author also found a significant increase in the coefficient of variance, *CV* of the shoulder- and hip-joint amplitude for an elderly subject, which indicated gait instability for the elderly. The author speculated that this increase in gait variability might be attributed to the heavy weight of the lower limb motors, and a direct stimulation to the wearer's lower limbs. Hence, the author proposed the development of a gait-assist wearable exoskeleton using interactive rhythmic stimulation to the upper limbs to overcome the aforementioned limitations.

In Chapter 3: Gait-assist wearable exoskeleton to the upper limbs: An experimental investigation, the author presented the development and evaluation of a gait-assist wearable exoskeleton using interactive rhythmic stimulation to the upper limbs. The author found that this stimulation statistically significantly increases the hip-swing amplitude for the upper-limb-assist condition at all lag times, and statistically significantly decreases the hip-swing period at the 40% lag time condition. Further, this stimulation does not adversely affect the *CV* of the hip-swing amplitude and period, and upper–lower–limbs' coordination for the elderly's gait. Hence, the author asserted that interactive rhythmic stimulation to the upper limbs could provide gait assist support for the elderly with gait stability.

In Chapter 4: General Discussion, the author asserted that the gait-assist wearable exoskeleton that provides interactive rhythmic stimulation to the upper limbs is a significant improvement over stimulation to the upper and lower limbs. First, although

no stimulations were provided to the lower limbs, stimulation to the upper limbs statistically significantly increases the hip-swing amplitude and gait speed for the elderly's gait, which indicated the presence of an upper–lower–limbs' neural coupling. Second, although no stimulations were applied to the lower limbs, stimulation to the upper limbs showed a symmetrical pattern in the upper–lower–limbs' coordination, which indicated upper–lower–limbs' coordination for the elderly. Third, stimulation to the upper limbs does not statistically significantly increase the *CV* of the hip-swing amplitude and period, which indicated gait stability for the elderly.

In Chapter 5: Conclusion, the author summarized that interactive rhythmic stimulation to the upper limbs has a positive effect for the elderly's gait as manifested through a statistically significant increase in the hip-swing amplitude and gait speed without adversely affecting their upper–lower–limbs' coordination, and gait stability. Hence, the author concluded that this stimulation at an optimal condition could provide a promising neurorehabilitation strategy for the elderly's gait.

In summary, this thesis addressed the importance of interactive rhythmic stimulation to the upper limbs and provides evidence that this stimulation has a positive effect for the elderly's gait. Therefore, we agree that this thesis meets the criteria to complete the degree of Doctor of Engineering.

CHAPTER 2. GAIT-ASSIST WEARABLE EXOSKELETON TO THE UPPER AND LOWER LIMBS: A PRELIMINARY INVESTIGATION

2.1 Approach

We carry out our investigation using a four-steps approach. First, we develop a gait-assist wearable exoskeleton that provides interactive rhythmic stimulation to the upper and lower limbs through phase synchronization of the foot contact timing and upper limbs based on the mutual entrainment principle in human-robot interaction (i.e., interpersonal synchronization). Second, we conduct overground walking experiments with healthy elderly adults under the non-assist (i.e., baseline condition) and assist condition. Third, we evaluate the effect of stimulation to the upper and lower limbs for the elderly's gait on spatial gait parameters (i.e., shoulder- and hip-joint amplitude), their corresponding *CV*s, and upper–lower–limbs' coordination using the shoulder and hip-joint angular displacement data from the upper and lower limb motor encoders, and compare the elderly's gait against the non-assist condition and the gait of healthy young adults. Finally, we evaluate the remaining problems associated with the exoskeleton.

2.2 Gait-assist Wearable Exoskeleton to the Upper and Lower limbs

The gait-assist wearable exoskeleton to the upper and lower limbs comprises: (1) hardware to provide motor torque (rhythmic stimulation) to the left and right upper and lower limbs of a subject, triggered by rhythmic signals, and (2) software to generate the rhythmic signals in synchronization with the walking rhythm of the subject based on the mutual entrainment principle.

2.2.1 Hardware Modules

The hardware comprises an actuator module, a control module, a sensor module and a power module. The weight of the wearable exoskeleton and control unit (i.e., I/O unit, power unit, motor controllers and PC) is 5.7 kg and 6.0 kg, respectively. Its overall weight is 11.7 kg. The actuator module is rigidly attached to a spiral harness that can be secured to the upper limbs (i.e., between the elbow and shoulder joint) and lower limbs (i.e., between the hip and knee joint) using a Velcro belt. The wearable exoskeleton is rigidly secured to the upper body (i.e., chest) and lower body (i.e., waist) of the subject using adjustable belts. Fig 1 shows the appearance of the hardware module of the wearable exoskeleton to the upper and lower limbs.

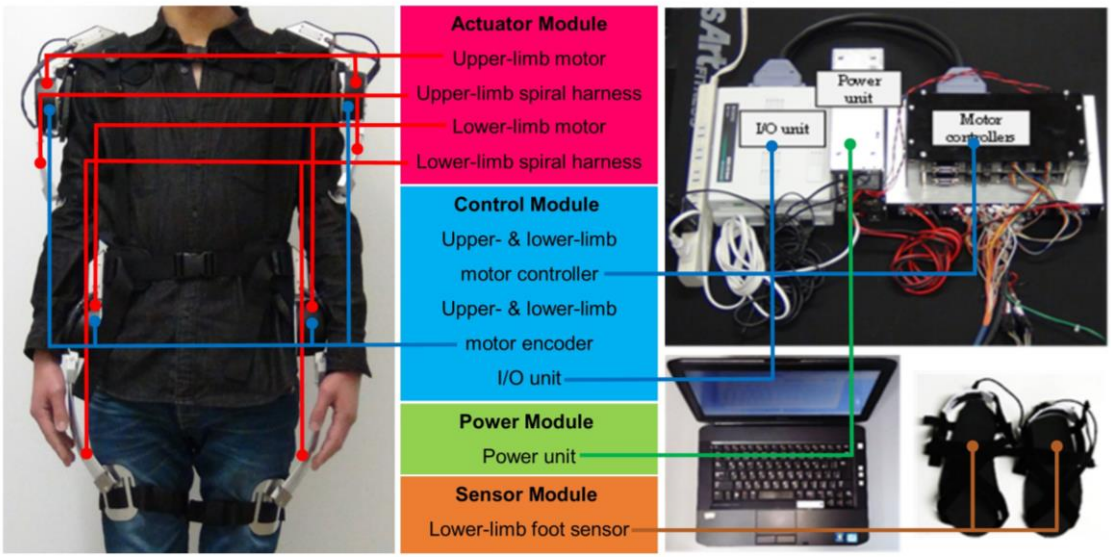

Fig 1. Appearance of gait-assist wearable exoskeleton to the upper and lower limbs.

The hardware module comprises the actuator, control, power and sensor modules. The actuator module comprises two upper-limb motors and upper-limb spiral harnesses, two lower-limb motors and lower-limb spiral harnesses. The control module comprises two upper- and lower-limb motor controllers, two upper- and lower-limb motor encoders and an I/O unit. The power module comprises an external power unit and an external on/off switch. The sensor module comprises two elongated tape switch foot sensor, which is inserted inside the shoe pad.

2.2.1.1 Actuator Module

This module comprises two three-phase upper- and lower-limb DC brushless motors, each of which provides an output torque to each of the upper and lower limbs, spiral harnesses, and a Velcro belt. The upper-limb motors have a maximum motor drive voltage of 24.0 V and a power rating of 100 W. The lower-limb motors have a maximum motor drive voltage of 24.0 V and a power rating of 600 W.

2.2.1.2 Control Module

This module comprises two upper- and lower-limb DC motor controllers, two upper- and lower-limb DC motor encoders, two I/O units (CONTEC, DIO-1616LX-USB, Japan) and an external PC (Dell, E5430, USA). The motor encoders provide the control interface between the upper and lower limbs, and the I/O units by detecting the subject's shoulder- and hip-joint angular displacements and sending this information to the I/O units. The motor controllers provide the control interface between the I/O unit and the upper- and lower-limb DC motors by causing the motors to output the desired torque to the subject's upper and lower limbs.

2.2.1.3 Power Module

This module comprises an external power unit and an external on/off switch. The external power unit provides power to the control module and drives the upper- and lower-limb DC motors. The external on/off switch switches on and off the electrical supply to the control modules and the upper and lower limb motors.

2.2.1.4 Sensor Module

This module comprises two elongated tape switch foot sensors (OJIDEN, OT-

21BP-G, Japan) placed below the shoe pad, which closes contact upon foot contact and vice-versa. Fig 2 shows the schematic diagram of the hardware module of the wearable exoskeleton to the upper and lower limbs.

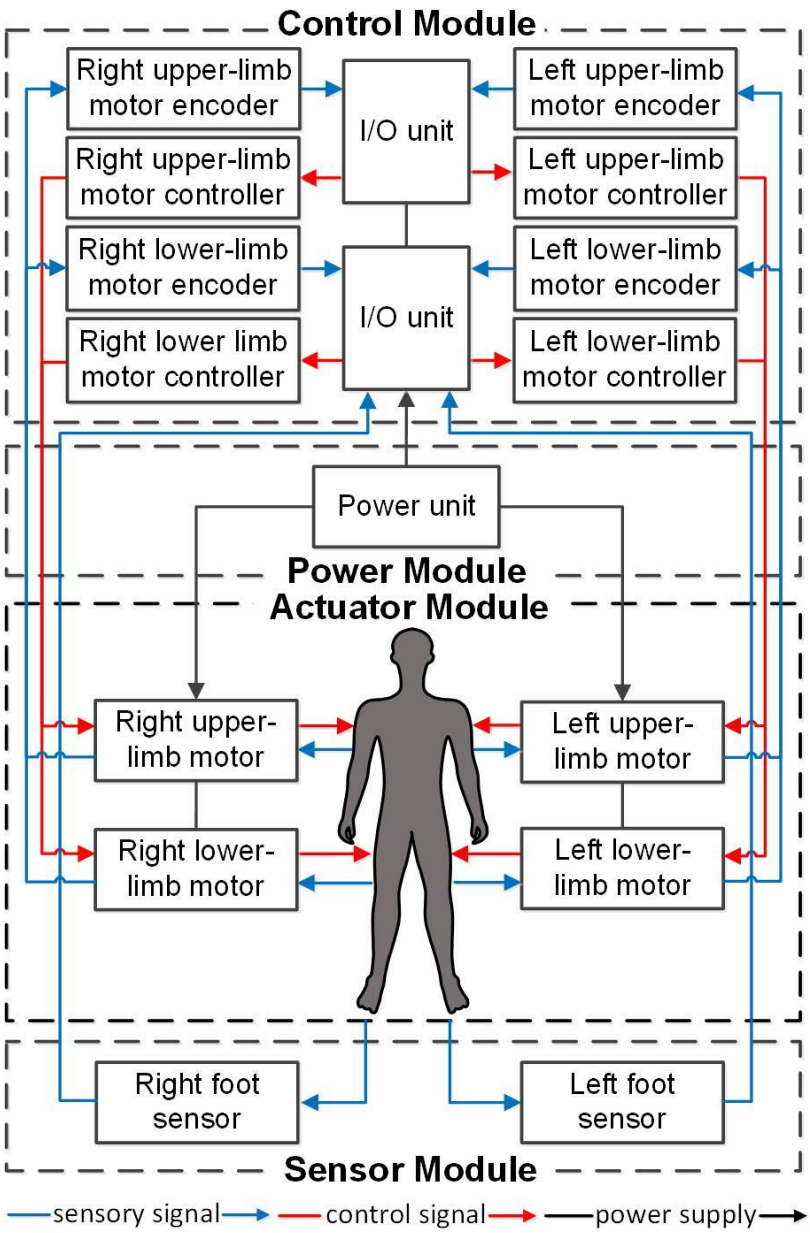

Fig 2. Schematic diagram of hardware module of gait-assist wearable exoskeleton to upper and lower limbs. The motor encoders detect the shoulder- and hip-joint angular displacements from the subject and input to the I/O units. The motor controllers output the desired motor torque from the I/O units to the motors. The power unit provides the electrical supply to the control module and the motors. The foot sensors detect the subject's footstep rhythm (i.e., timing) and input to the I/O unit.

2.2.2 Software Modules

The software comprises three modules. Module 1 (phase control module) controls the left and right upper-limb motor phases (i.e., their timing) by coordinating the phase differences of the left and right foot contact timing and the upper-limb motors torque to a target value based on the mutual entrainment principle. Module 2 (subject phase-input module) receives both of the subject's lower-limb foot contact timing via the foot sensors. Finally, Module 3 (motor torque output module) controls the magnitude and phase of each of the upper- and lower-limb output motor torques and outputs the desired magnitude and phase information to the subject. Fig 3 shows a schematic diagram of the software for the wearable exoskeleton to the upper and lower limbs.

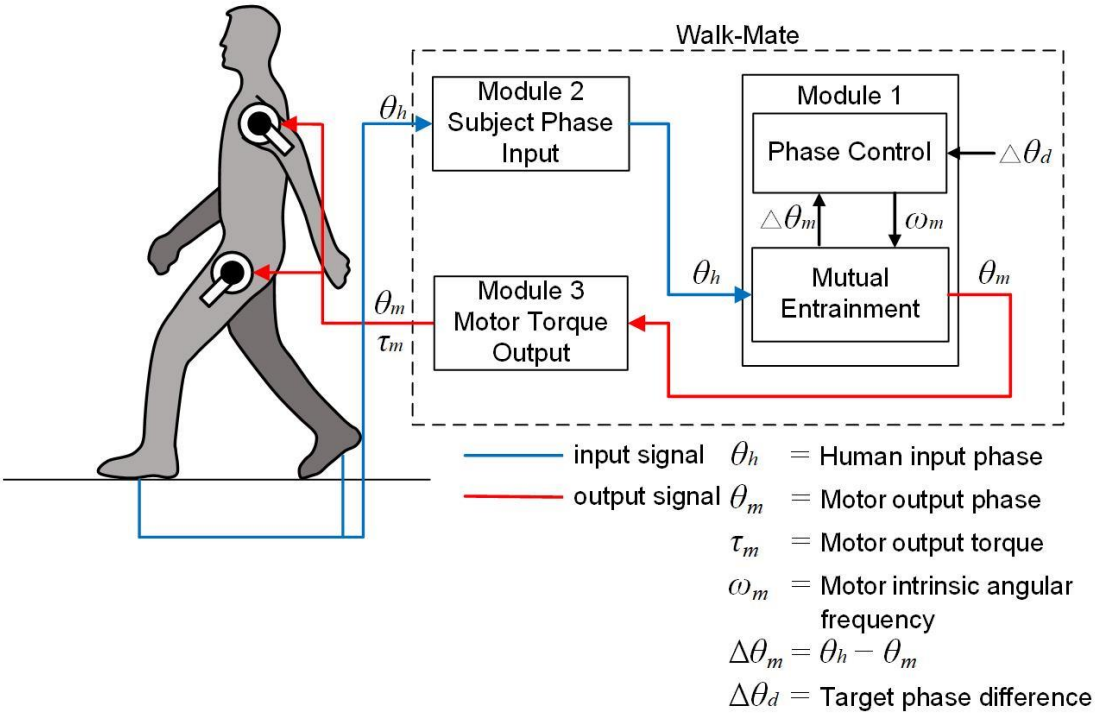

Fig 3. Schematic diagram of the software of the gait-assist wearable exoskeleton to the upper and lower limbs. The software module comprises module 1 (phase control module), module 2 (subject phase-input module) and module 3 (motor-torque output module). Module 1 controls the left and right upper-limbs' motor phases by coordinating the phase differences of the left and right foot contact timing and the upper-limb motors torque based on the mutual entrainment principle. Module 2 receives the left and right

foot contact timing from the left and right foot sensors and input this information to the I/O unit. Module 3 controls the magnitude and phase of the left and right upper- and lower-limbs output motor torque and outputs the desired magnitude and phase of the upper- and lower-limbs' motor torque to the subject.

2.2.2.1 Phase Control Module

This module comprises the mutual entrainment submodule and the phase control submodule. The mutual entrainment submodule controls the left upper-limb motor phases, $\theta_{m,l}$ such that the phase difference $\Delta\theta_{m,l}$ between the left foot contact timing $\theta_{h,l}$ and the left upper-limb-motor phases $\theta_{m,l}$ converges to 0°, where $\Delta\theta_{m,l} = \theta_{h,l} - \theta_{m,l}$. The phase $\theta_{h,l}$ is defined as the left humans' foot contact timing. The phase $\theta_{m,l}$ is defined as the left upper-limb-motor phase. The submodule also controls the right upper-limb motor phase in the same manner, in terms of the variables $\theta_{m,r}$, $\Delta\theta_{m,r}$ and $\theta_{h,r}$.

The phase control submodule comprises two nonlinear coupled oscillators based on the Kuramoto model (Kuramoto, 1984), which can be represented as

$$\dot{\theta}_{m,l} = \omega_{m.l} + K_{lr}\sin\left(\theta_{m,r} - \theta_{m,l}\right) + K_m \sin\left(\Delta\theta_{m,l}\right), \quad (5)$$

$$\dot{\theta}_{m,r} = \omega_{m,r} - K_{lr}\sin\left(\theta_{m,l} - \theta_{m,r}\right) + K_m \sin\left(\Delta\theta_{m,r}\right). \quad (6)$$

Here, $\omega_{m,l}$ and $\omega_{m,r}$ are variable intrinsic angular frequencies of the upper-limb-motors. K_{lr} is the coupling between the left and right upper-limb-motor phases, and K_m denotes the strength of the phase difference convergence between the foot contact timing and upper-limb motors. In this present study, we set $K_{lr} = 5.0$ and $K_m = 0.5$, following the parameters from the previous WalkMate framework (Miyake, 2009). Fig 4 is a schematic diagram showing the relationships between all phases and phase differences used in the phase control module.

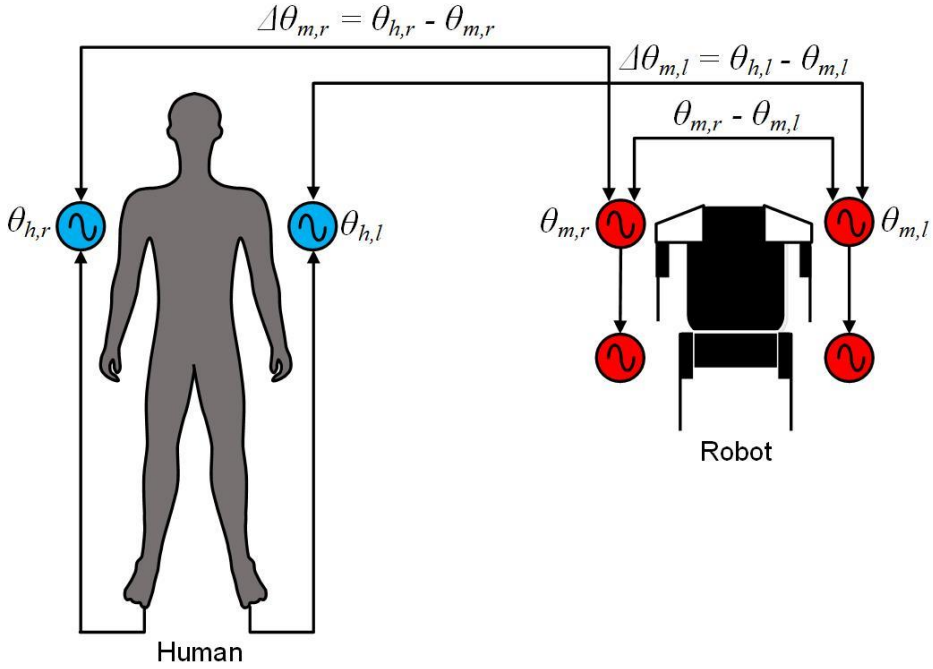

Fig 4. Schematic diagram of the definition of all phase and phase differences used in the phase control module. Here, $\theta_{h,r}$ and $\theta_{h,l}$ represent the right and left foot contact timing. $\theta_{m,r}$ and $\theta_{m,l}$ represent the right and left upper-limb-motor phases. $\Delta\theta_{m,l} = \theta_{h,l} - \theta_{m,l}$ and $\Delta\theta_{m,r} = \theta_{h,r} - \theta_{m,r}$ represent the phase difference between the left and right foot contact timing and upper-limb motors, respectively.

The phase difference control submodule controls the intrinsic angular frequencies $\omega_{m,l}$ and $\omega_{m,r}$, of the upper-limb motors by converging the phase differences $\Delta\theta_{m,l}$ and $\Delta\theta_{m,r}$ to a target phase difference, $\Delta\theta_d$. The operation of this submodule can be represented as:

$$\dot{\omega}_{m,l} = \varepsilon \sin(\Delta\theta_{m,l} - \Delta\theta_d), \tag{7}$$

$$\dot{\omega}_{m,r} = \varepsilon \sin(\Delta\theta_{m,r} - \Delta\theta_d). \tag{8}$$

Here, ε (> 0) is a control gain. In this study, we initialize ε to 0.16, $\Delta\theta_d$ to 0, and both $\omega_{m,l}$ and $\omega_{m,r}$ to 4.0 rad/s because the frequency of complete human gait cycles is about 1.0 Hz.

2.2.2.2 Subject Phase Input Module

This module receives the subject's left and right foot contact timing (i.e., phase) from the foot sensors during human locomotion. The control algorithm comprises four steps. First, both upper- and lower-limb motors were activated after four complete gait cycles. At that time, the left and right foot come into contact with the ground (i.e., $\theta_{hl} = 0°$ and $\theta_{hr} = \pi$). Second, the phase differences between the foot contact timing and its corresponding upper-limb motor phases, (i.e., $\Delta\theta_{m,l}$ and $\Delta\theta_{m,r}$) were updated in real time such that the phase differences converge to the target phase difference $\Delta\theta_d = 0°$. Third, the intrinsic angular frequencies of both upper-limb motors, $\omega_{m,l}$ and $\omega_{m,r}$, were updated using Equations (7) and (8) with the phase differences being updated from the second step. Fourth, the upper-limb motor phases θ_{ml} and θ_{mr} were updated using Equations (5) and (6) with the intrinsic angular frequencies updated from the third step. This cycle repeats from the second to the fourth steps during walking. Finally, the upper- and lower-limb motors stop 1.5s after the human stops walking. Fig 5 shows a flow-chart of the software control algorithm for the wearable exoskeleton to the upper and lower limbs.

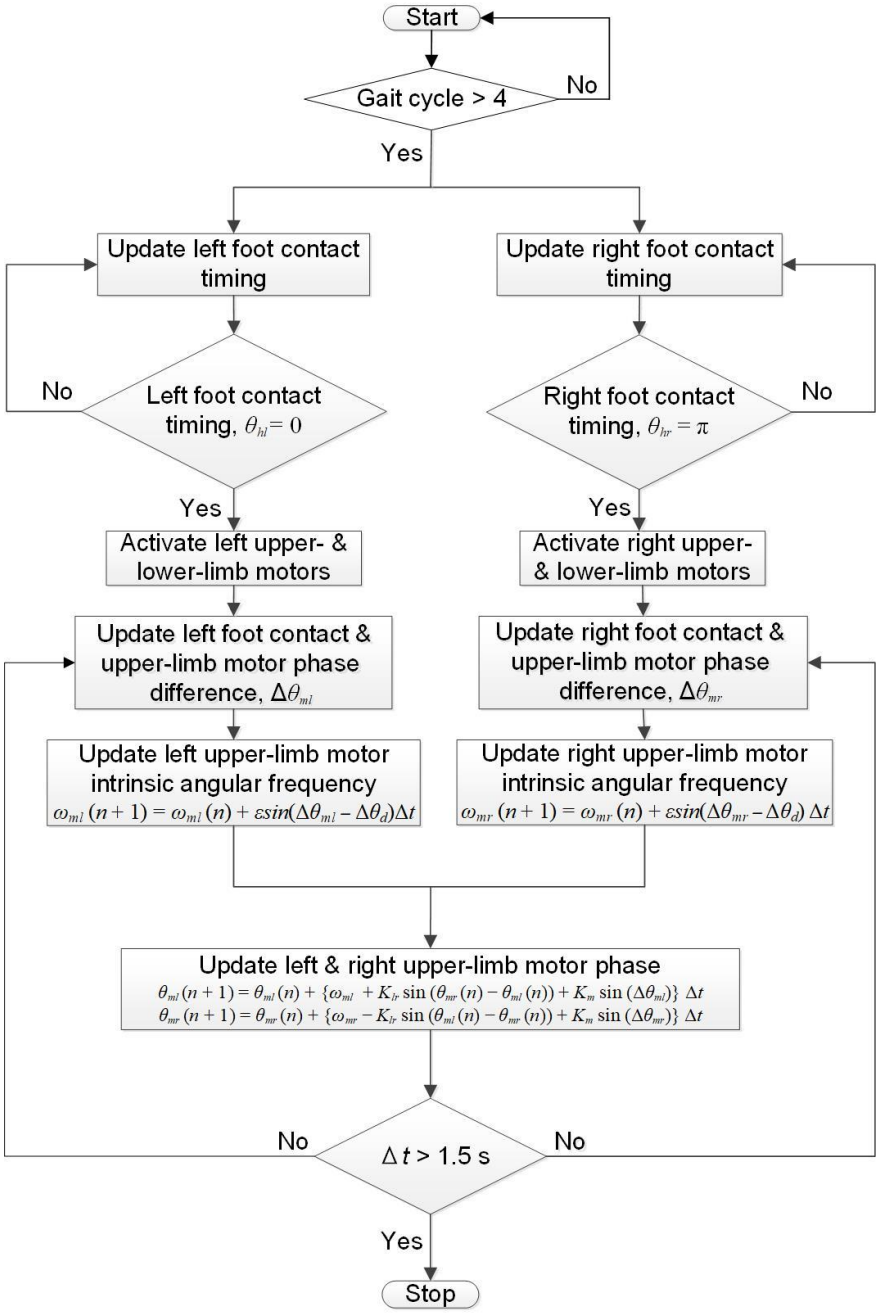

Fig 5. Flowchart of the software control algorithm of the wearable exoskeleton to the upper and lower limbs. The wearable exoskeleton starts after 4 complete gait cycles when the left and right foot comes into contact with the ground. The intrinsic angular frequencies of the left and right upper-limb motors are updated in real time using the phase control module by converging the phase difference between the foot contact timing and upper-limb motors to a target phase difference $\Delta\theta_d$. The phase of the left and right upper-limb motors are updated using the mutual entrainment module by the intrinsic angular frequencies of the left and right upper-limb motors.

2.2.2.3 Motor Torque Output Module

This module follows each foot contact timing during one complete human gait cycle with temporal control of the motor torque. The motor torque is applied at the contact point between the upper limbs and upper-limb spiral harnesses (i.e., just above elbow joint), and the lower limbs and lower-limb spiral harnesses (i.e., just above the knee joint). We implemented the output motor torque to the upper limbs at 15% lag time between the foot contact timing and upper-limb motors based on an experimental investigation with healthy young adults on a treadmill (Appendix 7.1).

In addition, we also implemented the phase difference of the output motor torque between the right and left upper- and lower-limbs, right and left upper-limbs, and right and left lower-limbs to 180º out of phase (i.e., anti-phase) following a natural human gait cycle. Fig 6 shows a phase diagram of the left and right upper- and lower-limb motors with respect to the foot contact timing for one complete gait cycle.

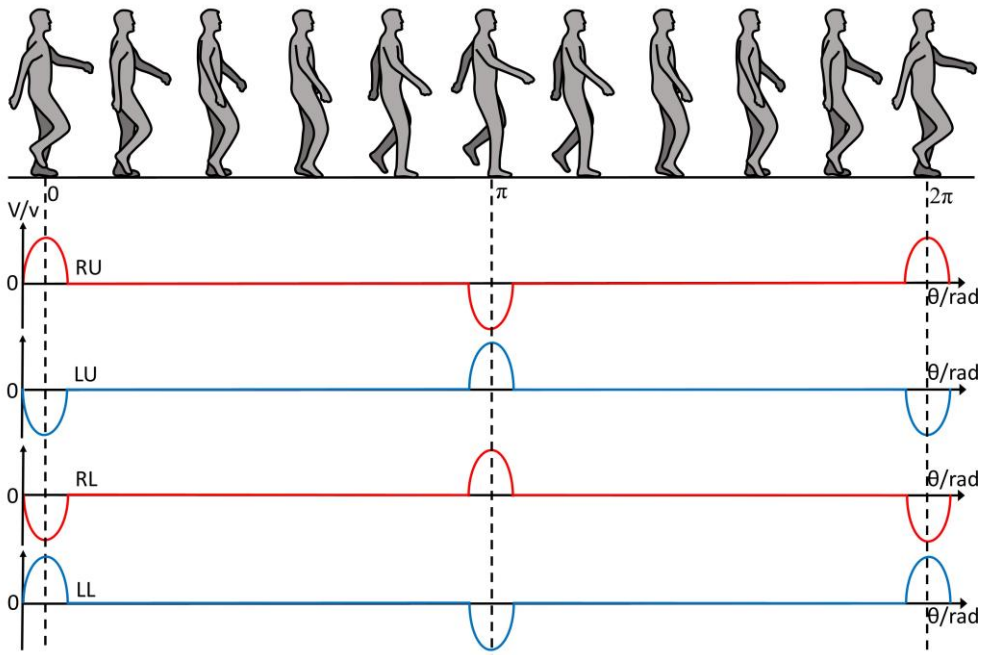

Fig 6. Phase diagram of left and right upper- and lower-limb motors with respect to the foot contact timing for one complete gait cycle. Here, RU, LU, RL, LL represent the output motor torque to the right upper-limb, left upper-limb, right lower-limb and left lower-limb, respectively for one complete gait cycle.

Further, we implemented the upper- and lower-limbs output motor torque using sigmoid function to ensure a smooth output motor torque for the subject. The increasing and decreasing function of the upper- and lower-limb motor torque were represented using the sigmoid and inverse sigmoid function, which can be represented as:

$$S_U(t) = \frac{1}{1+e^{-kt}} \times 100 \quad (9)$$

$$S_D(t) = \frac{1}{1+e^{kt}} \times 100 \quad (10)$$

Here, $S_U(t)$ and $S_D(t)$ represent the increasing and decreasing function of the output motor torque to upper- and lower-limbs respectively. t takes a value between –1 to 1. We also set k to an arbitrary value of 6.

2.3 Experiment Task

2.3.1 Ethics Statement

The experimental protocol in this study was approved by the Ethics Committee at the Tokyo Institute of Technology through written consent. We recruited healthy elderly subjects from the Machida Silver Centre in Tokyo, Japan. They were all free from documented neurological disorders. Before the start of the experiment, all participants were briefed about the experimental procedures and written informed consent was obtained.

2.3.2 Experiment Procedure

We evaluated the wearable exoskeleton by conducting walking experiments with 5 healthy elderly adults (2 males and 3 females). First, the subjects put on the wearable exoskeleton and walked at their own natural walking speed under two experimental conditions conducted randomly. They were the non-assist (i.e., baseline) and assist

conditions. For the non-assist condition, the subject put on the wearable exoskeleton but there was no output motor torque to the upper and lower limbs. For the assist condition, an output motor torque was applied to the upper and lower limbs at 15% lag time between the upper-limb motor torque onset timing and the foot contact timing. Two complete walking trials were conducted for each experimental condition with no rest time. For each trial, the subjects walked a horizontal distance of 55.4 m along the corridor. The experiment ended when the subjects had completed all experimental trials for each condition.

2.4 Gait Analysis

We performed a gait analysis of the shoulder- and hip-joint angular displacements using the time-series data obtained from the upper- and lower-limb motor encoders to evaluate the effect of interactive rhythmic stimulation applied to the upper and lower-limbs under the non-assist and assist conditions. The gait analysis comprised six steps.

First, we extracted each peak and trough of the time-series data for the right shoulder- and hip-joint angular displacements to calculate the peak-to-peak amplitudes of the shoulder- and hip-joint angular displacements for five complete stable gait cycles for each complete trial. Second, we calculated the mean peak-to-peak amplitude of the time-series data for five complete trials on the right shoulder- and hip-joint angular displacements to obtain the mean right shoulder- and hip-joint amplitude for each complete trial. Third, we calculated the mean of the mean right shoulder- and hip-joint amplitude for all subjects (n = 5). Fourth, we compared the mean right shoulder- and hip-joint amplitude between the non-assist and assist conditions. Fifth, we calculated and compared the CV of the right shoulder- and hip-joint amplitude for one complete

trial for the non-assist and assist conditions for each subject by removing the first and last five gait cycles of each complete trial due to acceleration and deceleration to determine the dispersion of the right shoulder- and hip-joint amplitude from their respective mean amplitude using equation (11).

$$CV = \frac{\sigma}{\mu} \tag{11}$$

Here, σ and μ is the standard deviation and mean of joint amplitude of one complete trial, respectively. Finally, we compared the anti-phase coordination between the right upper and lower limbs for one complete trial of each condition using phase diagram. We did not perform any statistical analysis between the non-assist and assist conditions on the right shoulder- and hip-joint amplitude and their respective *CV*s due to the small sample size (n = 5).

2.5 Results

Fig 7 shows an example of the time-series data on the right shoulder-joint angular displacements for the non-assist and assist condition for an elderly subject. The results show that the peak-to-peak amplitude of the right shoulder-joint angular displacement is significantly higher for the assist condition compared with the non-assist condition.

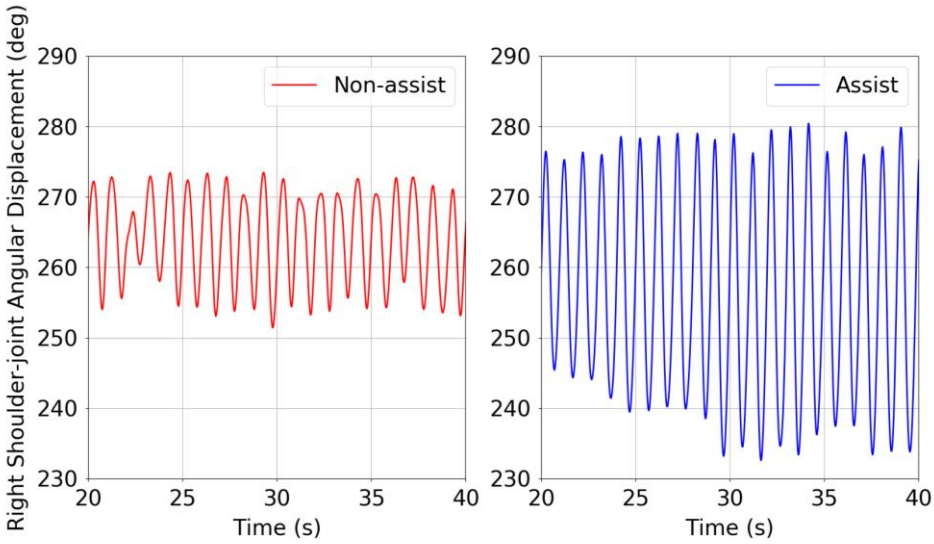

Fig 7. Example of the time-series data for the right shoulder-joint angular displacements of an elderly subject. Right shoulder-joint angular displacement under the (A) non-assist condition, and (B) assist condition.

Fig 8 shows the result of the analysis of the mean shoulder-joint amplitude for the elderly subjects. Table 1 gives the mean right shoulder- and hip-joint amplitude for each experimental condition. The result shows a significant increase in the mean right shoulder-joint amplitude from 24.9° to 40.5° for the non-assist and assist condition with a mean increment 15.6° with the elderly subjects. The result indicates that interactive rhythmic stimulation to the upper and lower limbs significantly increases the shoulder-joint amplitude for the assist condition against the non-assist condition with the elderly subject.

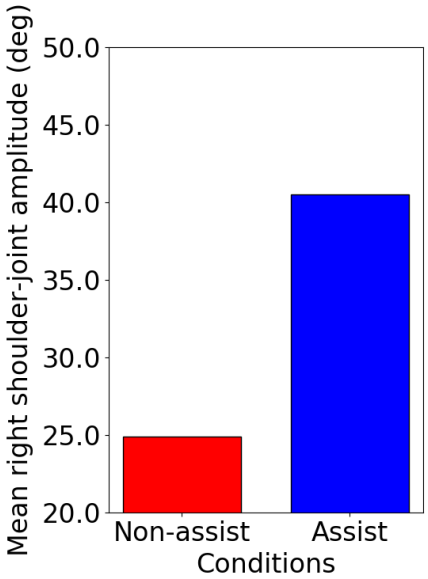

Fig 8. Analysis of the mean right shoulder-joint amplitude. The mean right shoulder-joint amplitude for the non-assist and assist conditions for the elderly subjects.

Table 1. Mean right shoulder- and hip-joint amplitude for each experimental condition.

Parameter	Condition	Mean
Shoulder-joint amplitude (°)	Non-assist	24.9
	Assist	40.5
Hip-joint amplitude (°)	Non-assist	39.2
	Assist	44.1

Fig 9 shows an example of the time-series data on the right hip-joint angular displacements for the non-assist and assist condition for an elderly subject. The result shows the peak-to-peak amplitude of the right hip-joint angular displacement is significantly higher for the assist condition compared with the non-assist condition.

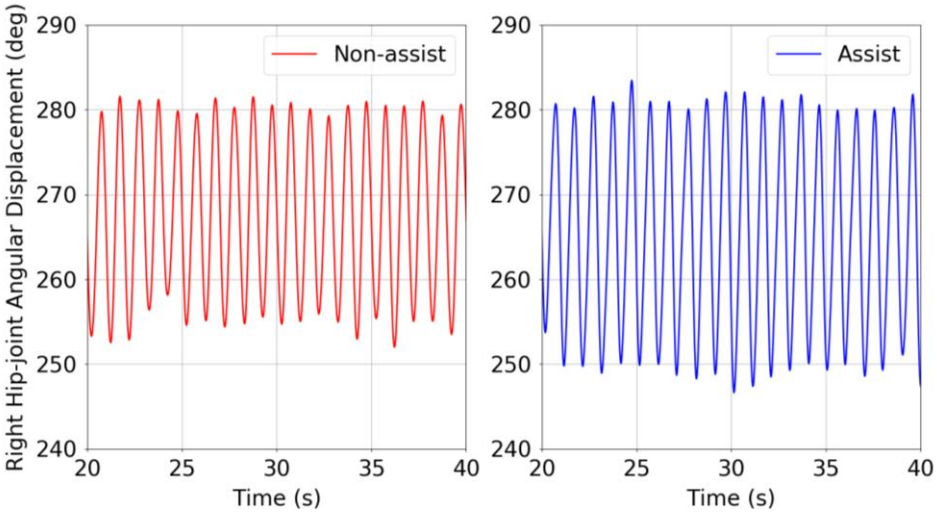

Fig 9. Example of the time-series data for the right hip-joint angular displacements of an elderly subject. Right hip-joint angular displacement under the (A) non-assist condition, and (B) assist condition.

Fig 10 shows the result of the analysis for the mean right hip-joint amplitude for the elderly subjects. The result shows a significant increase in the mean right hip-joint amplitude from 39.2° to 44.1° for the non-assist and assist conditions with a mean increment of 4.9°. The results indicate that interactive rhythmic stimulation to the upper and lower limbs significantly increases the hip-joint amplitude for the assist condition against the non-assist condition with the elderly subjects.

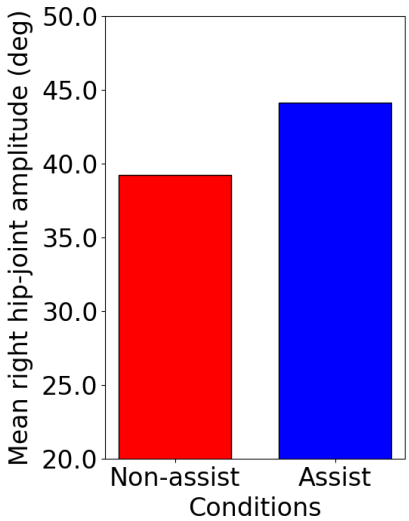

Fig 10. Analysis of the mean right hip-joint amplitude. The mean right hip-joint amplitude for the non-assist and assist conditions for the elderly subjects.

Fig 11 shows an example of the upper–lower–limbs' coordination diagram of the right shoulder- and hip-joint angular displacement for the non-assist and assist conditions for an elderly subject. The results showed a symmetrical pattern in the anti-phase coordination of the right upper and lower limbs between the non-assist and assist conditions for the elderly subject. The results indicate that interactive rhythmic stimulation to the upper and lower limbs does not adversely affect the elderly's upper–lower–limbs' coordination and is comparable with the non-assist condition.

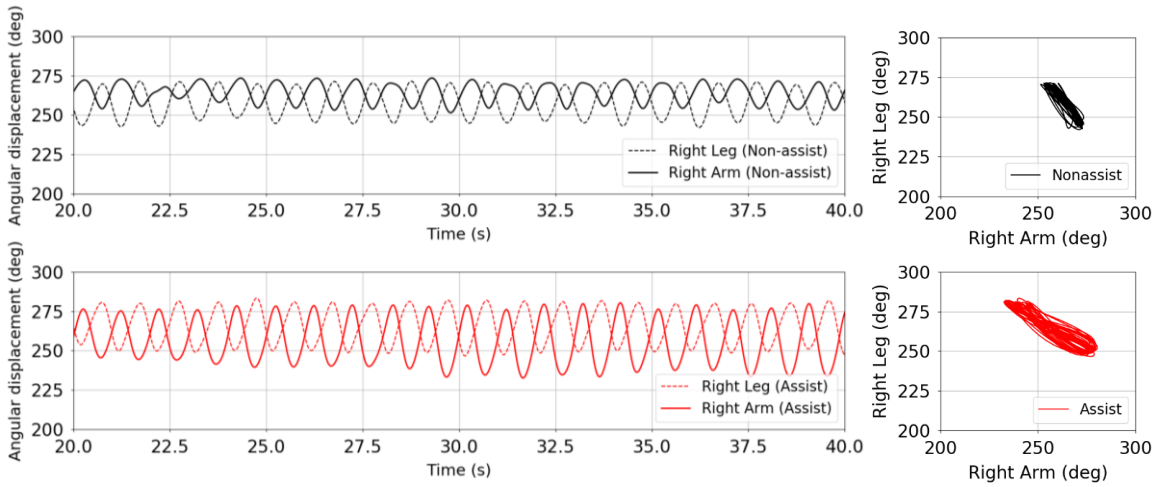

Fig 11. Upper–lower–limbs' coordination analysis of the right shoulder- and hip-joint angular displacement. The right shoulder- and hip-joint angular displacement for the non-assist and assist conditions for an elderly subject.

Fig 12 shows the result of the analysis of the *CV* of the right shoulder- and hip-joint amplitude for an elderly subject. The results showed a significant increase in the *CV* of the right shoulder and hip-joint amplitude from the non-assist to assist conditions. The results indicate that interactive rhythmic stimulation to the upper and lower limbs increases the elderly's gait instability.

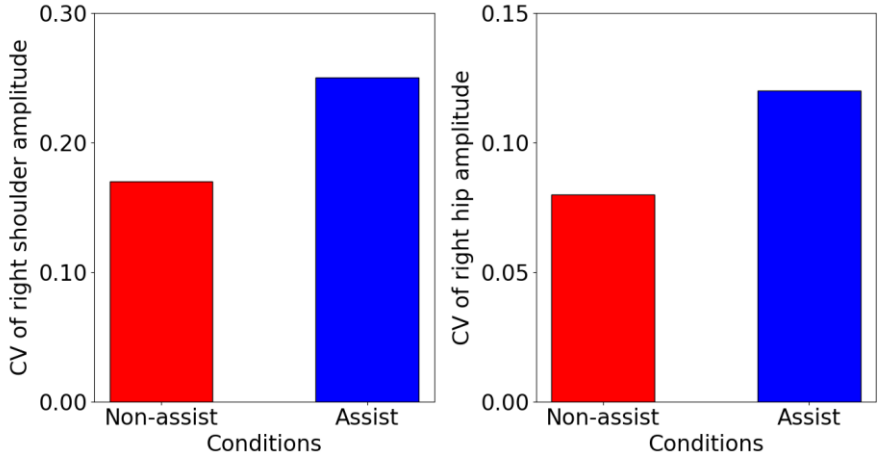

Fig 12. Analysis of the *CV* of right shoulder- and hip-joint amplitude. The *CV* of right shoulder- and hip-joint amplitude for the non-assist and assist conditions for an elderly subject.

2.6 Discussion

The gait-assist wearable exoskeleton developed in this study, the WalkMate, applied interactive rhythmic stimulation to the elderly subjects' upper and lower limbs, aiming to support their gait based on the principle of mutual entrainment (i.e., interpersonal coordination) in human-robot interaction. This support (i.e., active mode) is in contrast with that of previous power-assist wearable exoskeletons that aim to provide a direct torque to the wearer's lower limbs based on the master-slave control principle (i.e., passive mode). We hypothesize that this approach would improve the upper–lower–limbs' coordination, thereby providing gait-assist support for the elderly. To verify our hypothesis, we investigated the effect of such stimulation on spatial gait parameters (i.e., shoulder- and hip-joint amplitude), their corresponding *CV*s, and upper–lower–limbs' coordination by conducting walking experiments with healthy elderly subjects under the non-assist and assist conditions.

The results showed a significant increase in the mean right shoulder-joint amplitude for the assist condition compared with the non-assist condition, with a mean

increment of about 15.6°. It has been reported that a decrease in the arm-swing amplitude is associated with aging (Mirelman et al., 2015) with a decrease of 33.1% in healthy elderly adults (61–77 years) compared with healthy young adults (30–40 years). In this study, we observed a significant increase in the right shoulder-joint amplitude (i.e., arm-swing amplitude) by about 63% between the non-assist and assist conditions with the elderly subjects. Hence, the result indicates that interactive rhythmic stimulation to the upper and lower limbs could significantly increase the arm-swing amplitude for the elderly's gait, approaching that of healthy young adults.

In a second main result, we observed a significant increase in the mean right hip-joint amplitude for the assist condition compared with the non-assist condition, with a mean increment of about 4.9°. It has been reported that the step length was 4% shorter in healthy elderly adults compared with healthy young adults (DeVita and Hortobagyi, 2000). In addition, stride length was 6.7% (Ostrosky et al., 1994) and 10% (Winter et al., 1990) shorter in healthy elderly adults compared with healthy young adults, respectively. Further, hip angle was 7.3% smaller in healthy elderly adults compared with healthy young adults (Crosbie et al., 1997). In this study, we observed a significant increase in the right hip-joint amplitude by about 12.5% between the non-assist and assist condition with the healthy elderly subjects. Hence, the result indicates that interactive rhythmic stimulation to the upper and lower limbs could significantly increase the hip-joint amplitude for elderly's gait to be comparable to the gait of healthy young adults.

In a third main result, we observed a symmetrical pattern in the phase diagram of the upper and lower limbs between the between the non-assist and assist conditions for an elderly adult and is comparable with that of healthy young adults in a previous study (Serrien et al, 2000). It has been reported that elderly adults experienced a functional

decline in the anti-phase coordination between the ipsilateral limbs (i.e., same side of upper and lower limbs) (Serrien et al, 2000, Fujiyama et al., 2009) as manifested through an asymmetrical pattern in the phase diagram as compared with healthy young adults (Serrien et al., 2000). Hence, the result indicates that interactive rhythmic stimulation to the upper and lower limbs does not adversely affect the upper–lower–limbs' coordination for the elderly's gait and is comparable with that of healthy young adults.

However, in a fourth main result, we observed a significant increase in the *CV* of the right shoulder and hip-joint angular displacement from the non-assist to assist condition for an elderly subject. It has been reported that older adults exhibited decrease instability by walking slower (Kang and Dingwell, 2008), in spite of increased variability (Kang and Dingwell, 2008; Callisaya et al., 2010). Hence, the results indicate that interactive rhythmic stimulation to the upper and lower limbs increases the elderly's gait variability, which further indicates elderly's gait instability.

2.7 Limitations

Although stimulation to the upper and lower limbs significantly increases the shoulder- and hip-joint amplitude without adversely affecting the upper–lower–limbs' coordination, the results indicate a significant increase in their corresponding *CV*s with an elderly. We speculate that the increase in gait variability might be attributed to two remaining problems. First, stimulation to the lower limbs might cause gait instability for the elderly due to a direct application of an external motor torque to the wearer's lower limbs. Second, the additional weight imposed by the lower limb motors might cause gait instability for the elderly. To overcome the aforementioned limitations, we aimed to develop a gait-assist wearable exoskeleton using interactive rhythmic stimulation to the upper limbs to provide gait-assist support for the elderly.

CHAPTER 3. GAIT-ASSIST WEARABLE EXOSKELETON TO THE UPPER LIMBS: AN EXPERIMENTAL INVESTIGATION

3.1 Approach

We carry out our investigation using a four-step process. First, we evaluated the weight of the lower limb motors and a direct stimulation to the wearer's lower limbs might cause gait instability for the elderly. Second, we develop a gait-assist wearable exoskeleton using interactive rhythmic stimulation to the upper limbs through phase synchronization of the upper limbs and upper-limb-motors based on the mutual entrainment principle in human-robot interaction (i.e., interpersonal coordination) and upper–lower–limbs' neural coupling in human locomotion (i.e., intrapersonal coordination). Third, we conduct overground walking experiments with healthy elderly adults under the free (i.e., control condition) and upper-limb-assist condition at different lag times of the output motor torque to investigate the optimal upper-limb-assist condition. Finally, we evaluate the effect of stimulation to the upper limbs for the elderly's gait on a spatial (i.e., hip-swing amplitude) and temporal (i.e., hip-swing period) gait parameter, their corresponding *CV*s, and upper–lower–limbs' coordination using the arm- and hip-swing angular velocity data from the upper and lower limbs' wearable sensors, and compare the elderly's gait against the free condition and the gait of healthy young adults.

3.2 Gait-assist Wearable Exoskeleton to the Upper Limbs

The gait-assist wearable exoskeleton to the upper limbs comprises (1) hardware to provide motor torque (rhythmic stimulation) to the left and right upper limbs of a subject,

triggered by rhythmic signals, and (2) software to generate the rhythmic signals in synchronization with the walking rhythm of the subject based on the mutual entrainment principle.

3.2.1 Hardware Modules

The hardware comprises an actuator module, a control module, and a power module. Its overall weight is 5.8 kg. The actuator module is rigidly attached to an adjustable harness that can be secured to the upper limbs (i.e., between the elbow and shoulder joint) using a Velcro belt. The wearable exoskeleton is rigidly secured to the upper body (i.e., chest) and lower body (i.e., waist) of the subject using adjustable belts. Fig 13 shows the appearance of the hardware modules of the wearable exoskeleton to the upper limbs.

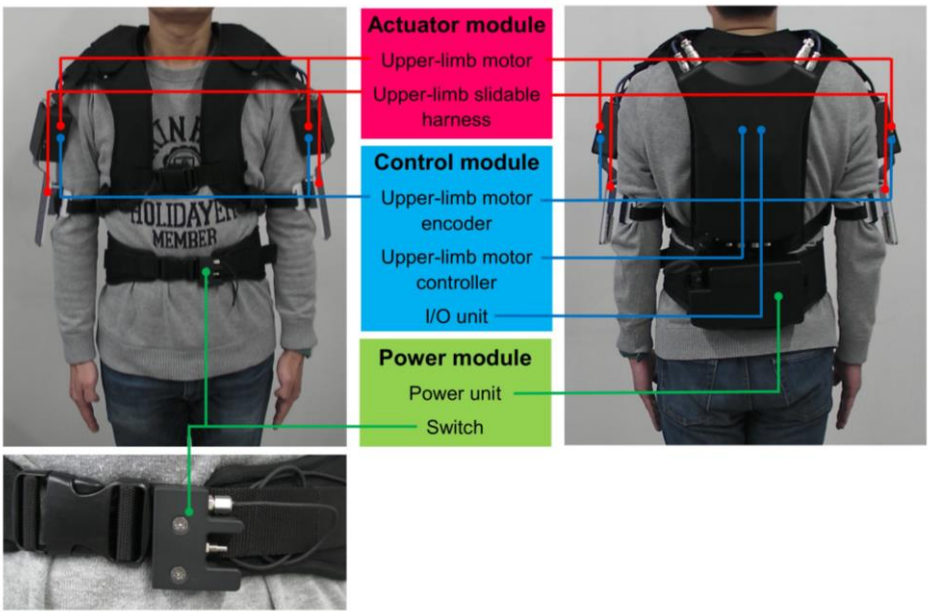

Fig 13. Appearance of gait-assist wearable exoskeleton to the upper limbs. The hardware module comprises the actuator, control and power modules. The actuator module comprises two upper-limb DC motors and slidable harnesses. The control module comprises two upper-limb DC motor encoders, two upper-limb DC motor controllers (i.e., hidden inside the cover) and an I/O unit (i.e., hidden inside the cover). The power module comprises an external power unit and an external on/off switch.

3.2.1.1 Actuator Module

This module comprises two three-phase DC brushless motors (DR-4316-X14B00420; Shinano Kenshi, Nagano, Japan), each of which provides an output torque to the upper limbs, adjustable harnesses, and a Velcro belt. The motors have a drive voltage of 24.0 V, a rated load current of 2.0 A, and a maximum thrust load of 3.8 N.

3.2.1.2 Control Module

This module comprises two upper-limb DC motor controllers, two upper-limb DC motor encoders, and an I/O unit. The encoders provide the control interface between the upper limbs and the I/O unit by detecting the subject's shoulder-joint angular displacement and sending this information to the I/O unit. The motor controllers provide the control interface between the I/O unit and the upper-limb DC motors by causing the motors to output the desired torque to the subject's upper limbs. An Android smartphone (ASUS Z00ED; Zenfone, Taiwan) controls the magnitude and phase of the output motor torque to the upper limbs through wireless communication with the I/O unit via Bluetooth.

3.2.1.3 Power Module

This module comprises an external power unit (7LPP545483AHR-1M01-WS; Hitachi, Japan) and an external on/off switch strapped to the adjustable belt at the waist level. The rechargeable external power unit provides power to the control module and drives the upper-limb DC motors. The external on/off switch acts as an emergency switch to enable the subject to override the human operator by switching off the motor torque to the upper limbs in case of an emergency or discomfort. Fig 14 shows the schematic diagram of the hardware module of the wearable exoskeleton to the upper

limbs.

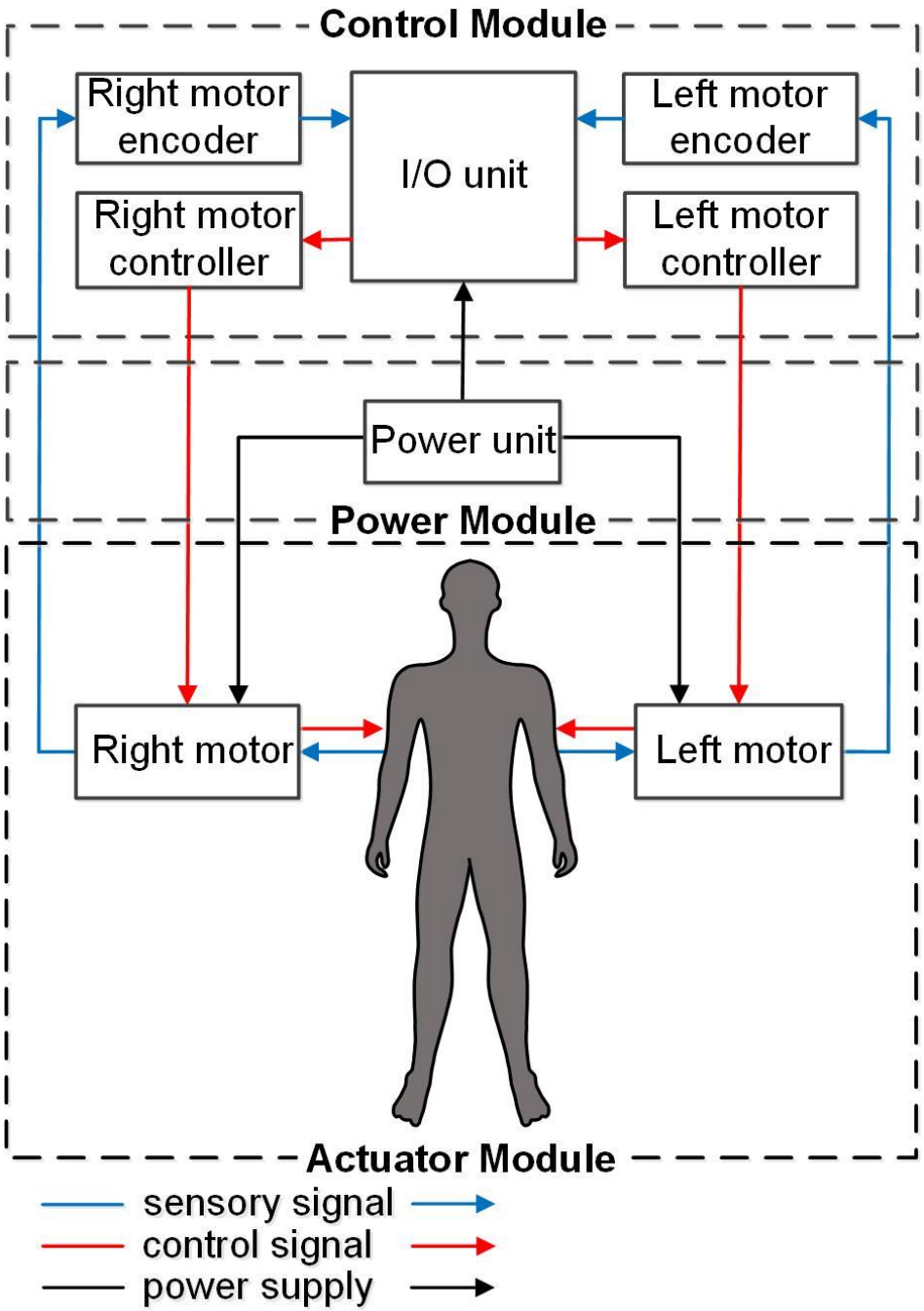

Fig 14. Schematic diagram of hardware module of the gait-assist wearable exoskeleton to the upper limbs. The upper-limb DC motor encoders detect the shoulder joints' angular displacement from the subject and input to the I/O unit. The upper-limb DC motor controllers output the desired motor torque from the I/O unit to the upper-limb DC motors. The power unit provides power to the control module and the upper-limb DC motors.

3.2.2 Software Modules

The software module comprises three modules. Module 1 (phase control module) controls the left and right upper-limb motor phases (i.e., their timing) by coordinating the phase differences of the left and right upper limbs and the upper-limb motors to a target based on the mutual entrainment principle. Module 2 (subject phase-input module) receives the subject's upper-limb angular displacements in real time via the upper-limb motor encoders. Finally, module 3 (motor-torque output module) controls the magnitude and phase for each of the upper-limb output motor torques and outputs the desired magnitude and phase information to the subject. Fig 15 shows a schematic diagram of the software for the wearable exoskeleton to the upper limbs.

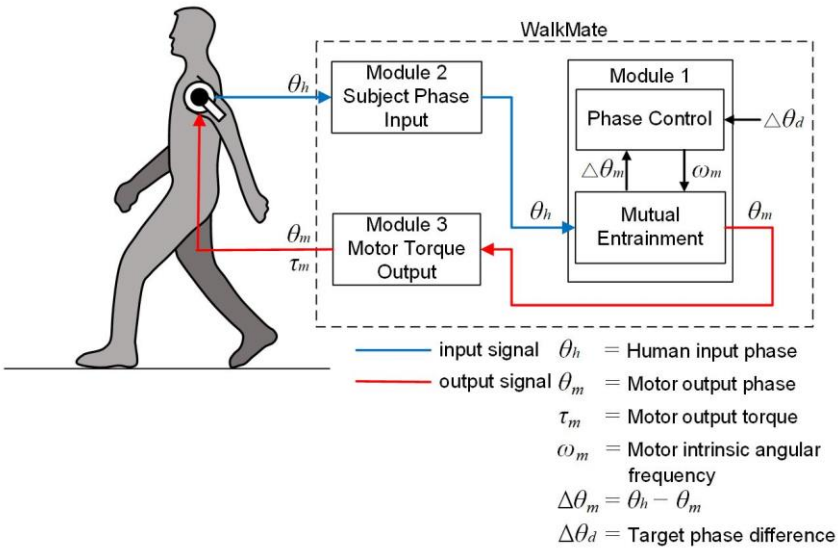

Fig 15. Schematic diagram of the software module of the gait-assist wearable exoskeleton to the upper limbs. The software module comprises module 1 (phase control module), module 2 (subject phase-input module), and module 3 (motor torque output module). Module 1 converges the phase difference between the left and right upper limbs and the upper-limb motor torque to a target value based on the mutual entrainment principle. Module 2 detects the left and right upper-limb angular displacement and input this information to the I/O unit. Module 3 controls the magnitude and phase of the left and right upper-limb motor torque and output the desired motor torque to the subject.

3.2.2.1 Phase Control Module

This module comprises the mutual entrainment submodule and the phase control submodule. The mutual entrainment submodule controls the left upper-limb motor phases, $\theta_{m,l}$ such that the phase differences, $\Delta\theta_{m,l}$ between the left upper limb arm-swing phases, $\theta_{h,l}$ and the left upper-limb motor phase, $\theta_{m,l}$ converge to 0°, where $\Delta\theta_{m,l} = \theta_{h,l} - \theta_{m,l}$. The phase $\theta_{h,l}$ is defined as the angle measured from the rearmost position of the left upper limb, with the rearmost position corresponding to 0º. The phase $\theta_{m,l}$ is defined as the motor phase that corresponds to the angle measured from the rearmost position. This submodule also controls the right upper-limb motor phase in the same manner, in terms of the variables $\theta_{m,r}$, $\Delta\theta_{m,r}$, and $\theta_{h,r}$.

The phase control submodule comprises two nonlinear coupled phase oscillators based on the Kuramoto model (Kuramoto, 1984), which can be represented as

$$\dot{\theta}_{m,l} = \omega_{m.l} + K_{lr}\sin\left(\theta_{m,r} - \theta_{m,l}\right) + K_m \sin\left(\Delta\theta_{m,l}\right), \quad (12)$$

$$\dot{\theta}_{m,r} = \omega_{m,r} - K_{lr}\sin\left(\theta_{m,l} - \theta_{m,r}\right) + K_m \sin\left(\Delta\theta_{m,r}\right). \quad (13)$$

Here, $\omega_{m,l}$ and $\omega_{m,r}$ are variable intrinsic angular frequencies of the upper-limb-motors. K_{lr} is the coupling between the left and right upper-limb motor phases, and K_m denotes the strength of the phase difference convergence between the upper limbs and motors. In the study, we set $K_{lr} = 5.0$ and $K_m = 0.5$, following the parameter values from the previous WalkMate framework (Miyake 2009). Fig 16 is a schematic diagram showing the relationships between all phases and phase differences used in the phase control module.

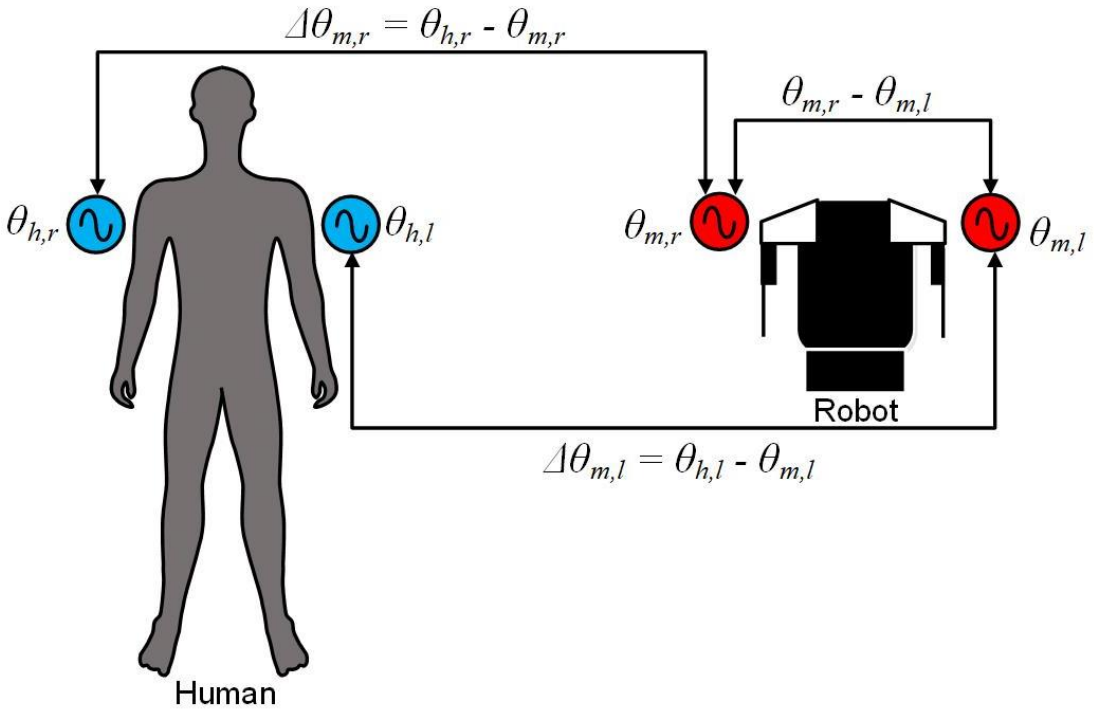

Fig 16. Schematic diagram of the definition of all phase and phase differences used in the phase control module. $\theta_{h,r}$ and $\theta_{h,l}$ represent the right and left upper limb arm-swing phases, respectively. $\theta_{m,r}$ and $\theta_{m,l}$ represent the right and left upper limb motor phases, respectively. $\Delta\theta_{m,l} = \theta_{h,l} - \theta_{m,l}$ and $\Delta\theta_{m,r} = \theta_{h,r} - \theta_{m,r}$ represent the phase difference between the left arm-swing and upper-limb motor, and right arm-swing and upper-limb motor, respectively.

The phase control submodule controls the intrinsic angular frequencies, $\omega_{m,l}$ and $\omega_{m,r}$, of the upper-limb motors by converging the phase differences, $\Delta\theta_{m,l}$ and $\Delta\theta_{m,r}$, to a target phase difference $\Delta\theta_d$. The operation of this submodule can be represented as:

$$\dot{\omega}_{m,l} = \varepsilon \sin(\Delta\theta_{m,l} - \Delta\theta_d) , \tag{14}$$

$$\dot{\omega}_{m,r} = \varepsilon \sin(\Delta\theta_{m,r} - \Delta\theta_d) . \tag{15}$$

Here, ε (> 0) is a control gain. In this study, we initialize ε to 0.16, $\Delta\theta_d$ to 0°, and both $\omega_{m,l}$ and $\omega_{m,r}$ to 4.0 rad/s, because the frequency of complete human gait cycles is about 1.0 Hz.

3.2.2.2 Subject Phase-input Module

This module receives the subject's upper-limb angular displacement from the upper-limb DC motor encoders. The control algorithm comprises four steps. First, both upper-limb motors were activated after four complete arm-swing cycles. At that time, both upper-limb were at their rearmost position (i.e., $\theta_{hl} = 0°$ and $\theta_{hr} = \pi$). Second, the phase differences between each upper-limb phase and its corresponding upper-limb motor phase (i.e., $\Delta\theta_{m,l}$ and $\Delta\theta_{m,r}$) were updated in real-time such that the phase differences approach the target phase difference $\Delta\theta_d = 0°$. Third, the intrinsic angular frequencies of both upper-limb motors, $\omega_{m,l}$ and $\omega_{m,r}$ were updated using Equations (14) and (15) with the phase differences being updated from the second step. Fourth, the upper-limb motor phases θ_{ml} and θ_{mr} were updated using Equations (12) and (13) with the intrinsic angular frequencies updated from the third step. This cycle repeats from the second to fourth steps during walking. Finally, the upper-limb motors stop when the operator switches off the exoskeleton using the Android phone controller or the end-user switches it off using the external switch. Fig 17 represents a flowchart of the software control algorithm for the wearable exoskeleton to the upper limbs.

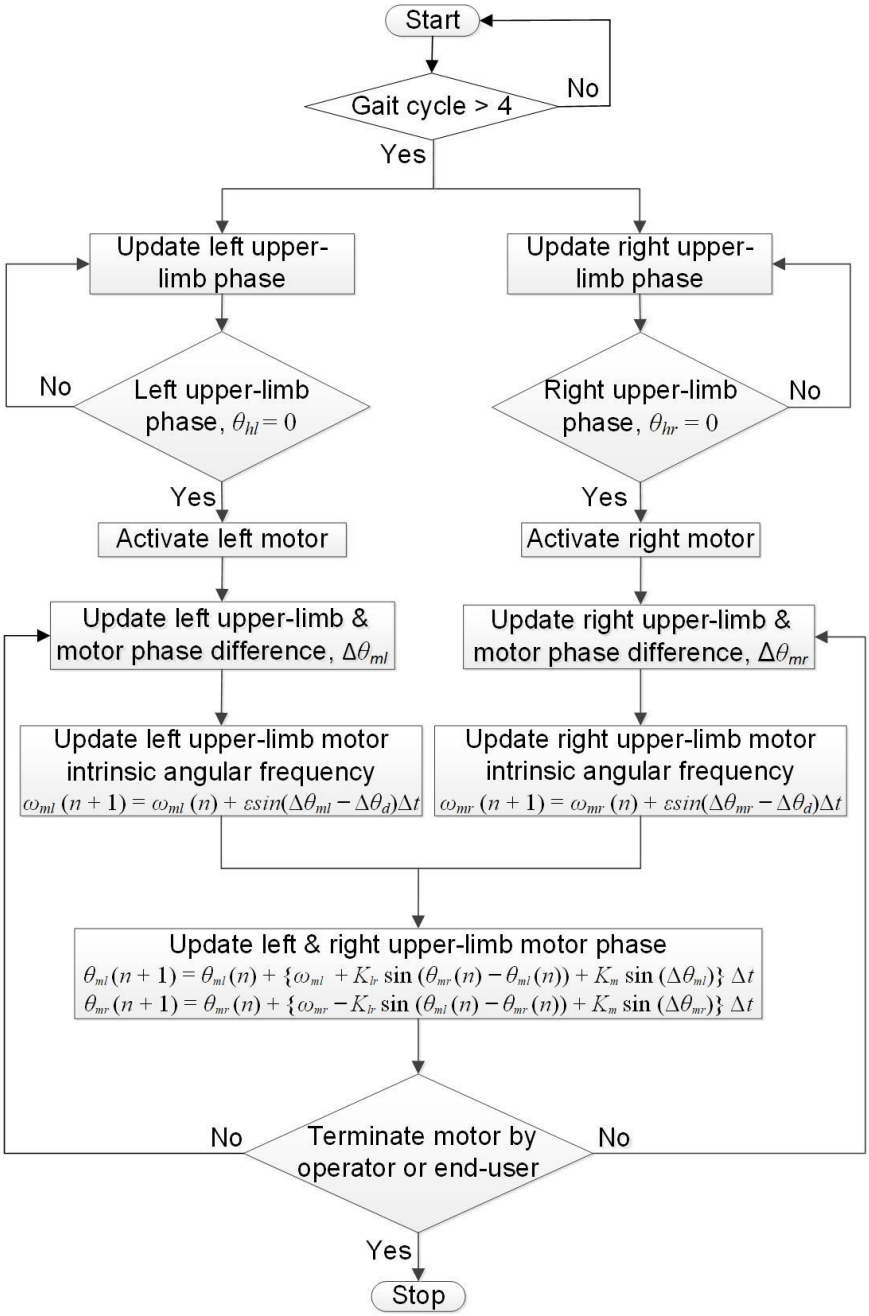

Fig 17. Flowchart of the software control algorithm of the gait-assist wearable exoskeleton to the upper limbs. The wearable exoskeleton starts after 4 complete gait cycles when the upper limbs were at the rearmost position. The left and right intrinsic angular frequencies of the upper-limb motors were updated in real-time by converging the phase difference between the left and right upper-limbs and upper-limb motors to a target phase difference, $\Delta\theta_d$. The left and right upper-limb motor phases were updated using the mutual entrainment module by the intrinsic angular frequencies of the left and right upper limb motors.

3.2.2.3 Motor Torque Output Module

This module follows each arm swing during one complete human gait cycle with temporal control of the motor torque. The upper-limb motor torque is applied at the contact point between the upper limb and the adjustable harness (i.e., just above the elbow joint). The phase of the output motor torque differs from the subject's arm-swing phase with respect to the rearmost position by an amount (i.e., lag time) that can be varied from 0% to 50% of one complete arm-swing cycle. The upper-limb-assist conditions for 0% and 50% lag times represent the output motor torque being applied to the upper limb at its rearward and foremost positions, respectively. However, because the foremost position corresponds to the exact time that the arm reverses its swing direction, using a 50% lag time might cause instability in the subject. We therefore restricted the maximum lag time to 40% in this study, where the upper limb is at an arm-swing position between the subject's frontal plane and the limb's foremost position. Fig 18 shows schematically the upper-limb-assist conditions for various lag times.

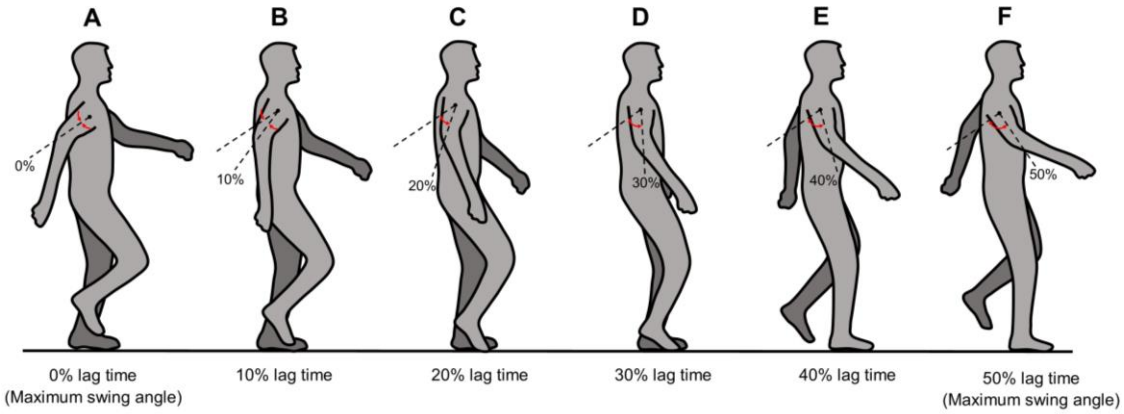

Fig 18. Schematic diagram of the upper-limb-assist conditions at the different lag times. (A) 0% (B) 10%, (C) 20%, (D) 30%, (E) 40%, and (F) 50%. 0% and 50% lag times correspond to the arm-swing phase at the rearward and foremost positions, respectively.

3.3 Experiment Task

3.3.1 Ethics Statement

The experiment protocol in this study was approved by the Ethics Committee at the Tokyo Institute of Technology through written consent. We recruited healthy elderly subjects from the Machida Silver Centre in Tokyo, Japan. They were all free from documented neurological disorders. Before the start of the experiment, all participants were briefed about the experimental procedures and written informed consent was obtained.

3.3.2 Participants

We evaluated the wearable exoskeleton by conducting walking experiments with 12 healthy elderly male subjects. The mean age of the subjects was 74.5 ± 2.6 years. The mean height and weight were 166.2 ± 5.1 cm and 63.3 ± 10.1 kg, respectively. Table 2 shows the mean age, height and weight of the subjects for the gait-assist wearable exoskeleton to the upper limbs.

Table 2: Experiment subjects for the gait-assist wearable exoskeleton to the upper limbs. Mean age, height and weight of the elderly subjects (mean ± SD).

Subjects	*N*	Age (years)	Height (cm)	Weight (kg)
Male	12	74.5 ± 2.6	166.2 ± 5.1	63.3 ± 10.1

3.3.3 Experimental Procedure

The experimental procedure comprised of two steps. First, the subjects walked a horizontal distance of 55.4 m along a corridor at their own natural speed with a natural arm swing. This process established a baseline called the “free condition”. Three

complete trials were conducted under this condition. Second, three experimental sessions were conducted. In each experimental session, the subjects put on the wearable exoskeleton and walked at their own natural walking speed under the upper-limb-assist conditions involving five different lag times (0%, 10%, 20%, 30%, and 40%) conducted randomly. For each condition, the subjects walked the same horizontal distance of 55.4 m along the corridor. Three complete trials were conducted for each condition. There was no rest time given between the first and second experimental sessions, but a rest time of about 5 min was given between the second and third sessions. The experiment ended when the subjects had completed all three experimental sessions.

During the experiment, each subject also wore a wearable sensor (TSND121; ATR-Promotion, Japan) on each of his upper and lower limbs. The sensor comprised an accelerometer and a gyroscope capable of measuring acceleration and angular velocity in all three dimensions. The sensor was rigidly secured to the upper and lower limbs using elastic Velcro belts at a vertical height of 5.0 cm and 15.0 cm above the elbow and knee joint on the sagittal plane, respectively. The time-series data from the wearable sensors were recorded during the experiment using a sampling frequency of 100 Hz and then transmitted to a portable laptop computer (Dell Latitude E5440; Dell, USA) via Bluetooth for off-line analysis. The sampling precision of the angular velocity is 0.01 degree per second. The time taken for each subject to complete each experiment trial was also measured using a digital stopwatch (HS44-001; Citizen, Japan) to calculate the average walking speed of each subject.

3.4 Gait Analysis

We performed a gait analysis of the left and right hip-swing angular displacements, hip-swing periods, their corresponding *CV*s, and upper–lower–limbs' coordination

using the time-series data obtained from the wearable sensors of the left and right upper and lower limbs to evaluate the effect of the interactive rhythmic stimulation applied to the upper limbs under all conditions. The gait analysis comprised twelfth steps.

First, we applied a fourth-order zero-phase shift Butterworth low-pass filter with a cut-off frequency of 6.0 Hz to the time-series data for the hip-swing angular velocity in the sagittal plane, because it has been reported that the frequencies for normal gait are within a narrow band, with the upper limit between 4.0 Hz to 6.0 Hz (Winter et al., 1974; Angeloni et al., 1994). Second, we performed a simple numerical integration of the time-series data on the hip-swing angular velocities using the trapezoidal rule to obtain the left and right hip-swing angular displacements, $\theta_{z,l}(t)$ and $\theta_{z,r}(t)$. Third, we applied a small recursive filter to $\theta_{z,l}(t)$ and $\theta_{z,r}(t)$ to correct for accumulation drift error caused by the numerical integration in the second step. Fourth, we repeated the same procedure to obtain the left and right arm-swing angular displacements. Fifth, we extracted each peak and trough of the corrected time-series data for the hip-swing angular displacements using a peak-detection algorithm to calculate the peak-to-peak hip-swing amplitudes for all complete stable gait cycles in each complete trial. Sixth, we calculated the mean peak-to-peak amplitude of the time-series data for the left and right hip-swing angular displacements, removing the first and last five gait cycles because of acceleration and deceleration issues, to obtain the mean left and right hip-swing amplitudes. Seventh, we calculated the mean hip-swing amplitude as the mean value of the mean left and right hip-swing amplitudes. Eighth, we calculated the time difference between two consecutive peaks and troughs of the time-series data for the left and right hip-swing angular displacements to calculate the mean left and right hip-swing periods. Ninth, we calculated the mean hip-swing period, which is the mean of the mean left and right hip-swing periods. Tenth, we calculated the mean CV of the left and right hip-

swing amplitude between the free and upper-limb-assist conditions for three complete trials to determine the dispersion of the hip-swing amplitude from the mean amplitude. Then we calculated the mean *CV* of the hip-swing amplitude as the mean of the mean left and right *CV* of the hip-swing amplitude. Eleventh, we repeated the same procedure for the mean *CV* of the hip-swing period. Finally, we compared the anti-phase coordination between the left and right arm-and hip-swing angular displacement for one complete trial of the free and upper-limb-assist condition at all lag times using phase diagram. Postprocessing of the time-series data from the wearable sensors was performed using the Scientific Computing Library, SciPy in Python (version 2.7) and numerical analysis of the time-series data was performed using a Microsoft Excel spreadsheet.

3.5 Statistical Analysis

Statistical analysis comprised a two-step process. First, we performed a statistical analysis of the mean hip-swing angular displacement, mean hip-swing period and their correspond *CV*s between the free condition and each of the upper-limb-assist conditions, using the Friedman test because of the nonparametric distribution of the numerical data ($n = 12$). Second, if a statistically significant difference existed from the previous test, we performed a multiple pair-wise Wilcoxon signed-rank test. To address the type-I and type-II errors introduced as a result of multiple pairwise testing, we performed a correction to the statistical test using the Bonferroni correction (Bland and Altman, 1995). All statistical analyses were performed using *R* (version 3.3.3). A statistically significant difference between the free condition and each of the upper-limb-assist conditions was confirmed at $p < 0.05$.

3.6 Results

Figs 19(A) to 19(D) show examples of the time-series data for both the right and left hip-swing angular displacements, for both the free condition and the upper-limb-assist condition with 40% lag time, respectively, for an elderly subject. These results showed that the peak-to-peak amplitude for each of the right and left hip-swing angular displacements is higher for the upper-limb-assist condition with a 40% lag time than for the free condition.

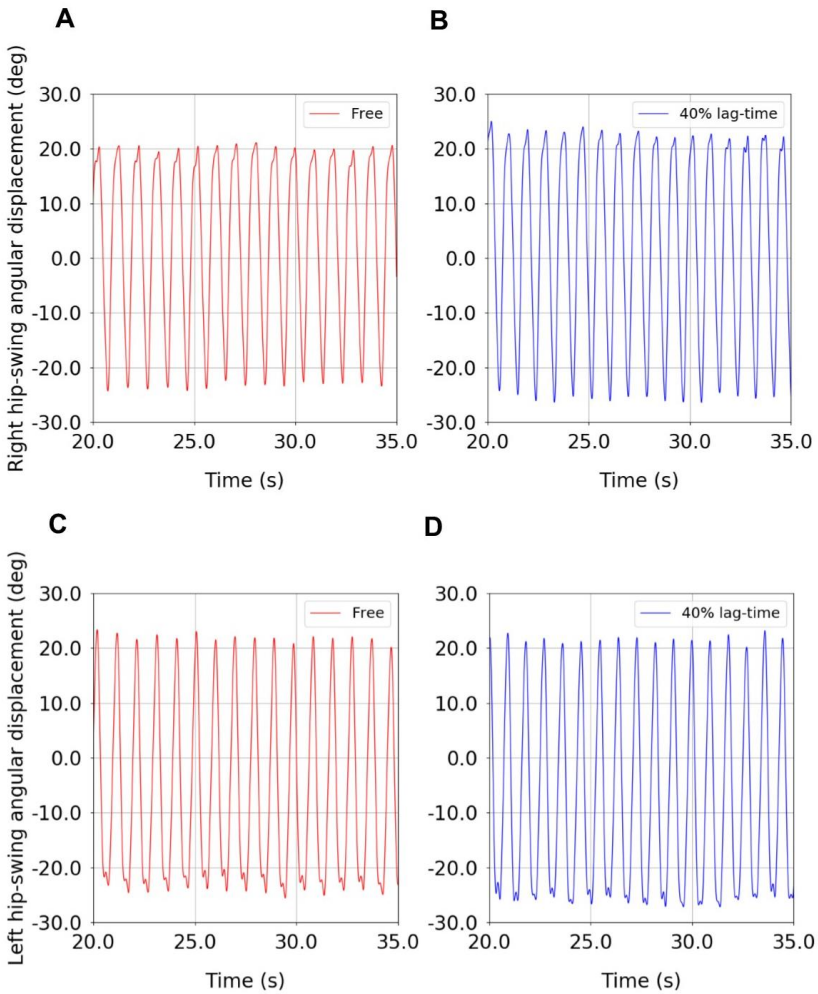

Fig 19. Example of the time-series data for the right and left hip-swing angular displacements for an elderly subject. Right hip-swing angular displacement under the (A) free condition; (B) upper-limb-assist condition with 40% lag time; Left hip-swing angular displacement under the (C) free condition; (D) upper-limb-assist condition with 40% lag time.

Fig 20 shows the result of the statistical analysis for the mean hip-swing amplitude for the elderly subjects. Table 3 gives the mean hip-swing amplitude, mean hip-swing period for each experimental condition, and the *p*-value for the upper-limb-assist conditions with respect to the free condition. A Friedman test revealed a significant effect of upper-limb conditions on the hip-swing amplitude ($A^2(5) = 27.1$, $p < 0.01$). A post hoc test using Wilcoxon signed-rank test with Bonferroni correction showed a statistically significant difference between the free condition and each of the upper-limb-assist conditions with respect to the mean hip-swing amplitude under all conditions ($p = 0.0024$). In particular, the mean hip-swing amplitude shows a statistically significant increase of about 2.8º from the free condition to each of the upper-limb-assist conditions. The results showed an increase in the mean hip-swing amplitude for each of the upper-limb-assist conditions against the free condition.

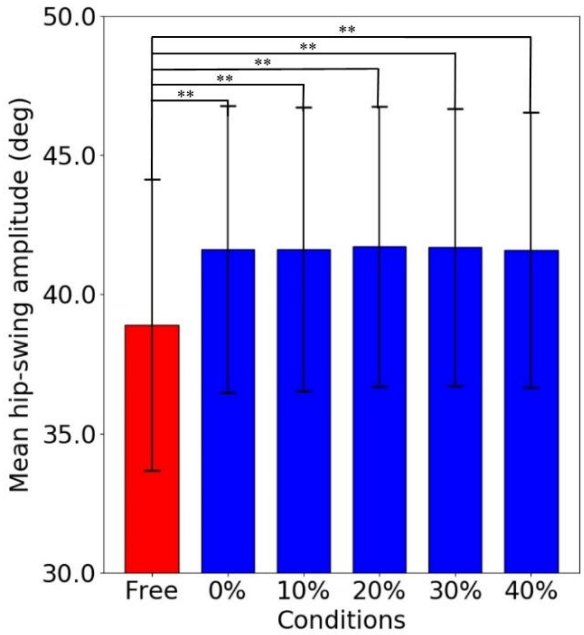

Fig 20. Statistical analysis of the mean hip-swing amplitude. The mean hip-swing amplitude for the free condition and each of the upper-limb-assist conditions for the elderly subjects at 0, 10, 20, 30, and 40% lag time. (**: $p < 0.01$).

Table 3. Mean and *p* values of the mean hip-swing amplitude and period (*: $p < 0.05$; **: $p < 0.01$)

Parameter	Condition	Mean (±SD)	*p*-value
Hip-swing amplitude (º)	Free	38.90 (± 5.24)	-
	0% lag time	41.62 (± 5.16)	0.0024**
	10% lag time	41.63 (± 5.10)	0.0024**
	20% lag time	41.72 (± 5.04)	0.0024**
	30% lag time	41.69 (± 4.98)	0.0024**
	40% lag time	41.60 (± 4.94)	0.0024**
Hip-swing period (ms)	Free	1000.5 (± 60.4)	-
	0% lag time	982.3 (± 67.5)	0.088
	10% lag time	980.1 (± 66.8)	0.081
	20% lag time	978.0 (± 66.7)	0.061
	30% lag time	974.9 (± 67.3)	0.061
	40% lag time	977.1 (± 67.3)	0.024*

Fig 21 shows the results of the statistical analysis of the mean hip-swing period for the elderly subjects. A Friedman test revealed a significant effect of upper-limb conditions on the hip-swing period ($A^2(5) = 17.2$, $p = 0.00412$). A post hoc test using Wilcoxon signed-rank test with Bonferroni correction showed a statistically significant difference between the free condition and the upper-limb-assist condition with a 40% lag time ($p = 0.024$), where the mean hip-swing period decreased on average by 23 ms. However, no statistically significant differences were observed for other upper-limb-assist conditions ($p = 0.088$, 0.081, 0.061, and 0.061, respectively).

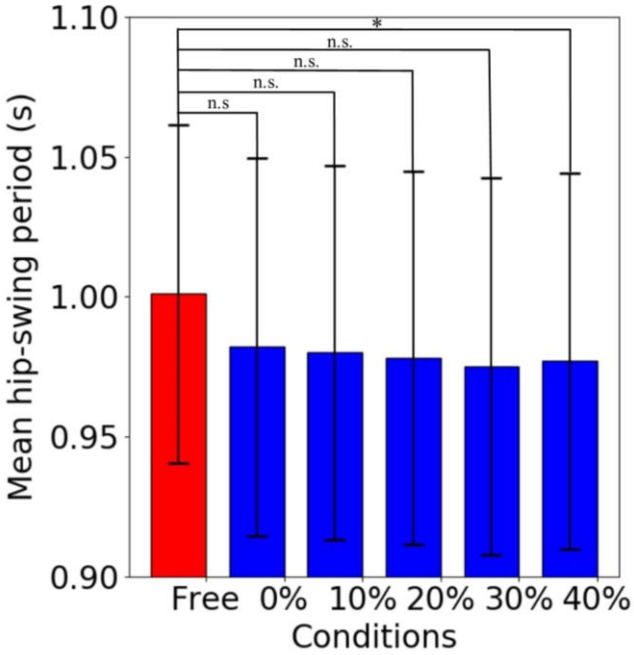

Fig 21. Statistical analysis of the mean hip-swing period. The mean hip-swing period for the free condition and each of the upper-limb-assist conditions for the elderly subjects at 0%, 10%, 20%, 30%, and 40% lag time. (*: $p < 0.05$, n.s.: non-significant).

Figs 22 and 23 shows examples of phase diagram of the right and left arm- and hip-swing angular displacement for the free and upper-limb-assist condition at all lag times for an elderly subject, respectively (Please refer to Appendix 7.13 for the phase diagram of all elderly subjects). The results showed a symmetrical pattern in the anti-phase coordination of the left and right upper and lower limbs between the free and upper-limb-assist condition at all lag times for the elderly subject. The results indicate that interactive rhythmic stimulation to the upper limbs does not adversely affect the elderly's upper–lower–limbs' coordination and is comparable with the free condition.

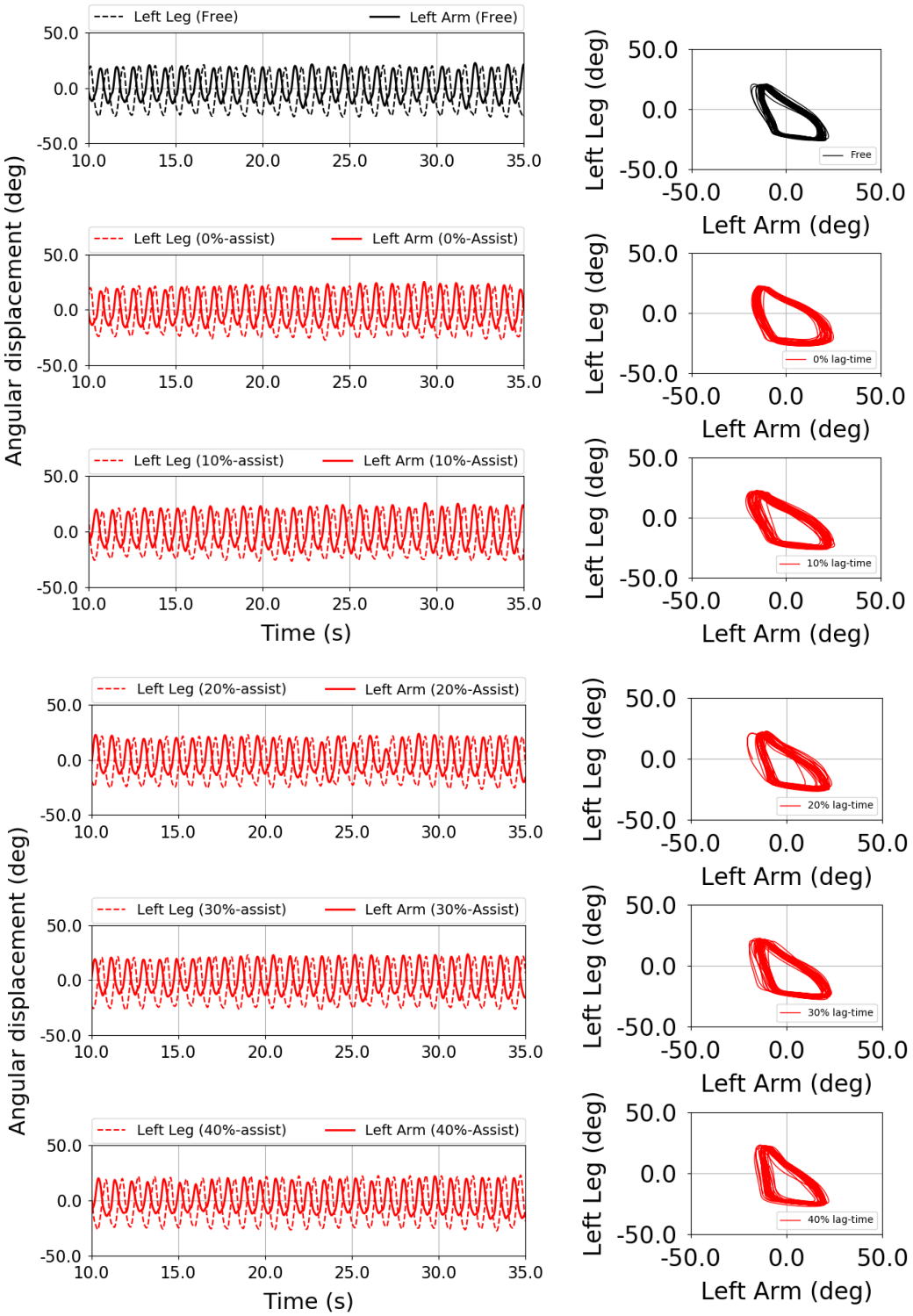

Fig 22. Phase diagram of the left arm- and hip-swing angular displacement. The left arm- and hip-swing angular displacement for the free and upper-limb-assist condition at all lag times for elderly subject 2.

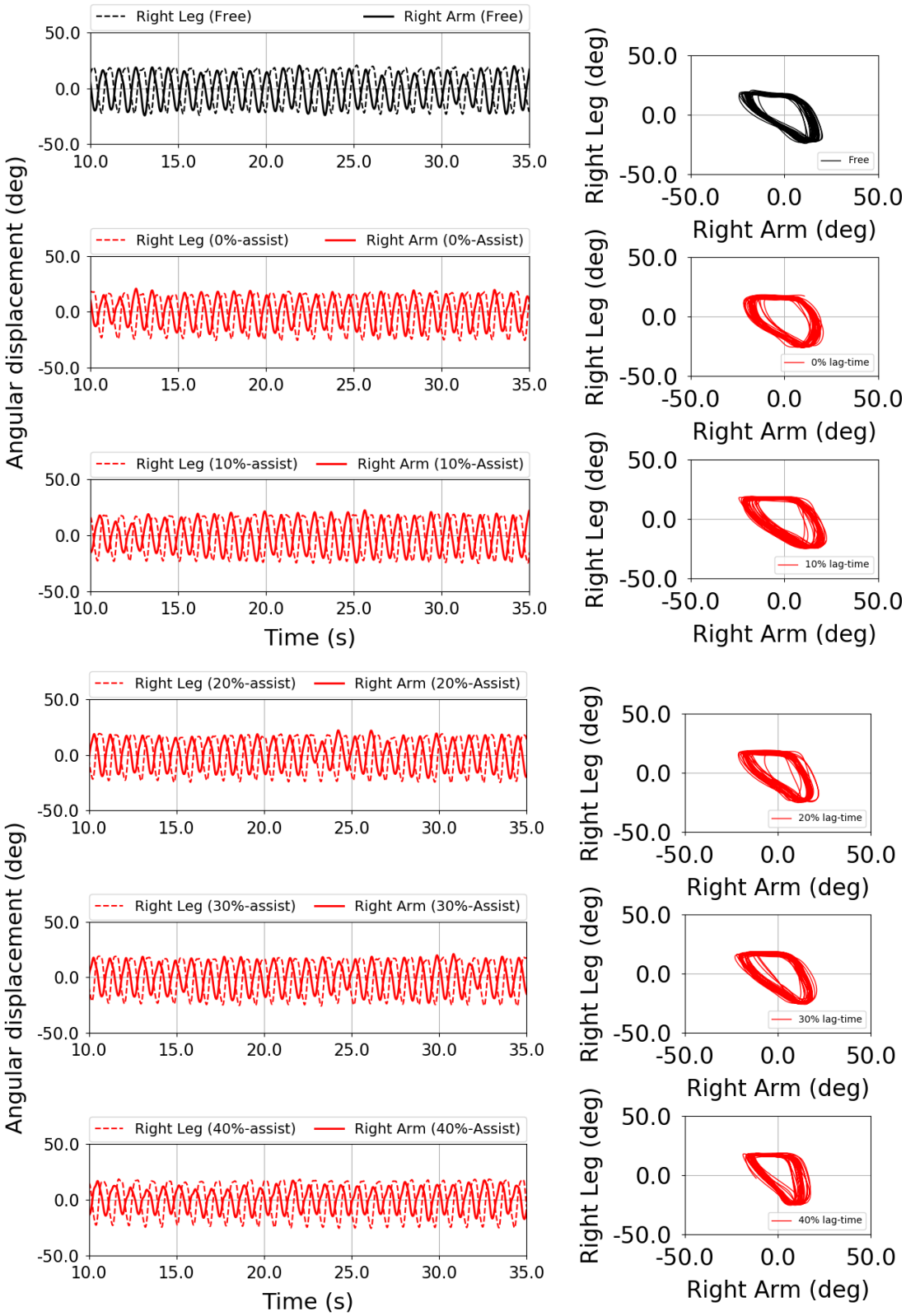

Fig 23. Phase diagram of the right arm- and hip-swing angular displacement. The right arm- and hip-swing angular displacement for the free and upper-limb-assist condition at all lag times for elderly subject 2.

Fig 24 shows the results of the statistical analysis for the mean *CV* of the hip-swing amplitude for the elderly subjects. A Friedman test revealed no significant effect of upper-limb conditions on the mean *CV* of the hip-swing amplitude ($A^2(5) = 6.381$, $p = 0.270$). The results showed no statistically significant difference in the mean *CV* of the hip-swing amplitude for each of the upper-limb-assist conditions against the free condition.

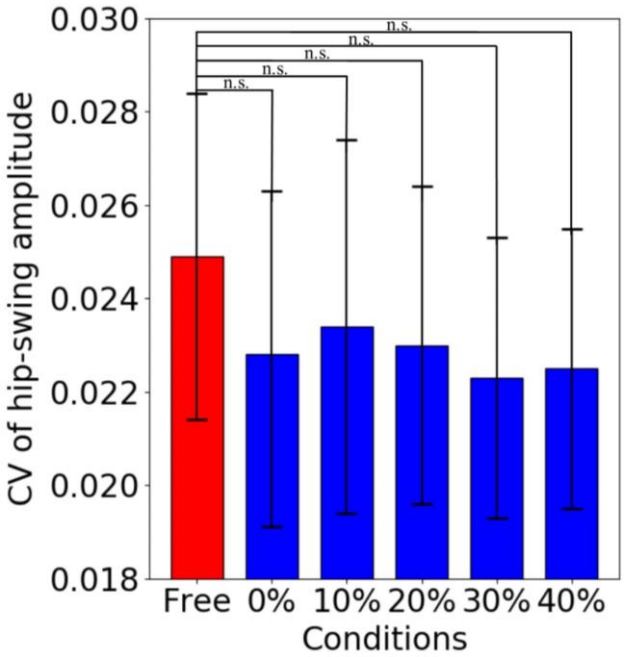

Fig 24. Statistical analysis of mean *CV* of hip-swing amplitude. The mean *CV* of hip-swing amplitude for the free condition and each of the upper-limb-assist conditions for the elderly subjects at 0, 10, 20, 30, and 40% lag time. (n.s.: non-significant).

Fig 25 shows the results of the statistical analysis of the mean *CV* of the hip-swing period for the elderly subjects. A Friedman test revealed no significant effect of upper-limb conditions on the mean *CV* of the hip-swing period ($A^2(5) = 3.1655$, $p = 0.6745$). The results showed no statistically significant difference in the mean *CV* of the hip-swing period for each of the upper-limb-assist conditions against the free condition.

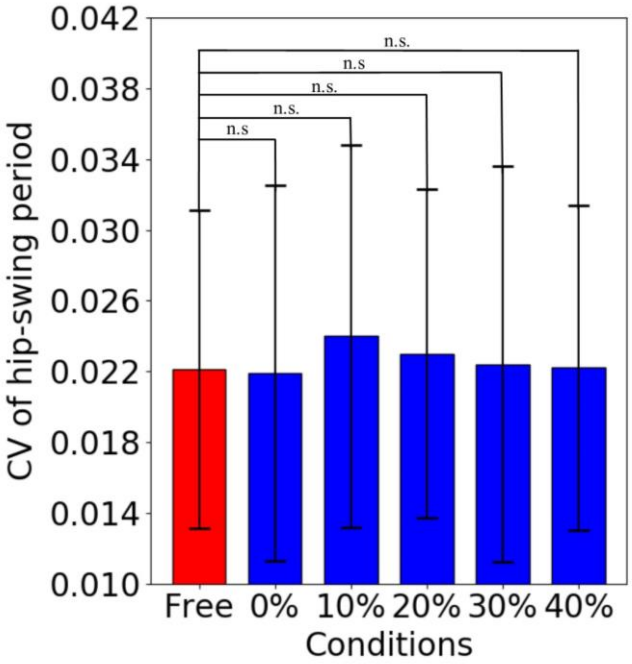

Fig 25. Statistical analysis of mean *CV* of hip-swing period. The mean *CV* of hip-swing period for the free condition and each of the upper-limb-assist conditions for the elderly subjects at 0, 10, 20, 30, and 40% lag time. (n.s.: non-significant).

3.7 Discussion

In pursuant to the remaining problems associated with the gait-assist wearable exoskeleton to the upper and lower limbs, the gait-assist wearable exoskeleton developed in this study, the WalkMate, applied interactive rhythmic stimulation to the elderly subjects' upper limbs, aiming to support their gait based on the principle of mutual entrainment (i.e., interpersonal coordination) in human–robot interaction and upper–lower–limbs' neural coupling (i.e., intrapersonal coordination) as mediated by central pattern generators. We postulate that this approach would provide stable gait-assist support to the wearer's lower limbs, and coordination to the upper and lower limbs based on the intrinsic mechanisms of upper–lower–limbs' neural coupling in human locomotion. To verify our hypothesis, we investigated the effect of such stimulation on a spatial (i.e., hip-swing amplitude) and temporal (i.e., hip-swing period) gait parameter,

their corresponding *CV*s, and upper–lower–limbs' coordination by conducting walking experiments with healthy elderly subjects.

It has been reported that changes in gait pattern with increasing age are associated with decreasing muscle strength and that there is a need for increased stability during locomotion with increasing age (Nigg et al., 1994). In addition, it has been reported that age causes a redistribution of joint torques and powers, with the elderly using their hip extensors more than young adults walking at the same speed (DeVita and Hortobagyi, 2000). We feel that it is important to assist healthy elderly subjects to regain their normal gait ability as a result of aging to assist them in their activities of daily living. In this regard, we consider our gait-assist wearable exoskeleton able to overcome the limitations of elderly's gait by encouraging voluntary efforts (i.e., active mode), thereby providing appropriate support to the lower limbs.

Although many power-assist wearable exoskeletons have been developed, these exoskeletons aim to provide a direct torque to the wearer's lower limb by controlling the gait trajectory to reach a target trajectory based on the master-slave control principle (Kawamoto et al., 2003; Riener et al., 2005; Veneman et al., 2007; Kim et al., 2010; Esquenaszi et al., 2012; Alexander et al., 2012; Alan et al., 2014; Bortole et al., 2015; Barbareschi et al., 2015; Yi et al., 2016, 2017; Chen et al., 2017; Deng et al., 2017; Lerner et al., 2017; Choi et al., 2018). Moreover, there is no direct comparison between the baseline condition (i.e., free walking) and the robot-assist condition. Hence, the effectiveness of the direct power-assist support of these wearable exoskeletons to the lower limbs remains unclear.

In contrast, in this study, we conducted walking experiments with healthy elderly subjects using the control condition (i.e., free walking) and upper-limb-assist condition at different lag times. The results showed a statistically significant increase in the mean

hip-swing amplitude for the upper-limb-assist condition at all lag times compared with the free condition, with a mean increment of about 7% (i.e., 2.8º). It has been reported that the step length was 4% shorter in healthy elderly adults compared with healthy young adults (DeVita and Hortobagyi, 2000). In addition, stride length was 6.7% (Ostrosky et al., 1994) and 10% (Winter et al., 1990) shorter in healthy elderly adults compared with healthy young adults, respectively. Further, hip angle was 7.3% smaller in healthy elderly adults compared with healthy young adults (Crosbie et al., 1997). In this study, although no stimulations were applied to the lower limbs, we observed a statistically significant increase in the hip-swing amplitude by about 7% between the free condition and each upper-limb-assist condition at different lag times with the healthy elderly subjects. Hence, the result indicates that interactive rhythmic stimulation to the upper limbs could effectively increase the hip-swing amplitude for elderly adults' gait to be comparable to the gait of healthy young adults.

In addition, Lerner et al. (2017) reported that power-assist support to the wearer's knee joint showed a statistically significant increase in the peak hip extension of children with cerebral palsy by 8º between the baseline walking condition (i.e., free walking) and the power-assist condition. Although the increase in the mean hip-swing amplitude in our present study is smaller than that measured in the previous study (Lerner et al., 2017), it should be noted that all the participants in the previous study are unhealthy subjects, whereas all our participants are healthy subjects. Hence, the result supports the hypothesis that applying appropriate interactive rhythmic stimulation to the elderly adult's upper limbs would affect their lower limbs as manifested through an increase in the hip-swing amplitude.

We speculate from the results that the mutual entrainment resulting from such stimulation would activate the central pattern generators of the upper limbs, thereby

stimulating the lower limbs as mediated through a cooperative relationship (intra-synchronization) between the upper and lower limbs. Such as relationship has been reported in terms of upper–1ower–1imbs' neural coupling in many previous studies (Delwaide et al., 1977; Baldissera et al., 1982, 1988; Guadagnoli et al., 2000; Dietz et al., 2001; Zehr et al., 2001; Zehr and Haridas, 2003; Frigon et al., 2004; Huang and Ferris, 2004, 2009; Zehr and Duysens, 2004; Kawashima et al., 2008). In particular, the soleus muscles of the lower limbs could be activated (Huang and Ferris, 2004, 2009; Kawashima et al., 2008) and the presynaptic inhibition could be suppressed (Zehr and Duysens, 2004) by the stimulation of the upper limbs via the upper–1ower–limbs' neural coupling.

In a second main result, although no stimulations were applied to the lower limbs, we observed a statistically significant decrease in the mean hip-swing period of the subjects for the upper-limb-assist condition with 40% lag time compared with the free condition. However, there is no statistically significant difference between the upper-limb-assist condition with a 0%, 10%, 20%, and 30% lag time, and the free condition. It has been reported that the stride velocity of healthy elderly adults is 7.9% lower than that of healthy young adults (Ostrosky et al., 1994). In addition, it has been reported that there are 7.7% (DeVita and Hortobagyi, 2000) and 2.3% (Krasovsky et al., 2014) reported decreases in the swing time of healthy elderly adults compared with healthy young adults. In this study, we observed a statistically significant decrease in the hip-swing period by 2.3% (i.e., 23 ms) between the free condition as compared with the upper-limb-assist condition at 40% lag time. Although the decrease in the hip-swing period (i.e., increase in the gait speed) is smaller in our present study compared with that measured by DeVita and Hortobagyi (2000), it is comparable with the results presented by Krasovsky et al. (2014). Hence, the result indicates that interactive

rhythmic stimulation to the upper limbs could increase the gait speed of the elderly to be comparable to the gait of healthy young adults.

Although this decrease in the hip-swing period is small, the result indicates that interactive rhythmic stimulation to the upper limbs at an optimal arm-swing position can increase the arm-swing activity. Because it has been reported in previous studies that an increase in arm-swing activity increases the gait speed (Eke-Okoro et al., 1997; Marks, 1997; Long et al., 2011), the results indicate the possibility that interactive rhythmic stimulation to the upper limbs could increase the gait speed with these healthy elderly subjects due to an increase in arm-swing-activity, particularly at a 40% lag time. Moreover, it has been reported in a previous study that postural changes of the upper limb affect the reflex transmission of the lower limbs, which is maximal when the upper limb is at an angle of 45º with respect to the frontal plane (Delwaide et al., 1977). This position corresponds to the arm-swing position of the upper limbs at a 40% lag time in our study. It would be possible that stimulation at this arm-swing position could activate the soleus reflex of the lower limbs significantly, again leading to increased gait speed. Therefore, the effect of the stimulation on the gait speed might be optimized for the 40% lag time.

In a third main result, although no stimulation were applied to the lower limbs, we observed a symmetrical pattern in the phase diagram of the left and right arm- and hip-swing angular displacements between the free and upper-limb-assist condition at all lag times for an elderly adult and is comparable with that of a healthy young adult in a previous study (Serrien et al, 2000). However, this is in contrast with the asymmetrical pattern in the phase diagram of an elderly subject in the previous study (Serrien et al., 2000). Therefore, the results indicate that interactive rhythmic stimulation to the upper limbs does not adversely affect the upper–lower–limbs' coordination for the elderly's

gait and is comparable with that of healthy young adults.

In a fourth main result, we observed no statistically significant difference in the mean *CV*s of the hip-swing amplitude and period for the upper-limb-assist condition at all lag times compared with the free condition. It has been reported that older adults exhibited decreased instability by walking slower (Kang and Dingwell, 2008), in spite of increased variability (Kang and Dingwell, 2008; Callisaya et al., 2010). Although stimulation to the upper limbs does not statistically significantly decrease the elderly's gait variability, the results indicate that stimulation to the upper limbs does not adversely affect the elderly's gait stability which is comparable with the free (i.e., stable) condition.

In summary, interactive rhythmic stimulation to the upper limbs statistically significantly increases the hip-swing amplitude and gait speed for the elderly's gait without adversely affecting their gait stability, and upper–lower–limbs' coordination. Therefore, interactive rhythmic stimulation to the upper limbs at an optimal lag time condition could offer a promising neurorehabilitation strategy for the elderly's gait.

3.8 Limitations

However, there are some limitations in our present study. First, the weight of the gait-assist wearable exoskeleton used is heavy (5.8 kg) for the elderly subjects. Although our results showed a statistically significant increase in the hip-swing amplitude and gait speed of these subjects, the marginal change indicates that the weight of the wearable exoskeleton might have counteracted the benefits of the interactive rhythmic stimulation. Because of this possibility, the development of a lightweight gait-assist wearable exoskeleton for the elderly is underway. Second, the sample size of our elderly subjects ($n = 12$) can be considered small. Our preliminary results showed that some inter-subject variability exists even for healthy elderly subjects in the hip-swing amplitude and hip-

swing period. Thus, there is a need to increase the sample size of the elderly subjects to minimize the effect of this variability. Third, we have only conducted three experimental sessions for each experimental condition on the same day. In order to account for the effect of neuroplasticity, there is a need to conduct more experimental sessions over a longer time frame including "free" walking experiments immediately after walking experiments using the wearable exoskeleton (i.e., "wash-out" effect).

Despite the aforementioned limitations, our results suggest that the WalkMate gait-assist wearable exoskeleton succeeds in generating interactive rhythmic stimulation in synchronization with an elderly subject's arm swing, based on the mutual entrainment principle. Moreover, this principle plays an important role in establishing intrapersonal coordination between the upper and lower limbs of the subjects. In addition, it should also be noted that the autonomous gait ability of subjects has been an important aspect of the establishment of this principle.

CHAPTER 4. GENERAL DISCUSSION

4.1 Gait-assist Wearable Exoskeletons to the Upper Limbs

We have well developed a gait-assist wearable exoskeleton, WalkMate that provides interactive rhythmic stimulation to the upper limbs based on the mutual entrainment principle in human-robot interaction to provide gait-assist support for the elderly's gait. Further, we have well developed the gait-assist wearable exoskeleton to provide coordination to the upper and lower limbs for the elderly's gait. In addition, we have positively evaluated our gait-assist wearable exoskeleton that provides stimulation to the upper limbs as manifested through an improvement in the elderly's hip-swing amplitude and gait speed without adversely affecting the elderly's gait stability, and upper–lower–limbs' coordination.

4.2 Gait-assist Wearable Exoskeletons

The gait-assist wearable exoskeleton that provides interactive rhythmic stimulation to the upper limbs is a significant improvement over the wearable exoskeleton that provides stimulation to the upper and lower limbs. First, the gait-assist wearable exoskeleton that provides stimulation to the upper and lower limbs significantly increases the *CV* of the shoulder- and hip-joint amplitude for the elderly's gait. However, the gait-assist wearable exoskeleton that provides stimulation to the upper limbs does not statistically significantly increase the *CV* of the hip-swing amplitude and period for the elderly's gait, which indicates gait stability for the elderly. Second, the gait-assist wearable exoskeleton that provides stimulation to the upper limbs showed a symmetrical pattern in the phase diagram of the arm- and hip-swing angular displacements which indicates upper–lower–limbs' coordination for the elderly's gait

although no stimulations were applied to the lower limbs. Third, the gait-assist wearable exoskeleton that provides stimulation to the upper limbs statistically significantly increases the hip-swing amplitude and statistically significantly decreases the hip-swing period, although no stimulations were applied to the lower limbs.

4.3 Main Results

In a first main result, the result shows that interactive rhythmic stimulation to the upper and lower limbs significantly increases the hip-joint amplitude for the elderly's gait by 12.5% from the non-assist to assist conditions. However, although we did not provide any stimulation to the wearer's lower limbs, the results show that stimulation to the upper limbs statistically significantly increases the hip-swing amplitude by 7% at the upper-limb-assist condition at all lag times and statistically significantly decreases the hip swing period by 2.3% at the 40% lag time condition. Therefore, the results indicate that stimulation to the upper limbs could provide gait-assist support for the elderly, which might be mediated by an upper–lower–limbs' neural coupling in human locomotion. This is in contrary with all previous power-assist wearable exoskeletons, which aimed to provide support to the wearer's lower limbs through the application of a motor torque.

In a second main result, the results show that interactive rhythmic stimulation to the upper and lower limbs significantly increases in the *CV* of the shoulder- and hip-joint amplitude, but stimulation to the upper limbs does not show any statistically significant difference in the *CV* of the hip-swing amplitude and period between the free and upper-limb-assist conditions at all lag times. Therefore, the results indicate that interactive rhythmic stimulation to the upper limbs does not adversely affect the

elderly's gait stability as compared with stimulation to the upper and lower limbs. Further, the results indicate that stimulation to the upper limbs could provide gait stability for the elderly.

In a third main result, interactive rhythmic stimulation to the upper and lower limbs showed a symmetrical pattern in the upper–lower– limbs' coordination between the non-assist and assist condition for the elderly's gait. However, although no stimulations were applied to the upper limbs, it is interesting to note that stimulation to the upper limbs also showed a symmetrical pattern in the upper–lower–limbs' coordination between the free and upper-limb-assist condition at all lag times for the elderly's gait. Therefore, the results indicate that stimulation to the upper limbs does not adversely affect the elderly's upper–lower–limbs' coordination and could provide coordination to the upper and lower limbs for the elderly.

4.4 Power-assist Wearable Exoskeletons

Previous power-assist wearable exoskeletons aimed to provide a direct power-assist support to the wearer's lower limbs using the master-slave control principle (i.e., passive mode) without considering the global dynamics of upper–lower–limbs' coordination in human locomotion. On the other hand, the gait-assist wearable exoskeleton, WalkMate that provides interactive rhythmic stimulation to the upper limbs aimed to provide gait-assist support to the wearer's lower limbs using the mutual entrainment principle (i.e., active mode) in human-robot interaction as well as upper–lower–limbs' neural coupling in human locomotion. We hypothesize that the gait-assist wearable exoskeleton, WalkMate that provides interactive rhythmic stimulation to the upper limbs would encourage voluntary effort (i.e., active mode), thereby providing

support for the elderly's gait as compared with the master-slave control (i.e., passive mode) in most previous power-assist wearable exoskeletons.

CHAPTER 5. CONCLUSION

5.1 Conclusion

We have well developed a gait-assist wearable exoskeleton, WalkMate that provides interactive rhythmic stimulation to the upper limbs for the elderly's gait. The gait-assist wearable exoskeleton that provides stimulation to the upper limbs is a significant improvement over the wearable exoskeleton that provides stimulation to the upper and lower limbs. Although no stimulations were applied to the lower limbs, stimulation to the upper limbs statistically significantly increases the hip-swing amplitude at the upper-limb-assist condition at all lag times and statistically significantly decreases the hip-swing period at 40% lag time condition. In addition, although no stimulations were applied to the lower limbs, stimulation to the upper limbs showed a symmetrical pattern in the elderly's upper–lower–limbs' coordination, which indicates upper–lower–limbs' coordination for the elderly. Further, stimulation to the upper and lower limbs significantly increases the *CV* of the shoulder- and hip-joint amplitude for the elderly's gait but stimulation to the lower limbs does not statistically significantly increase the *CV* of the hip-swing amplitude and period, which indicates gait stability for the elderly. In summary, the gait-assist wearable exoskeleton that provides interactive rhythmic stimulation to the upper limbs at an optimal lag time condition could offer a promising neurorehabilitation strategy for the elderly's gait.

5.2 Future Work

We have five research plans for the future. First, we recruited male-only subjects for this study. Because there are gender differences in gait patterns due to a different

range of bodily mass and the position of the center of gravity, we plan to evaluate the effect of stimulation to the upper limbs on female subjects' gait. Second, we plan to conduct experiments on walking for longer periods including "wash-out" effects due to the effect of neuroplasticity. Third, we plan to investigate the effect of interactive rhythmic stimulation to the upper limbs on the upper–lower–limbs' coordination for the elderly's gait using continuous relative phase (CRP) difference of the upper- and lower-limbs' angular displacement (Van Emmerik and Wagenaar, 1996; Eke-Okoro et al., 1997; Wagenaar and Van Emmerik, 2000) and their respective *CV*. Fourth, we plan to investigate the effect of stimulation to the upper limbs on the left-right gait asymmetry for the elderly's gait (Nagano et al., 2013) by applying a variable torque to the left and right upper limbs. Finally, it has been reported that elderly adults with lower extremity dysfunction rely excessively on the passive action of the hip flexors to provide propulsion in the late stance to enhance stability (McGibbon and Krebs, 2004). Hence, we aim to extend our experiments to this group of elderly adults as well as patients with neurological disorders such as hemiplegia and Parkinson's disease.

CHAPTER 6. REFERENCES

1. Alan, T.A., Stefano, M.M.D.R., Ye, D., Conor, J.W. (2014). Stronger, smarter, softer: Next generation wearable robots. *IEEE Robot. Auto. Mag.* 21, 22–33.
2. Alexander, N.S., Jonathan, K., Edward, D.L. (2012). Design and evaluation of an orthotic knee-extension assist. *IEEE T. Neur. Sys. Reh.* 20, 678–687.
3. Angeloni, C., Riley, P.O., Krebs, D.E. (1994). Frequency content of whole body gait kinematic data. *IEEE Trans. Rehabil. Eng*. 2, 40–46.
4. Baldissera, F., Cavallari, P., Civaschi, P. (1982). Preferential coupling between voluntary movements of ipsilateral limbs. *Neurosci. Lett*. 34, 95–100.
5. Baldissera, F., Cavallari, P., Leocani, L. (1998). Cyclic modulation of the H-reflex in a wrist flexor during rhythmic flexion-extension movements of the ipsilateral foot. *Exp. Brain Res*. 118, 427–430.
6. Barbareschi, G., Richard, R., Thornton, M., Carlson, T. (2015). Statistically vs dynamically balanced gait: analysis of a robotic exoskeleton compared with a human. *Conf. Proc. Ann. Int. Conf. Med. Bio. Soc*. Milan, Italy, 6728–6731.
7. Bland, J.M., and Altman, D.G. (1995). Multiple significance tests: The Bonferroni method. *BMJ* 310, 170.
8. Bortole, M., Venkatakrishnan, A., Zhu, F., Moreno, J.C., Francisco, G.E., Pons, J.L., et al. (2015). The H2 robotic exoskeleton for gait rehabilitation after stroke: Early findings from a clinical study. *J. NeuroEng. Rehabil.* 12, 54.
9. Callisaya, M.L., Blizzard, L., Schmidt, M.D., McGinley, J.L., Srikanth, V.K. (2010). Ageing and gait variability-population-based study of older people. *Age and Ageing*. 39, 191–197.
10. Chen, B., Zhong, C., Zhao, X., Ma, H., Guan, X., Li, X., et al. (2017). A wearable

exoskeleton suit for motion assistance to paralyzed patients. *J. Ortho. Tran.* 11, 7–18.

11. Choi, H., Seo, K., Hyung, S., Shim, Y., and Lim, S. (2018). Compact hip-force sensor for a gait-assistance exoskeleton system. *Sensors*, 18, 566.
12. Cohen, A.H., Holmes, P.J., Rand, R.H. (1982). The nature of the coupling between segmental oscillators of the lamprey spinal generator for locomotion: a mathematical model. *J. Math. Bio*. 13, 345–369.
13. Cromwell, R.L., Newton, R.A., (2004). Relationship between balance and gait stability in healthy older adults. *J. Aging and Phys. Activ*. 11, 90–100.
14. Crosbie, J., Vachalathiti, R., Smith, R. (1997). Age, gender and speed effects on spinal kinematics during walking. *Gait and Posture*. 5, 13–20.
15. Deitz, V., Fouad, K., Bastiaanse, C.M. (2001). Neuronal coordination of arm and leg movements during human locomotion. *Eur. J. Neurosci*. 14, 1906–1914.
16. Delwaide, P.J., Figel, C., Richelle, C. (1977). Effects of postural changes of the upper limb on reflex transmission in the lower limb. Cervicolumbar reflex interactions in man. *J. Neurol. Neurosurg. Psychiatry*. 40, 616–621.
17. Deng, J., Wang, P., Li, M., Guo, W., Zha, F., and Wang, X. (2017). Structure design of active power-assist lower limb exoskeleton APAL robot. *Adv. Mech. Eng.* 9, 1–11. doi: 10.1177/1687814017735791.
18. DeVita, P., Hortobagyi, T. (2000). Age causes a redistribution of joint torques and powers during gait. *J. Appl. Physiol*. 88, 1804–1811.
19. Eke-Okoro, S.T., Gregoric, M., Larsson, L.E. (1997). Alterations in gait resulting from deliberate changes of arm-swing amplitude and phase. *Clin. Biomech*. *(Bristol, Avon)* 12, 516–521.
20. Esquenazi, A., Talaty, M., Packel, A., Saulino, M. (2012). The ReWalk powered

exoskeleton to restore ambulatory function to individuals with thoracic-level motor-complete spinal cord injury. *Am. J. Phys. Med. Rehabil.* 00, 1–11.

21. Frigon, A., Collins, D.F., Zehr, E.P. (2004). Effect of rhythmic arm movement on reflexes in the legs: Modulation of soleus H-reflexes and somatosensory conditioning. *J. Neurophysiol*. 91, 1516–1523.
22. Fujiyama, H., Garry, M.I., Levin, O., Swinnen, S.P., Summers, J.J. (2009). Age-related differences in inhibitory processes during interlimb coordination. *Brain Res*. 1262, 38– 47.
23. Graafmans, W.C., Ooms, M.E., Hofstee, M.A., Bezemer, P.D., Bouter, L.M., Lips, P. (1996). Falls in the elderly: a prospective study of risk factors and risk profiles. *Am. J. Epidemiol*. 143, 1129–1136.
24. Guadagnoli, M.A., Etnyre, B., Rodrigue, M.L. (2000). A test of a dual central pattern generator hypothesis for subcortical control of locomotion. *J. Electromyogr. Kinesiol*. 10, 241–247.
25. Haga, H., Shibata, H., Shichita, K., Matsuzaki, T., Hatano, S. (1986). Falls in the institutionalized elderly in Japan. *Arch. Gerontol. Geriat*. 5, 1–9.
26. Huang, J.H., Ferris, D.P. (2004). Neural coupling between upper and lower limbs during recumbent stepping. *J. Appl. Physiol*. 97, 1299–2004.
27. Huang, H.J., Ferris, D.P. (2009). Upper and lower limb muscle activation is bidirectionally and ipsilaterally coupled. *Med. Sci. Sports Exerc*. 41, 1778–1789.
28. Kang, H.G., Dingwell J.B. (2008). Effects of walking speed, strength and range of motion on gait stability in healthy older adults. *J. Biomech.* 41, 2899–2905.
29. Kannus, P., Palvanen, M., Niemi, S., Parkkari, S., Natri, A., Vuori, I., Jarvinen, M. (1999). Increasing number and incidence of fall-induced severe head injuries in older adults, nationwide statistics in Finland in 1970–1995 and prediction for the

future. *Am. J. Epidemiol*. 149, 143–150.

30. Kawamoto, H., Lee, S., Kanbe, S., Sankai, Y. (2003). Power assist method for HAL-3 using EMG-based feedback controller. *Conf. Proc. IEEE Int. Conf. Syst. Man. Cybern.* San Francisco, CA, USA, 1648–1653.
31. Kawashima, N., Nozaki, D., Abe, M.O., Nakazawa, K. (2008). Shaping appropriate locomotive motor output through interlimb neural pathway within spinal cord in humans. *J. Neurophysiol*. 99, 2946–2955.
32. Kim, S.H., Banala, S.K., Brackbill, E.A., Agrawal, S.K., Krishnamoorthy, V., Scholz, J.P. (2010). Robot-assisted modifications of gait in healthy individuals. *Exp. Brain Res*. 202, 809–824.
33. Krasovsky, T., Lamontagne, A., Feldman, A.G., Levin, M.F. (2014). Effects of walking speed on gait stability and interlimb coordination in younger and older adults. *Gait Posture*. 39, 378–385.
34. Kuramoto, Y. (1984). *Chemical oscillations, waves and turbulence*, Heidelberg: Springer-Verlag.
35. Laufer, Y. (2005). Effect of age on characteristics of forward and backward gait at preferred and accelerated walking speed. *J. Gerontol*. 60A, 627–632.
36. Lerner, Z.F., Damiano, D.L., and Bulea, T.C. (2017). The effects of exoskeleton assisted knee extension on lower-extremity gait kinematics, kinetics, and muscle activity in children with cerebral palsy. *Sci. Rep.* 7, 13512.
37. Long, J.T., Groner, J.B., Eastwood, D.C., Dillingham, T.R., Grover, P., Harris, G.F. (2011). Implications of arm restraint on lower extremity kinetics during gait. *J. Exp. Clin. Med*. 3, 200–206.
38. Marks, R. (1997). The effects of restricted arm swing during normal locomotion. *Biomed. Sci. Instrum*. 33, 209–215.

39. McGibbon, C.A., Krebs, D.E. (2004). Discriminating age and disability effects in locomotion: neuromuscular adaptations in musculoskeletal pathology. *J. Appl Physiol*. 96, 149–160.

40. Mirelman, A., Bemad-Elazeri, H., Nobel, T., Thaler, A., Peruzzi, A., Plotnik, M., Giladi, N., Haudorff, J.M. (2015). Effects of aging on arm swing during gait: the role of gait speed and dual tasking. *PLoS One*. 10, 1–11.

41. Miyake, Y. (2009). Interpersonal synchronization of body motion and the Walk-Mate walking support robot. *IEEE Trans. Robot*. 25, 638–644.

42. Nagano, H., Begg, R.K., Sparrow, W.A., Taylor, S. (2013). A comparison of treadmill and overground walking effects on step cycle asymmetry in young and older individuals. *J. Appl. Biomech*. 29, 188–193.

43. Nigg, B.M., Fisher, V., Ronsky, J.L. (1994). Gait characteristics as a function of age and gender. *Gait Posture*. 2, 213–220.

44. Ostrosky, K.M., VanSwearingen, J.M., Burdett, R.G., Gee, Z. (1994). A comparison of gait characteristics in young and old subjects. *Phys. Ther*. 74, 637–644.

45. Riener, R., Lunenburger, L., Jezernik, S., Anderschitz, M., Colombo, G., Dietz, V. (2005). Patient-cooperative strategies for robot-aided treadmill training: first experimental results. *IEEE T. Neur. Sys. Reh*. 13, 380–394.

46. Rubenstein, L.Z., Josephson, K.R. (2002). The epidemiology of falls and syncope. *Clin. Geriatr. Med*. 18, 141–158.

47. Salzman, B. (2010). Gait and balance disorders in older adults. *Am. Fam. Physician*, 82, 61–68.

48. Serrien, D.J., Swinnen, S.P., Stelmach, G.E. (2000). Age-relayed deterioration of coordinated interlimb behavior. *J. Gerontology*. 55, 295–303.

49. Shinkai, S., Kumagai, S., Fujiwara, Y., Amano, H., Yoshida, Y., Watanabe, S., et al.

(2003). Predictors for the onset of functional decline among initially non-disabled older people living in a community during a 6-year follow-up. *Geriatr. Gerontol. Int*. 3, 31–39.

50. Strausser, K.A., Kazerooni, H. (2011). The development and testing of a human machine interface for a mobile medical exoskeleton. *Conf. Proc. IEEE Int. Conf. Int. Robot. Sys*. San Francisco, CA, USA, 4911–4916.
51. Taga, G., Yamaguchi, Y., Shimizu, H. (1991). Self-organized control of bipedal locomotion by neutral oscillators in unpredictable environment. *Biol. Cybern*. 65, 147–159.
52. Van Emmerik, R.E.A., Wagenaar, R.C. (1996). Effects of walking velocity on relative phase dynamics in the trunk in human walking. *J. Biomech*. 29, 1175–1184.
53. Veneman, J.F., Kruidhof, R., Hekman, E.E.G., Ekkelenkamp, R., Van Asseldonk, E.H.F., Van der Kooij, H. (2007). Design and evaluation of the LOPES exoskeleton robot for interactive gait rehabilitation. *IEEE T. Neur. Sys. Reh*.15, 379–386.
54. Wagenaar, R.C., Van Emmerik, R.E.A. (2000). Resonant frequencies of arms and legs identify different walking patterns. *J. Biomech*. 33, 853–861.
55. Winter, D.A., Patia, A.E., Frank, J.S., Walt, S.E. (1990). Biomechanical walking pattern changes in the fit and healthy elderly. *Phys. Ther*. 70, 340–347.
56. Winter, D.A., Sidwall, H.G., Hobson, D.A. (1974). Measurement and reduction of noise in kinematics of locomotion. *J. Biomech*. 2, 40–46.
57. World Population Data Sheet. Available from: https://www.prb.org/wp-content/uploads/2018/08/2018_WPDS.pdf. Accessed 2019.
58. Long, Y., Du, Z.J., Wang, W.D., Dong, W. (2016). Development of a wearable exoskeleton rehabilitation system based on hybrid control mode. *Int. J. Adv. Robot. Sys.* 13, 1–10.

59. Long, Y., Du, Z.J., Chen, C.F., Wang, W.D., Dong, W. (2017). Development of a lower extremity wearable exoskeleton with double compact elastic module: preliminary experiments. *Mech. Sci.* 8, 249–258.

60. Yuasa, H., Ito, M. (1990). Coordination of many oscillators and generation of locomotory patterns. *Biol. Cybern*. 63, 177–184.

61. Zehr, E. P., Collins, D. F., and Chua, R. (2001). Human interlimb reflexes evoked by electrical stimulation of cutaneous nerves innervating the hand and foot. *Exp. Brain Res.* 140, 495–504.

62. Zehr, E. P., and Duysens, J. (2004). Regulation of arm and leg movement during human locomotion. *Neuroscientist*. 10, 347–361.

63. Zehr, E. P., and Haridas, C. (2003). Modulation of cutaneous reflexes in arm muscles during walking: further evidence of similar control mechanisms for rhythmic human arm and leg movements. *Exp. Brain Res*. 149, 260–266.

CHAPTER 7. APPENDIX

7.1 Preliminary Investigation of Phase Difference Between Foot Contact Timing and Upper Limbs

To determine the phase difference between the upper-limb arm-swing and the foot contact timing, we conducted a preliminary experimental investigation with 6 healthy young subjects (4 males and 2 females). Table 4 shows the mean age, height and weight of the subjects. The mean age of the male and female subjects are 24.3 ± 1.7 years and 27.0 ± 2.8 years, respectively. The mean weight of the male and female subjects are 73.0 ± 7.3 kg and 46.0 ± 1.4 kg, respectively. The mean height of the male and female subjects are 170.8 ± 7.8 cm and 155.5 ± 3.5 cm, respectively.

Table 4: Experimental subjects for preliminary investigation of phase difference between foot contact timing and upper limbs. Mean age, height and weight of the subjects (mean ± SD).

Subjects	*n*	Age (years)	Height (cm)	Weight (kg)
Male	4	24.3 ± 1.7	73.0 ± 7.3	170.8 ± 7.8
Female	2	27.0 ± 2.8	46.0 ± 1.4	155.5 ± 3.5

The experimental procedure comprises six steps. First, each subject practiced walking on a treadmill (SportsArt Fitness, T650MES, Japan) for about 1 min. Second, after each participant had confirmed their comfortable walking speed, six reflective markers were placed at the right shoulder, elbow, wrist, hip, knee and ankle of each subject. Third, each subject walked at a natural walking speed on a treadmill for about 10s and kinematics data was captured using a motion capture system (Nobby Tech, VENUS 3D, Japan). Fourth, we analyzed the right shoulder joint angular displacement using the angle between three reflective markers at the shoulder, elbow and hip. Fifth,

we analyzed the right ankle position using the marker placed on the ankle to determine the right foot contact timing. Sixth, we compared the right foot contact timing and the right shoulder joint angular displacement to determine the mean phase (i.e., timing) difference between the foot contact timing, forward arm-swing, and backward arm-swing with all subjects.

Table 5 shows the results of the phase (i.e., timing) difference between the right foot contact timing, forward arm-swing and backward arm-swing. Fig 26 shows the time-series plot of the right shoulder-joint angular displacement and the vertical displacement of the right ankle for four complete gait cycles. The left and right vertical axes show the right ankle vertical displacement and right shoulder-joint angular displacement, respectively. The right shoulder-joint angular displacement was measured with respect to the frontal plane of the subject at 0º. The right ankle vertical displacement was measured with respect to the height of the treadmill 0.32 m above the ground.

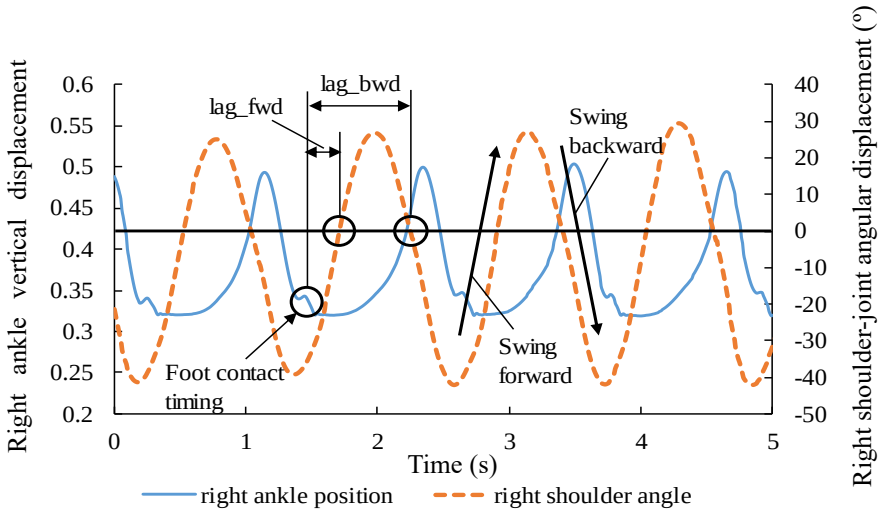

Fig 26. Lag time analysis of right foot contact timing and right shoulder-joint angular displacement. Here, lag_fwd and lag_bwd represent the lag time for the forward and backward arm-swing, respectively. The graph shows a forward and backward lag times between 15% to 20%, and 60% to 70% of one complete one-swing cycle between the right shoulder-joint angular displacement and the right ankle vertical displacement, respectively.

The result showed a lag time between 15% to 20% (mean = 17.6 ± 2.7%) between the right foot contact timing and the forward arm-swing phase of one complete gait cycle. The result also showed a lag time between 60% to 70% (mean = 66.5 ± 3.3%) between the right foot contact timing and the backward arm-swing phase of one complete gait cycle. Therefore, we implemented an output motor torque onset timing of 15% lag time between the left foot contact timing and the left upper-limb motor in the motor-torque output module.

Table 5: Result analysis of phase difference between foot contact timing and upper limb. Mean value and standard deviation (*SD*) of lag time between right foot contact timing, and rest position of right forward and backward arm-swing phases for one complete gait cycle expressed as a percentage.

Subject	Forward lag time (%)	Backward lag time (%)
1	19.9	67.6
2	15.1	65.6
3	17.2	70.2
4	21.5	63.6
5	14.4	62.3
6	17.7	69.4
Mean (±SD)	17.6 (±2.7)	66.5 (±3.3)

7.2 Gait Analysis of Gait-assist Wearable Exoskeleton to the Upper Limbs

A simple numerical integration of the hip-swing angular velocity time-series data in the sagittal plane using trapezoidal rule to obtain the hip-swing angular displacement can be represented as:

$$\theta_z = \int_0^t \omega_z dt \tag{1}$$

Here, θ_z is the hip-swing angular displacement in the sagittal plane, t is the time interval for one complete hip-swing cycle, and ω_z is the hip-swing angular velocity in the sagittal plane.

A small recursive filter to θ_z to correct for accumulation drift error due to numerical integration can be represented as:

$$\theta_z^{'}(n) = \theta_z(n) - \theta_z(n-1) + K\theta_z(n-1) \tag{2}$$

Here, $\theta_z^{'}(n)$ is the corrected hip-swing angular displacement in the sagittal plane, n is the length of the hip-swing time-series data and K is 0.995.

The mean left or right hip-swing amplitude was calculated by taking the mean of the peak-to-peak amplitude of the left or right hip-swing angular displacement time-series data, which can be represented as:

$$\bar{\theta} = \frac{1}{l}\sum_{n=1}^{l}\left[\theta_p(n) - \theta_t(n)\right] \tag{3}$$

Here, $\overline{\theta_h}$ is the mean left or right hip-swing amplitude, θ_p and θ_t is the left or right hip-swing angular displacement at each peak and trough, respectively, and l is the number of complete gait cycles excluding the first and last five complete gait cycles. The gait

analysis for the mean left or right arm-swing amplitude is similar to that for the hip-swing amplitude.

The mean left or right hip-swing period was calculated by taking the mean of the time difference between two consecutive peaks and troughs of the left or right hip-swing angular displacement time-series data, which can be represented as:

$$\overline{T_h} = \frac{1}{2l}\sum_{n=1}^{l}[(t_p(n+1)-t_p(n))+(t_t(n+1)-t_t(n))] \quad (4)$$

Here, $\overline{T_h}$ is the mean left or right hip-swing period, t_p and t_t is the corresponding time of each peak and trough of the left or right hip-swing angular displacement, and l is the number of complete gait cycles excluding the first and last five complete gait cycles. The gait analysis for the mean left or right arm-swing period is similar to that for the hip-swing period.

The mean coefficient of variance of the left or right hip-swing amplitude was calculated by taking the mean of the ratio of the standard deviation and mean of each complete trial for three complete trials which can be represented as:

$$\overline{CV}_h = \frac{1}{3}\sum_{n=1}^{3}\left(\frac{\sigma}{\mu}\right) \quad (5)$$

Here, $\overline{CV}_h$ is the mean coefficient of variance of the left or right hip-swing amplitude, σ is the standard deviation of the left or right hip-swing amplitude for each complete trial, and μ is the mean of the left or right hip-swing amplitude for each complete trial. The gait analysis for the mean coefficient of variance of the left or right arm- and hip-swing period, and left or right arm-swing amplitude is similar to that for the hip-swing amplitude.

7.3 Numerical Data for Fig 20

Table 6: Results for analysis of mean hip-swing amplitude for the free and upper-limb-assist conditions at different lag time in degree.

	Subjects	Hip-swing amplitude (°)					
		Free	0% lag time	10% lag time	20% lag time	30% lag time	40% lag time
1	Subject 1	44.40	48.68	48.23	48.47	48.48	48.30
2	Subject 2	42.39	43.58	43.73	44.12	43.84	43.39
3	Subject 3	41.63	45.12	45.24	45.34	45.18	45.05
4	Subject 4	37.50	39.83	39.67	40.01	39.79	39.77
5	Subject 5	39.59	42.04	41.88	42.01	42.09	41.35
6	Subject 6	30.65	31.89	32.10	32.38	32.57	32.67
7	Subject 7	32.87	35.84	35.88	36.12	36.01	36.29
8	Subject 8	31.11	34.59	34.53	34.45	34.83	34.46
9	Subject 9	42.72	43.68	43.60	43.92	43.26	43.74
10	Subject 10	44.44	47.30	47.48	47.42	47.42	47.64
11	Subject 11	45.44	47.34	47.31	46.66	47.07	46.75
12	Subject 12	34.01	39.62	39.89	39.71	39.76	39.83
	Mean	38.90	41.62	41.63	41.72	41.69	41.60
	SD	5.24	5.16	5.10	5.04	4.98	4.94

7.4 Numerical Data for Fig 21

Table 7: Results for analysis of mean hip-swing period for the free and upper-limb-assist conditions at different lag time in ms.

	Subjects	Hip-swing period (ms)					
		Free	0% lag time	10% lag time	20% lag time	30% lag time	40% lag time
1	Subject 1	972.0	952.2	930.8	916.2	918.6	930.2
2	Subject 2	937.5	928.9	933.4	931.4	925.0	922.6
3	Subject 3	1048.9	1049.0	1048.2	1050.1	1044.9	1038.3
4	Subject 4	894.9	903.1	900.4	902.1	904.4	899.3
5	Subject 5	993.1	952.3	947.8	954.5	954.2	959.6
6	Subject 6	1003.9	991.2	984.0	991.0	986.8	980.3
7	Subject 7	940.1	934.0	938.3	929.9	933.6	933.6
8	Subject 8	1075.6	1052.5	1048.6	1040.8	1033.9	1048.2
9	Subject 9	1097.1	1114.2	1106.9	1104.6	1110.3	1109.0
10	Subject 10	1071.1	1050.9	1055.2	1052.3	1047.2	1050.9
11	Subject 11	1012.6	976.8	981.2	973.7	962.4	972.2
12	Subject 12	959.3	882.9	886.3	888.9	877.9	881.1
	Mean	1000.5	982.3	980.1	978.0	974.9	977.1
	SD	60.4	67.5	66.8	66.7	67.3	67.3

7.5 Numerical Data for Fig 22

Table 8: Results for analysis of mean *CV* of hip-swing amplitude for the free and upper-limb-assist conditions at different lag time.

	Subjects	*CV* of hip-swing amplitude					
		Free	0% lag time	10% lag time	20% lag time	30% lag time	40% lag time
1	Subject 1	0.0246	0.0197	0.0214	0.0192	0.0250	0.0200
2	Subject 2	0.0244	0.0296	0.0268	0.0263	0.0229	0.0264
3	Subject 3	0.0244	0.0194	0.0211	0.0217	0.0177	0.0224
4	Subject 4	0.0290	0.0258	0.0291	0.0244	0.0219	0.0224
5	Subject 5	0.0284	0.0240	0.0278	0.0294	0.0223	0.0263
6	Subject 6	0.0254	0.0242	0.0267	0.0255	0.0208	0.0236
7	Subject 7	0.0217	0.0227	0.0198	0.0205	0.0211	0.0212
8	Subject 8	0.0305	0.0209	0.0231	0.0217	0.0250	0.0236
9	Subject 9	0.0206	0.0186	0.0166	0.0203	0.0168	0.0192
10	Subject 10	0.0214	0.0233	0.0258	0.0224	0.0265	0.0255
11	Subject 11	0.0196	0.0173	0.0174	0.0176	0.0206	0.0157
12	Subject 12	0.0290	0.0287	0.0247	0.0269	0.0268	0.0242
	Mean	0.0249	0.0228	0.0234	0.0230	0.0223	0.0225
	SD	0.0035	0.0037	0.0040	0.0034	0.0030	0.0030

7.6 Numerical Data for Fig 23

Table 9: Results for analysis of mean *CV* of hip-swing period for the free and upper-limb-assist conditions at different lag time.

	Subjects	*CV* of hip-swing period					
		Free	0% lag time	10% lag time	20% lag time	30% lag time	40% lag time
1	Subject 1	0.0246	0.0340	0.0355	0.0322	0.0364	0.0327
2	Subject 2	0.0161	0.0215	0.0248	0.0241	0.0259	0.0249
3	Subject 3	0.0129	0.0113	0.0126	0.0148	0.0118	0.0154
4	Subject 4	0.0185	0.0205	0.0267	0.0223	0.0265	0.0248
5	Subject 5	0.0205	0.0197	0.0285	0.0212	0.0166	0.0233
6	Subject 6	0.0189	0.0186	0.0180	0.0118	0.0152	0.0180
7	Subject 7	0.0177	0.0157	0.0132	0.0144	0.0113	0.0147
8	Subject 8	0.0215	0.0088	0.0160	0.0127	0.0149	0.0123
9	Subject 9	0.0179	0.0233	0.0183	0.0304	0.0177	0.0136
10	Subject 10	0.0388	0.0501	0.0510	0.0427	0.0510	0.0440
11	Subject 11	0.0145	0.0140	0.0140	0.0165	0.0157	0.0138
12	Subject 12	0.0432	0.0253	0.0297	0.0329	0.0258	0.0288
	Mean	0.0221	0.0219	0.0240	0.0230	0.0224	0.0222
	SD	0.0090	0.0106	0.0108	0.0093	0.0112	0.0092

7.7 Numerical Data for Gait Speed

Table 10: Results for analysis of average gait speed for the free and upper-limb-assist conditions at different lag time in m/s.

	Subjects	Average Speed (m/s)					
		Free	0% lag time	10% lag time	20% lag time	30% lag time	40% lag time
1	Subject 1	1.46	1.49	1.52	1.53	1.53	1.52
2	Subject 2	1.61	1.61	1.61	1.60	1.63	1.61
3	Subject 3	1.31	1.35	1.35	1.34	1.35	1.35
4	Subject 4	1.41	1.42	1.41	1.42	1.42	1.43
5	Subject 5	1.59	1.71	1.66	1.66	1.69	1.65
6	Subject 6	1.12	1.11	1.12	1.12	1.13	1.12
7	Subject 7	1.30	1.32	1.31	1.33	1.31	1.31
8	Subject 8	1.10	1.12	1.14	1.13	1.15	1.12
9	Subject 9	1.31	1.30	1.31	1.30	1.27	1.29
10	Subject 10	1.44	1.46	1.47	1.46	1.48	1.45
11	Subject 11	1.47	1.52	1.51	1.52	1.50	1.51
12	Subject 12	1.43	1.58	1.59	1.59	1.59	1.60
	Mean	1.38	1.42	1.42	1.42	1.42	1.41
	SD	0.15	0.18	0.17	0.17	0.18	0.17

7.8 Statistical Analysis of Mean Arm-swing Amplitude, Mean Arm-swing Period and their Corresponding *CV*s

Table 11. Mean and *p* values of the mean arm-swing amplitude, mean arm-swing period and *CV* of arm-swing amplitude for each experiment condition (*: $p < 0.05$; **: $p < 0.01$)

Parameter	Condition	Mean (±SD)	*p*-value
Arm-swing amplitude (º)	Free	34.88 (± 10.64)	-
	0% lag time	42.43 (± 8.20)	0.10500
	10% lag time	42.67 (± 7.57)	0.08055
	20% lag time	40.99 (± 6.85)	0.13430
	30% lag time	39.40 (± 7.25)	1.00000
	40% lag time	39.81 (± 5.02)	1.00000
Arm-swing period (ms)	Free	1000.5 (± 60.4)	-
	0% lag time	982.3 (± 67.5)	0.212400
	10% lag time	980.1 (± 66.8)	0.080500
	20% lag time	978.0 (± 66.7)	0.061050
	30% lag time	974.9 (± 67.3)	0.061050
	40% lag time	977.1 (± 67.3)	0.024415*
CV of arm-swing amplitude	Free	0.0987 (± 0.0413)	-
	0% lag time	0.1224 (± 0.0311)	0.10255
	10% lag time	0.1139 (± 0.0276)	1.00000
	20% lag time	0.1221 (± 0.0360)	0.35155
	30% lag time	0.1252 (± 0.0390)	0.06105
	40% lag time	0.1068 (± 0.0328)	1.00000

Table 11 gives the mean arm-swing amplitude, mean arm-swing period, *CV* of arm-swing amplitude for each experimental condition, and their corresponding *p*-value for the upper-limb-assist conditions with respect to the free condition. A Friedman test revealed a significant effect of upper-limb conditions on the arm-swing amplitude ($A^2(5)$

= 13.286, p = 0.02084). A post hoc test using Wilcoxon signed-rank test with Bonferroni correction showed no statistically significant difference between the free condition and each of the upper-limb-assist conditions with respect to the mean arm-swing amplitude under all conditions (p = 0.10500, 0.08055, 0.13430, 1.00000 and 1.00000, respectively).

In addition, a Friedman test revealed a significant effect of upper-limb conditions on the arm-swing period ($A^2(5)$ = 15.085, p = 0.01). A post hoc test using Wilcoxon signed-rank test with Bonferroni correction showed a statistically significant difference between the free condition and the upper-limb-assist condition with a 40% lag time (p = 0.024415). However, no statistically significant differences were observed for other upper-limb-assist conditions (p = 0.212400, 0.080500, 0.061050, and 0.061050, respectively).

In addition, a Friedman test revealed a significant effect of upper-limb conditions on the *CV* of arm-swing amplitude ($A^2(5)$ = 12.19, p = 0.03227). A post hoc test using Wilcoxon signed-rank test with Bonferroni correction showed no statistically significant difference between the free condition and each of the upper-limb-assist conditions with respect to the *CV* of arm-swing amplitude under all conditions (p = 0.10255, 1.00000, 0.35155, 0.06105 and 1.00000, respectively).

Further, a Friedman test revealed no significant effect of the upper-limb conditions on the *CV* of arm-swing period ($A^2(5)$ = 6.2892, p = 0.2791).

7.9 Numerical data for Fig 27

Table 12: Results for analysis of mean arm-swing amplitude for the free and upper-limb-assist conditions at different lag time in degree.

	Subjects	Arm-swing amplitude (deg)					
		Free	0% lag time	10% lag time	20% lag time	30% lag time	40% lag time
1	Subject 1	18.29	57.94	48.55	48.08	47.66	50.28
2	Subject 2	35.63	35.92	38.75	36.20	34.10	37.72
3	Subject 3	25.72	32.85	35.82	34.28	32.28	36.58
4	Subject 4	25.97	30.83	28.71	29.77	30.58	35.14
5	Subject 5	45.26	43.06	41.16	38.51	38.65	41.75
6	Subject 6	51.89	47.60	50.87	53.23	51.27	38.80
7	Subject 7	34.85	46.29	48.37	42.73	40.07	35.42
8	Subject 8	47.17	51.55	53.42	50.31	52.43	44.83
9	Subject 9	20.20	35.84	35.30	35.81	33.33	37.19
10	Subject 10	47.05	46.89	45.44	43.92	39.92	46.35
11	Subject 11	34.20	47.28	50.45	43.56	40.56	41.30
12	Subject 12	32.31	33.12	35.17	35.42	31.90	32.36
	Mean	34.88	42.43	42.67	40.99	39.40	39.81
	SD	10.64	8.20	7.57	6.85	7.25	5.02

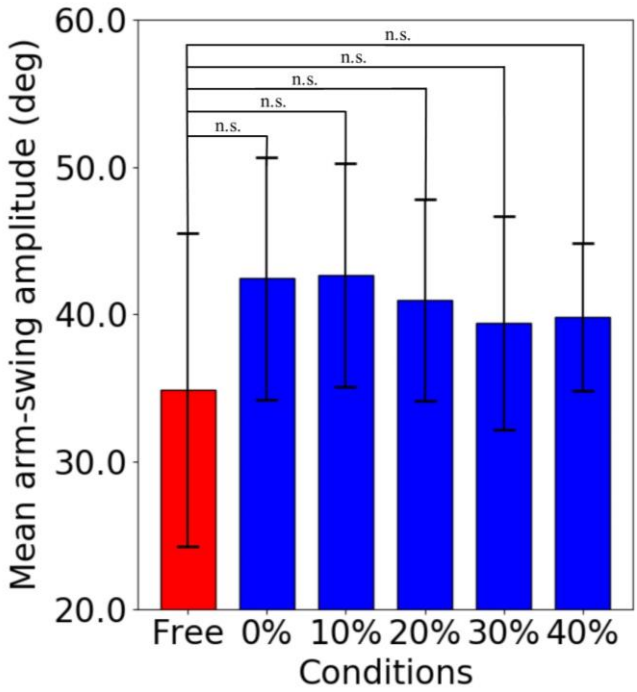

Fig 27. Statistical analysis of mean arm-swing amplitude. The mean arm-swing amplitude for the free condition and each of the upper-limb-assist conditions for the elderly subjects at 0, 10, 20, 30, and 40% lag time. (n.s.: non-significant).

Fig 27 shows the results of the statistical analysis of the mean arm-swing amplitude for the healthy elderly subjects. The results showed that there is no statistically significant difference in the mean arm-swing amplitude between the “free” and upper-limb-assist condition at all lag time. Hence, the results indicate that interactive rhythmic stimulation to the upper limbs does not statistically significantly increase the arm-swing amplitude for the elderly’s gait.

7.10 Numerical data for Fig 28

Table 13: Results for analysis of mean arm-swing period for the free and upper-limb-assist conditions at different lag time in ms.

	Subjects	Arm-swing period (ms)					
		Free	0% lag time	10% lag time	20% lag time	30% lag time	40% lag time
1	Subject 1	964	967	932	915	920	936
2	Subject 2	938	929	934	933	926	923
3	Subject 3	1049	1048	1048	1050	1045	1039
4	Subject 4	895	903	902	902	905	899
5	Subject 5	993	952	950	955	953	960
6	Subject 6	1004	990	984	991	988	981
7	Subject 7	940	934	939	930	934	934
8	Subject 8	1076	1053	1049	1042	1035	1049
9	Subject 9	1097	1114	1107	1105	1110	1110
10	Subject 10	1072	1051	1053	1052	1046	1051
11	Subject 11	1012	977	981	973	964	972
12	Subject 12	960	883	886	889	879	882
	Mean	1000	983	980	978	975	978
	SD	61	67	66	67	67	67

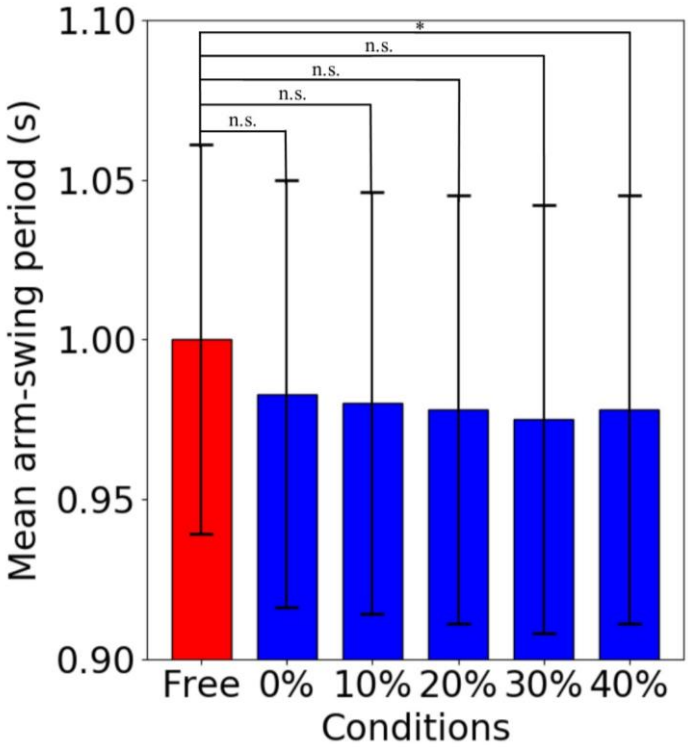

Fig 28. Statistical analysis of mean arm-swing period. The mean arm-swing period for the free condition and each of the upper-limb-assist conditions for the elderly subjects at 0, 10, 20, 30, and 40% lag time. (*: $p < 0.05$, n.s.: non-significant).

Fig 28 shows the results of the statistical analysis of the mean arm-swing period for the healthy elderly subjects. The results showed a statistically significant difference between the free condition and the upper-limb-assist condition with a 40% lag time ($p = 0.02415$), where the mean arm-swing period decreased on average by 23 ms. However, no statistically significant differences were observed for other upper-limb-assist conditions ($p = 0.2124$, 0.0805, 0.06105, and 0.06105, respectively).

7.11 Numerical data for Fig 29

Table 14: Results for analysis of mean *CV* of arm-swing amplitude for the free and upper-limb-assist conditions at different lag time.

	Subjects	*CV* of arm-swing amplitude					
		Free	0% lag time	10% lag time	20% lag time	30% lag time	40% lag time
1	Subject 1	0.1916	0.1636	0.1354	0.1639	0.1666	0.0992
2	Subject 2	0.0802	0.1317	0.1182	0.1272	0.0924	0.1035
3	Subject 3	0.0946	0.1369	0.1325	0.1390	0.1421	0.1328
4	Subject 4	0.0937	0.1345	0.1708	0.1718	0.1686	0.1268
5	Subject 5	0.0754	0.1082	0.1298	0.1310	0.1280	0.1404
6	Subject 6	0.0579	0.1253	0.0844	0.0583	0.0555	0.0425
7	Subject 7	0.0699	0.0868	0.0730	0.0940	0.1188	0.1105
8	Subject 8	0.0615	0.0666	0.0811	0.0794	0.0689	0.0607
9	Subject 9	0.1643	0.1560	0.1094	0.1337	0.1750	0.1475
10	Subject 10	0.0730	0.1151	0.1201	0.1343	0.1342	0.0831
11	Subject 11	0.0812	0.0794	0.0833	0.0719	0.0897	0.0858
12	Subject 12	0.1412	0.1651	0.1290	0.1604	0.1623	0.1483
	Mean	0.0987	0.1224	0.1139	0.1221	0.1252	0.1068
	SD	0.0413	0.0311	0.0276	0.0360	0.0390	0.0328

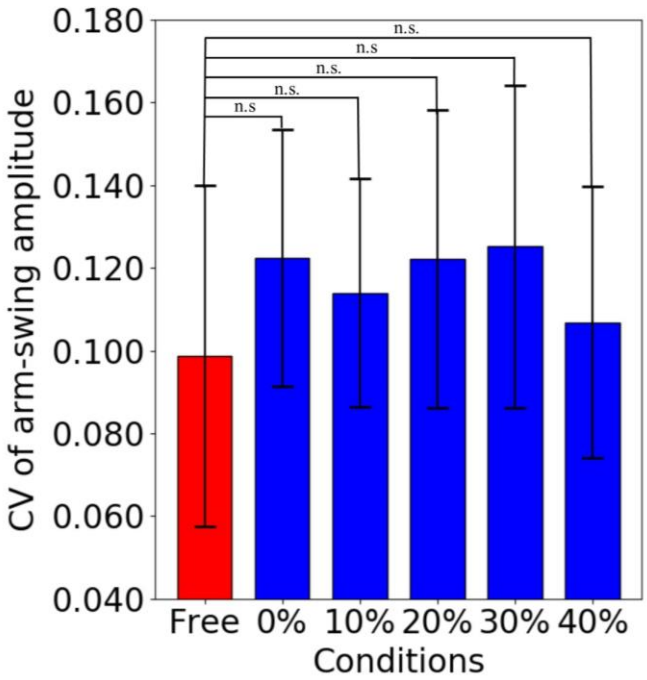

Fig 29. Statistical analysis of *CV* of arm-swing amplitude. The *CV* of arm-swing amplitude for the free condition and each of the upper-limb-assist conditions for the elderly subjects at 0, 10, 20, 30, and 40% lag time. (n.s.: non-significant).

Fig 29 shows the results of the statistical analysis of the *CV* of the arm-swing amplitude for the healthy elderly subjects. The results showed that there is no statistically significant difference in the *CV* of the arm-swing amplitude between the "free" and upper-limb-assist condition at all lag time. Hence, the results indicate that interactive rhythmic stimulation to the upper limbs does not cause any gait instability for the elderly's gait and is comparable with the "free" condition (i.e., stable condition).

7.12 Numerical data for Fig 30

Table 15: Results for analysis of mean *CV* of arm-swing period for the free and upper-limb-assist conditions at different lag time.

	Subjects	*CV* of arm-swing period					
		Free	0% lag time	10% lag time	20% lag time	30% lag time	40% lag time
1	Subject 1	0.0294	0.0268	0.0187	0.0224	0.0219	0.0199
2	Subject 2	0.0153	0.0184	0.0135	0.0148	0.0201	0.0158
3	Subject 3	0.0219	0.0245	0.0257	0.0256	0.0270	0.0288
4	Subject 4	0.0146	0.0180	0.0185	0.0191	0.0180	0.0146
5	Subject 5	0.0150	0.0157	0.0199	0.0218	0.0139	0.0205
6	Subject 6	0.0154	0.0270	0.0158	0.0114	0.0156	0.0187
7	Subject 7	0.0169	0.0157	0.0143	0.0142	0.0155	0.0153
8	Subject 8	0.0138	0.0149	0.0169	0.0165	0.0170	0.0170
9	Subject 9	0.0190	0.0188	0.0143	0.0197	0.0233	0.0206
10	Subject 10	0.0151	0.0153	0.0168	0.0204	0.0210	0.0163
11	Subject 11	0.0158	0.0114	0.0106	0.0127	0.0142	0.0127
12	Subject 12	0.0188	0.0201	0.0215	0.0204	0.0204	0.0254
	Mean	0.0176	0.0189	0.0172	0.0183	0.0190	0.0188
	SD	0.0042	0.0047	0.0039	0.0041	0.0038	0.0044

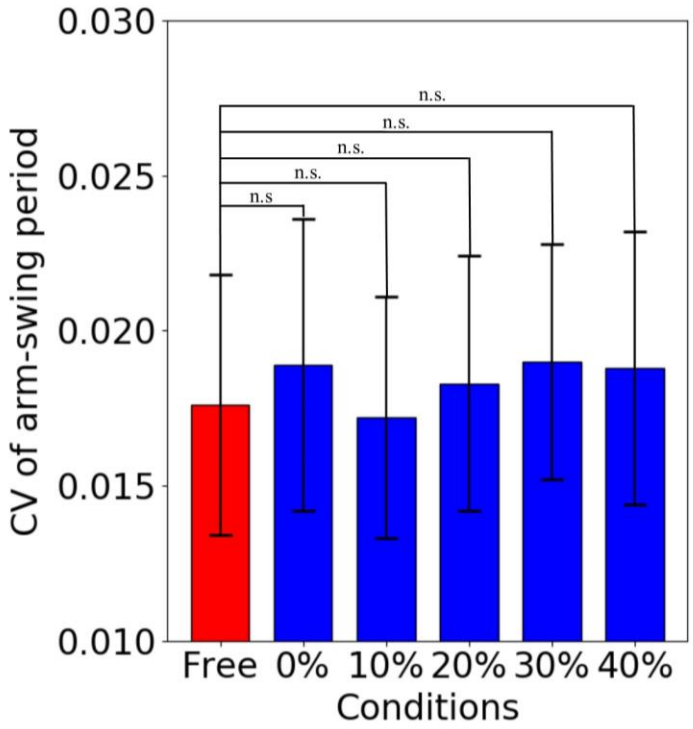

Fig 30. Statistical analysis of *CV* of arm-swing period. The *CV* of arm-swing period for the free condition and each of the upper-limb-assist conditions for the elderly subjects at 0, 10, 20, 30, and 40% lag time. (n.s.: non-significant).

Fig 30 shows the results of the statistical analysis of the *CV* of the arm-swing period for the healthy elderly subjects. The results showed that there is no statistically significant difference in the *CV* of the arm-swing period between the "free" and upper-limb-assist condition at all lag time. Hence, the results indicate that interactive rhythmic stimulation to the upper limbs does not cause any gait instability for the elderly's gait and is comparable with the "free" condition (i.e., stable condition).

7.13 Phase diagram for stimulation to upper limbs

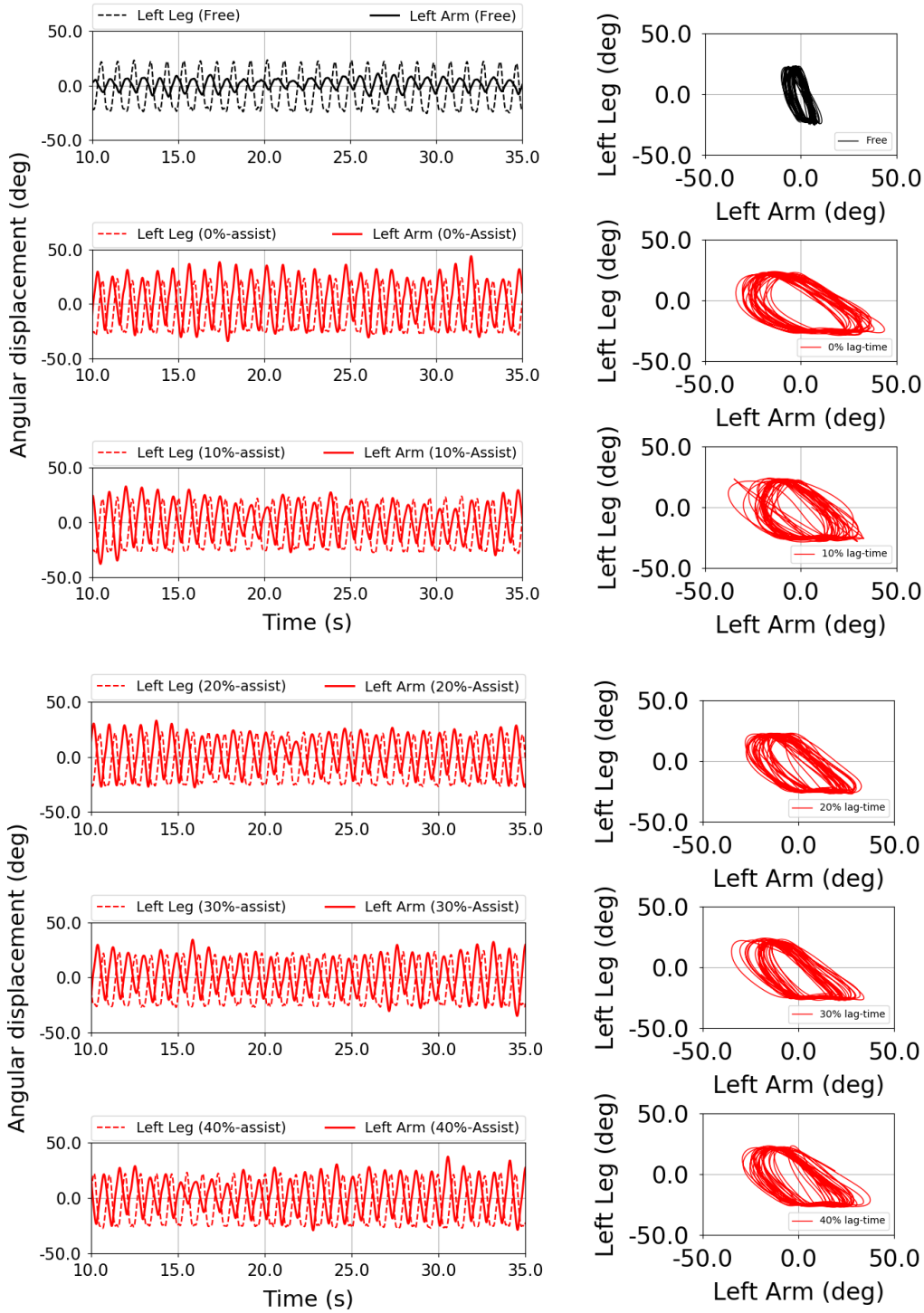

Fig 31. Phase diagram of the left arm- and hip-swing angular displacement for subject 1.

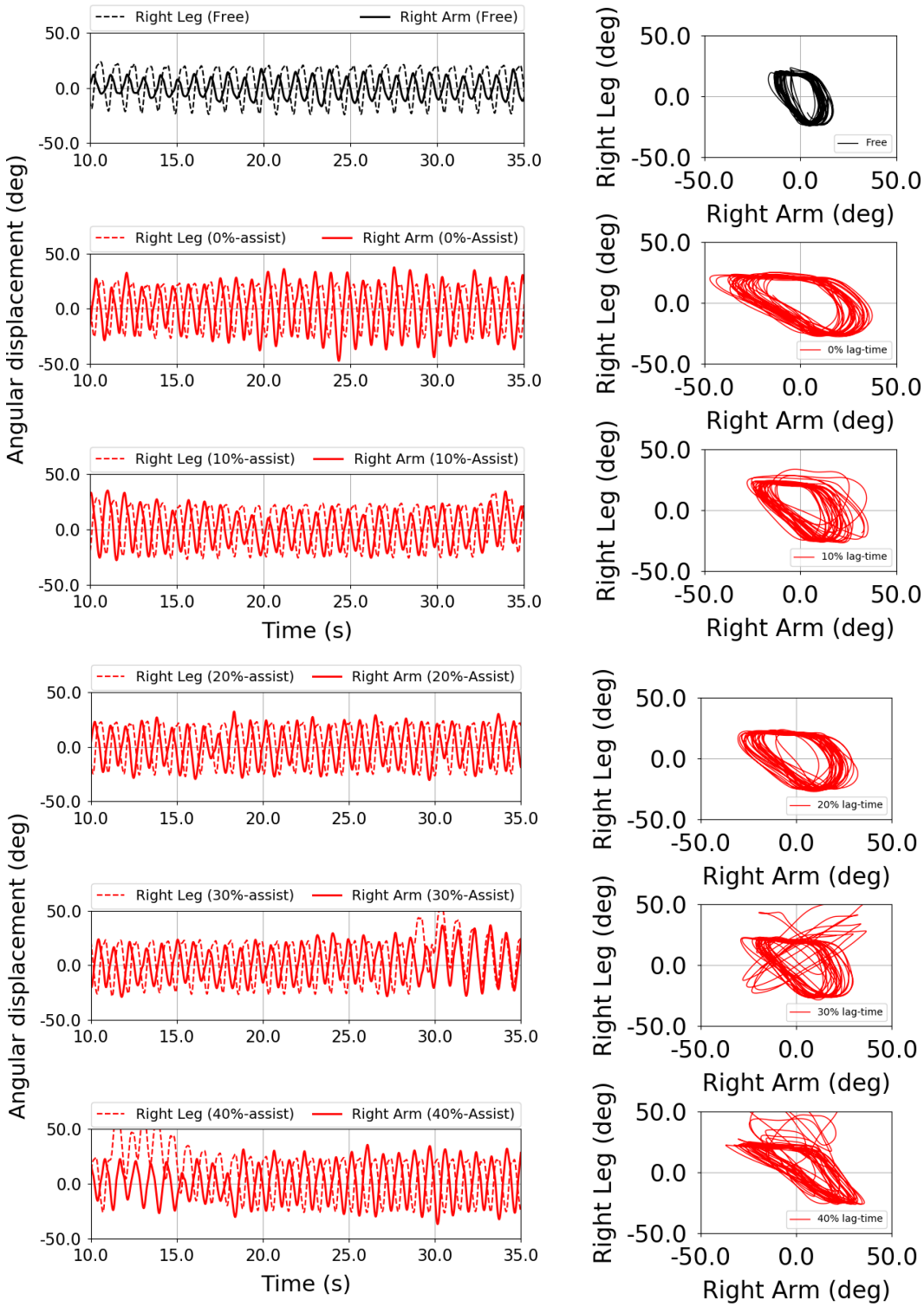

Fig 32. Phase diagram of the right arm- and hip-swing angular displacement for subject 1.

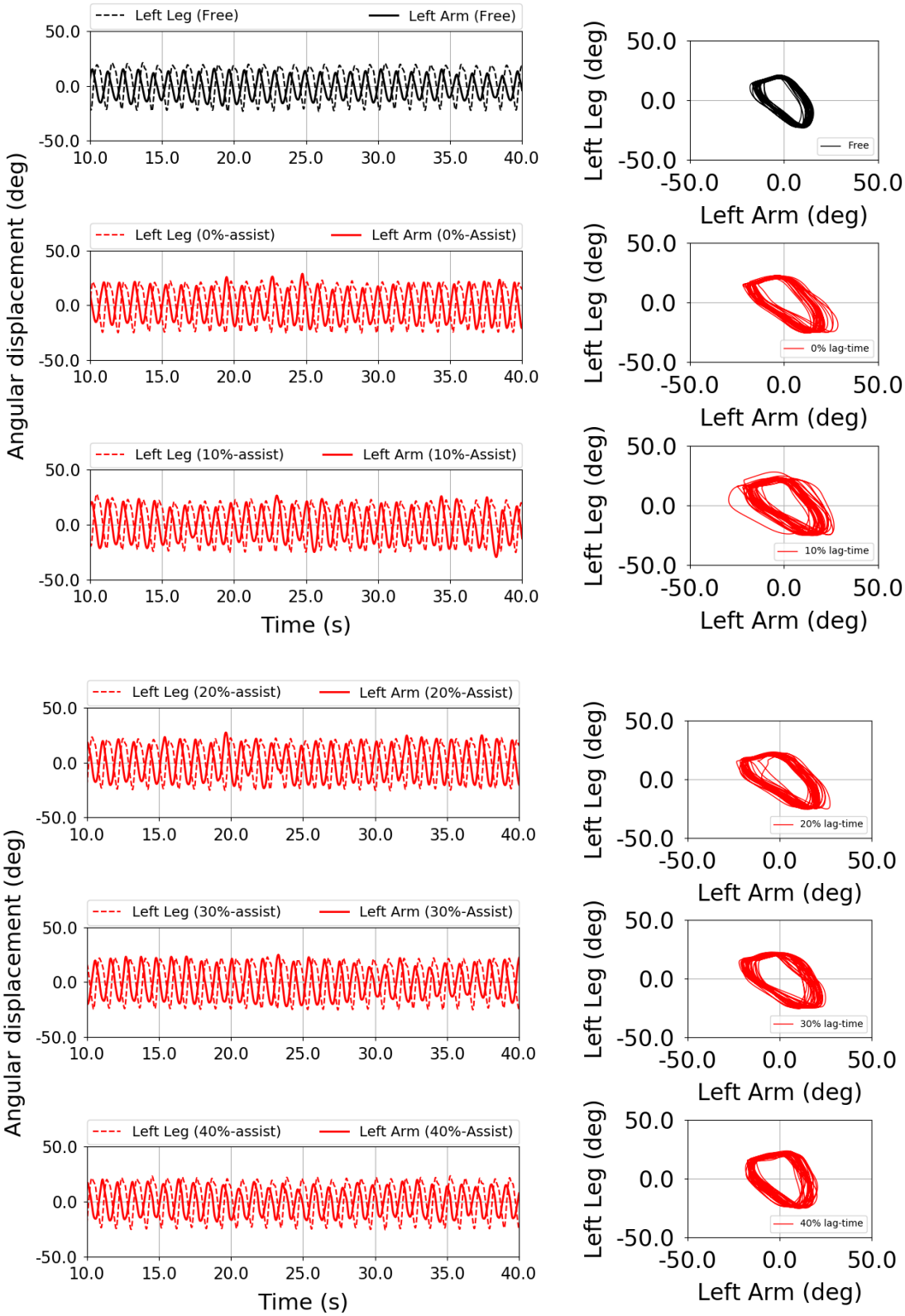

Fig 33. Phase diagram of the left arm- and hip-swing angular displacement for subject 3.

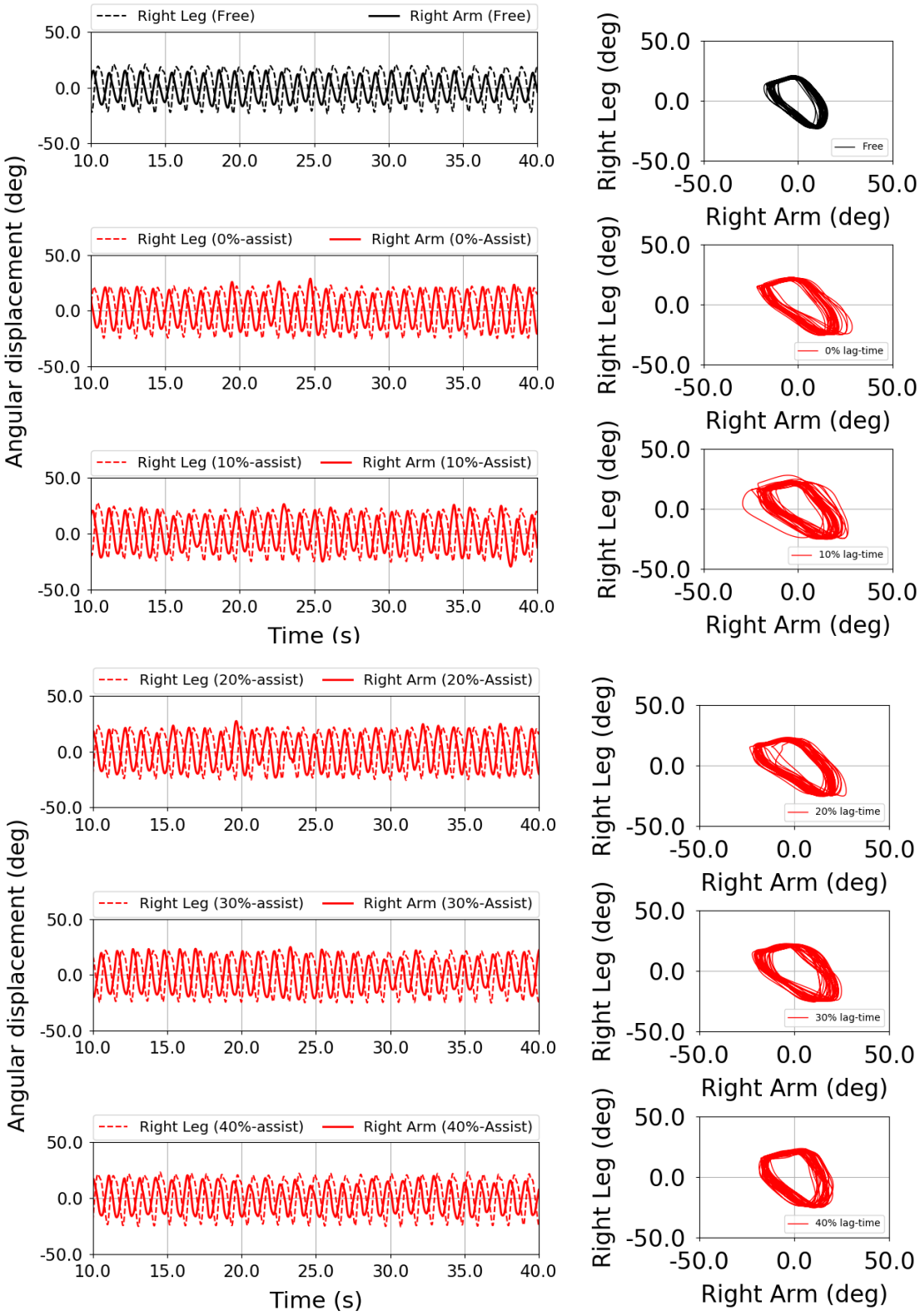

Fig 34. Phase diagram of the right arm- and hip-swing angular displacement for subject 3.

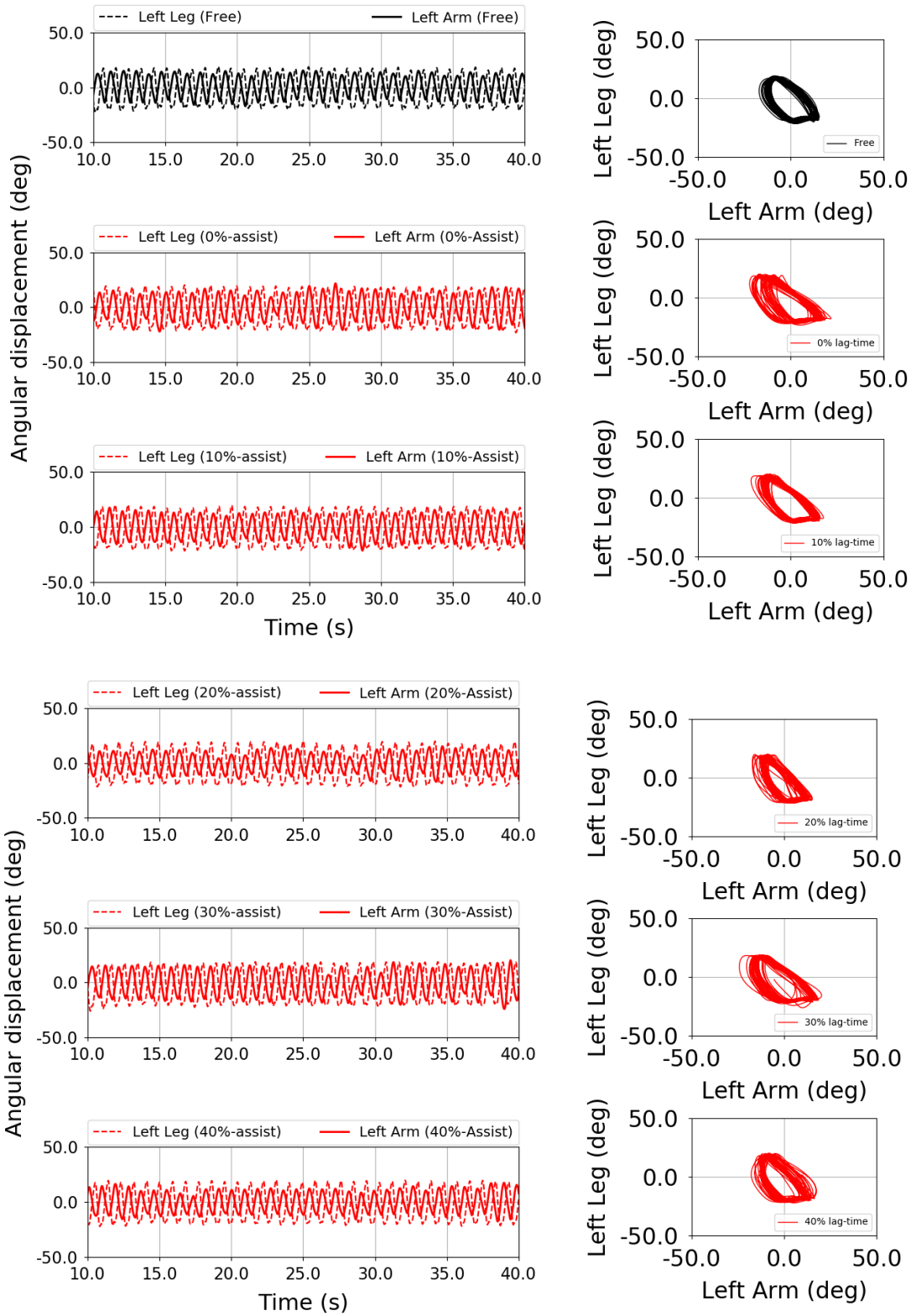

Fig 35. Phase diagram of the left arm- and hip-swing angular displacement for subject 4.

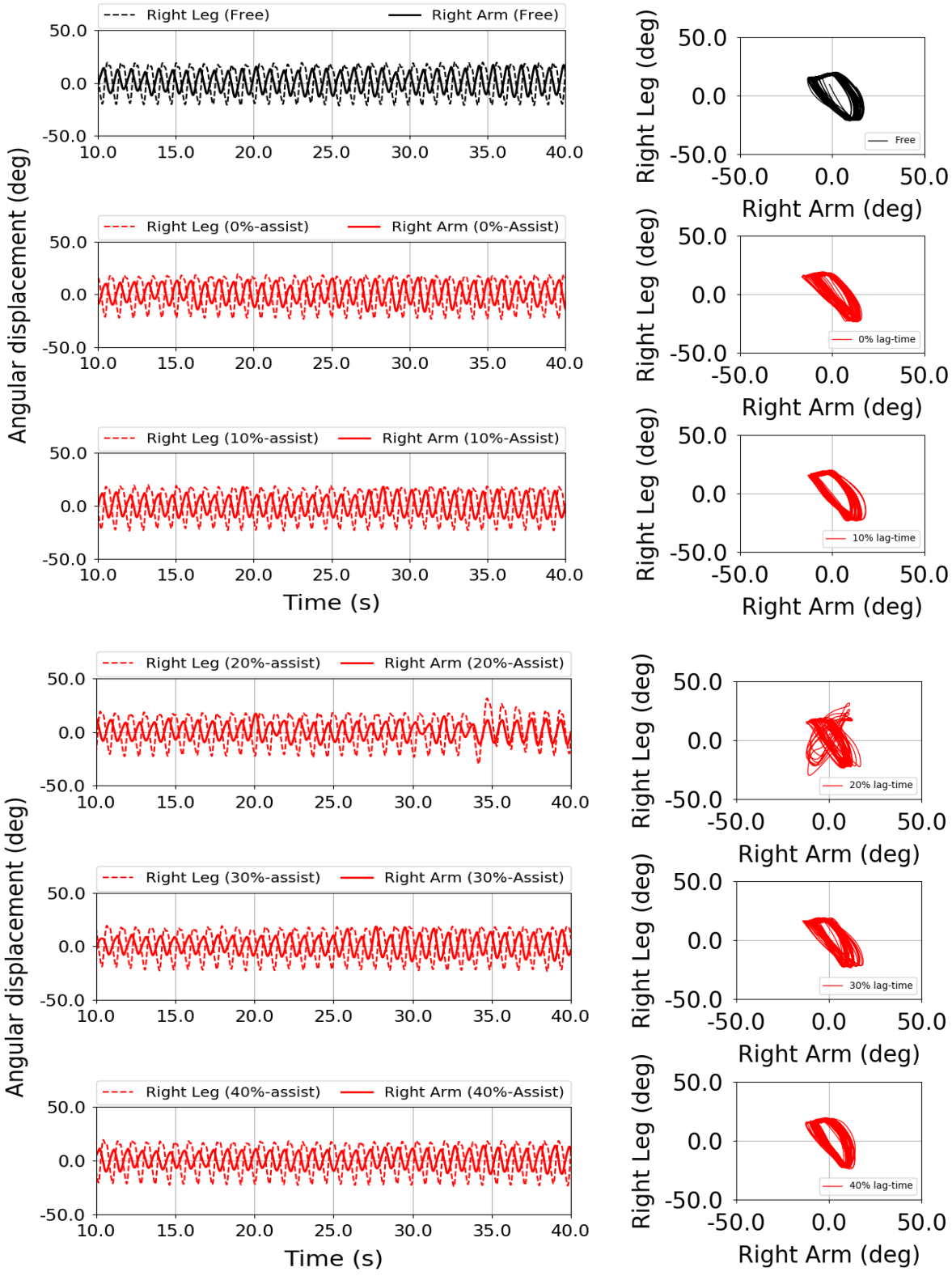

Fig 36. Phase diagram of the right arm- and hip-swing angular displacement for subject 4.

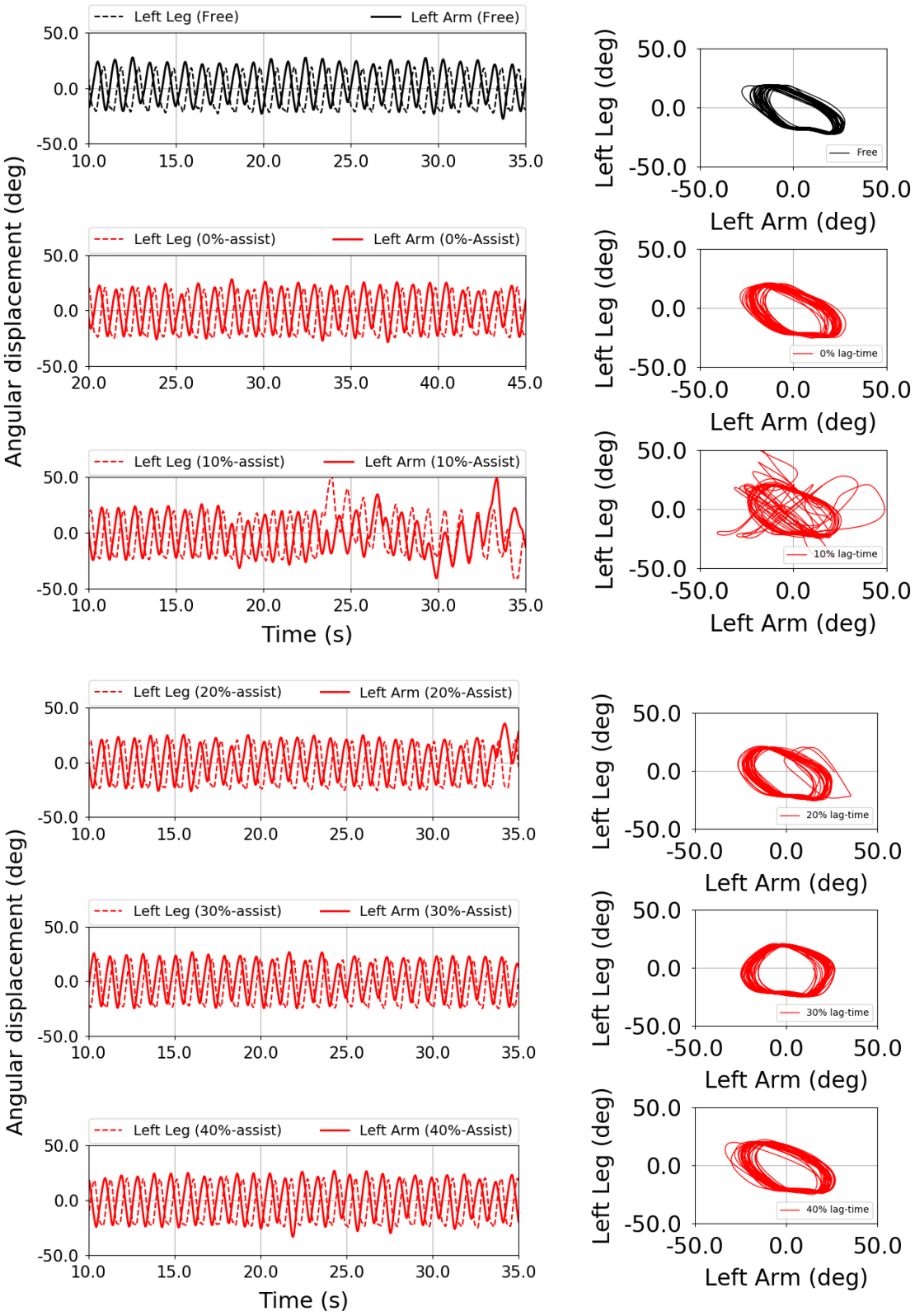

Fig 37. Phase diagram of the left arm- and hip-swing angular displacement for subject 5.

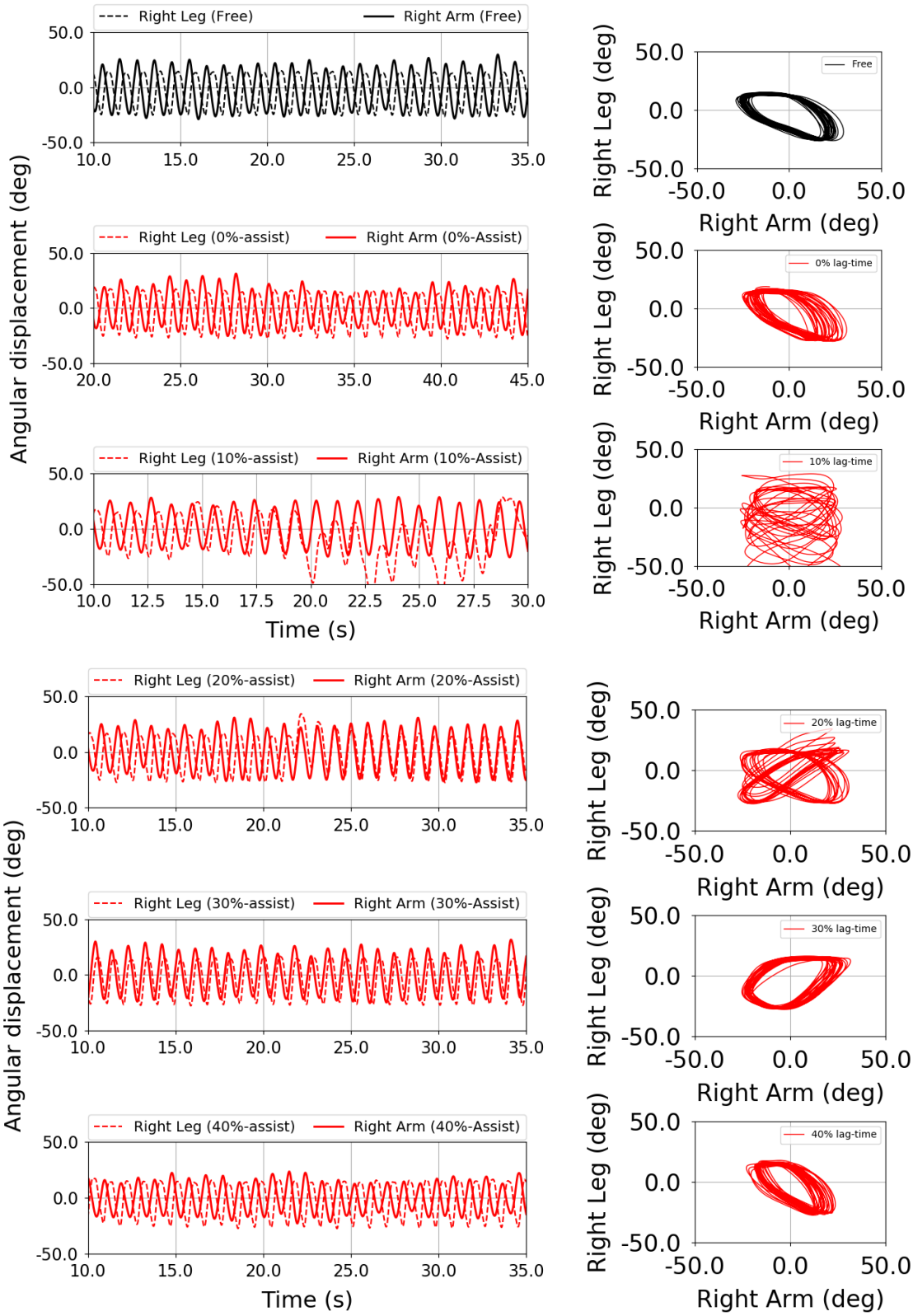

Fig 38. Phase diagram of the right arm- and hip-swing angular displacement for subject 5.

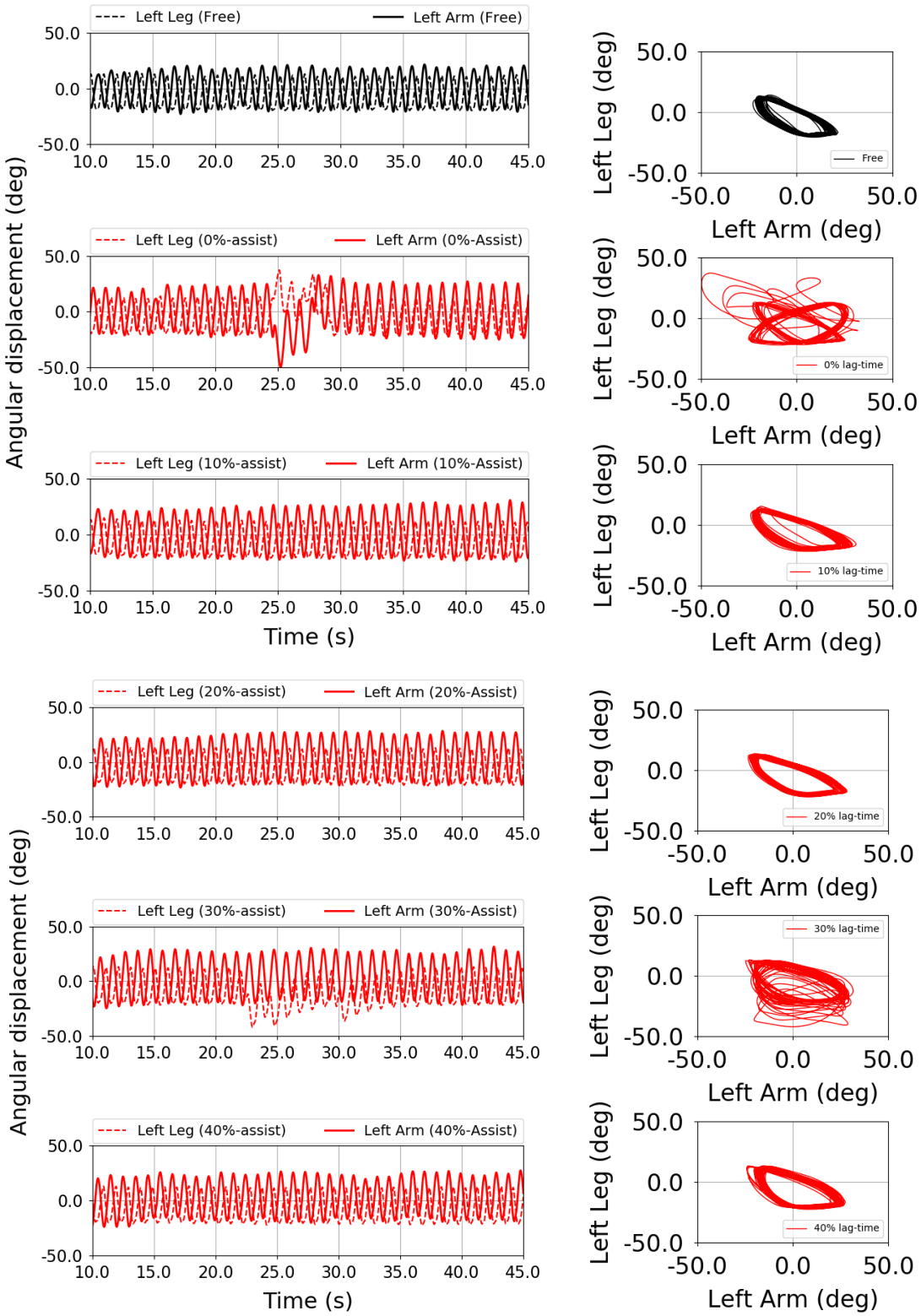

Fig 39. Phase diagram of the left arm- and hip-swing angular displacement for subject 6.

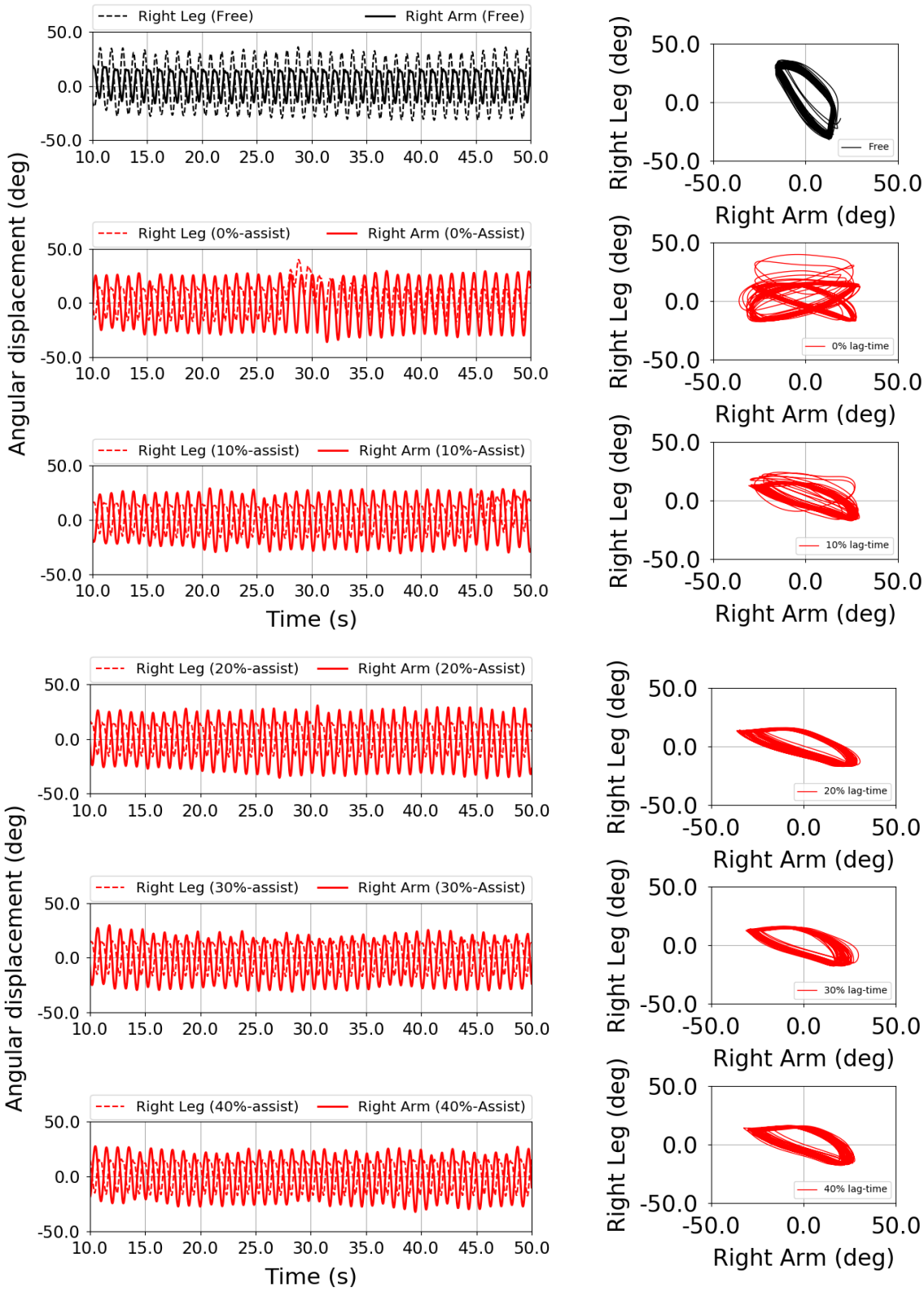

Fig 40. Phase diagram of the right arm- and hip-swing angular displacement for subject 6.

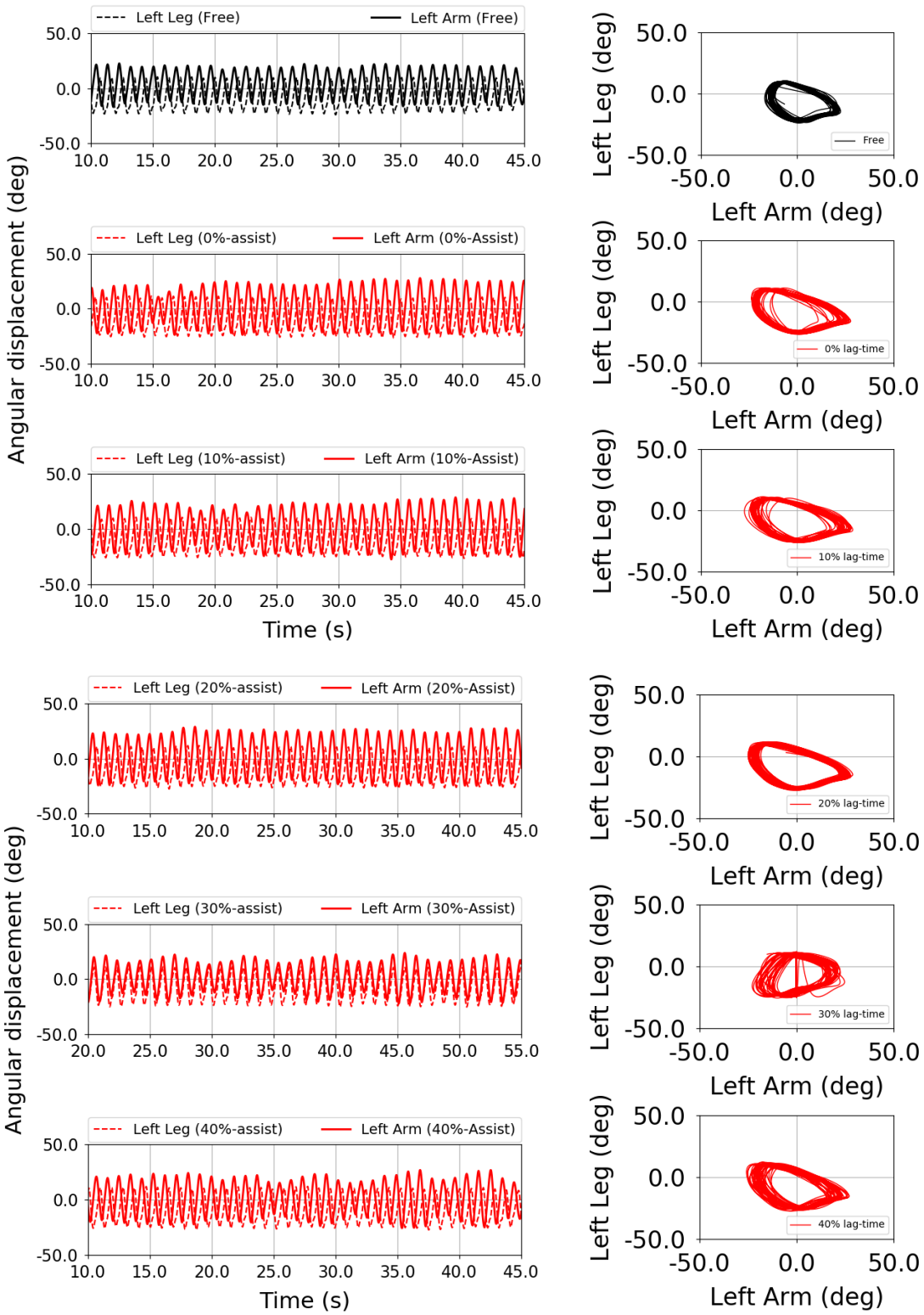

Fig 41. Phase diagram of the left arm- and hip-swing angular displacement for subject 7.

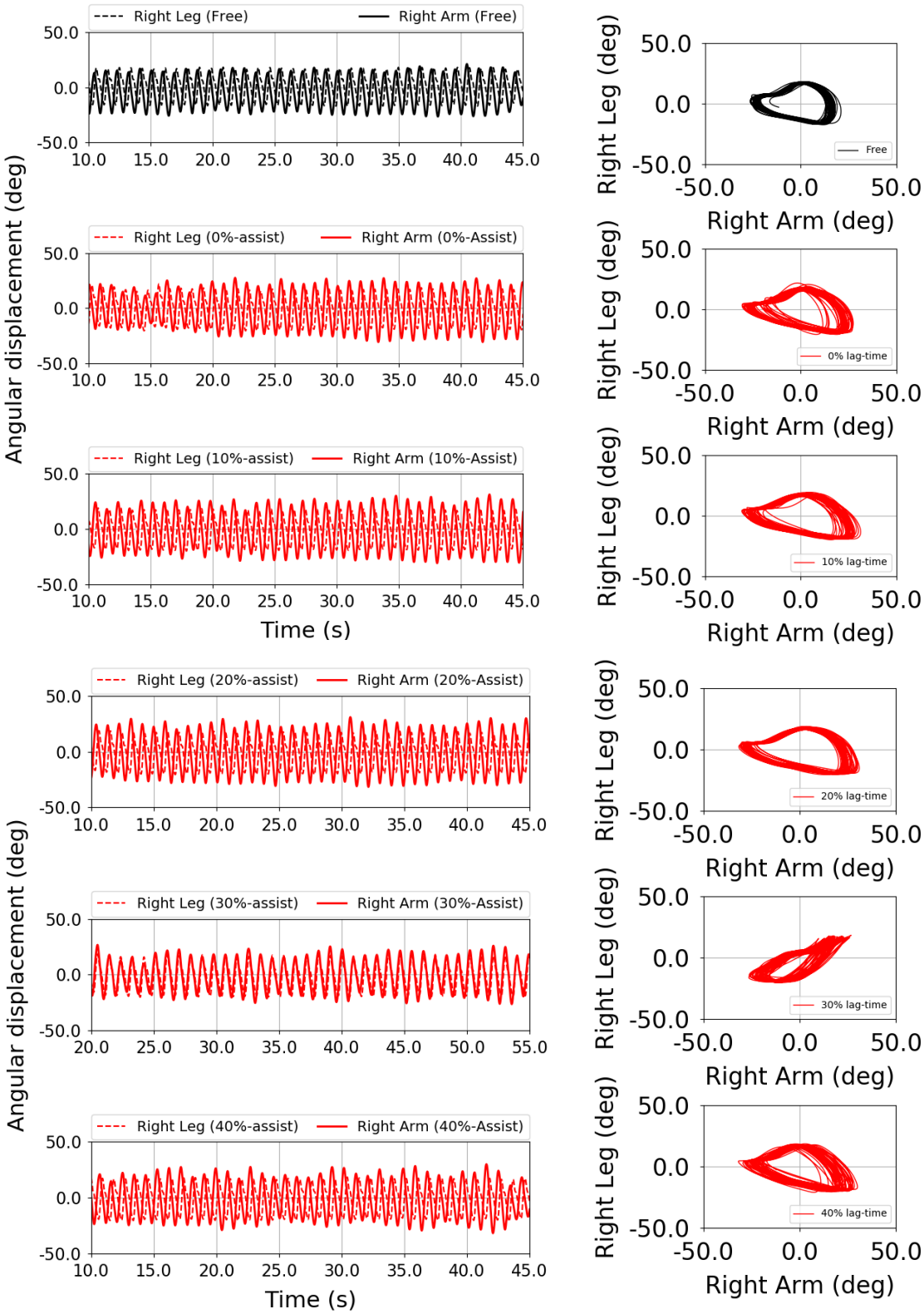

Fig 42. Phase diagram of the right arm- and hip-swing angular displacement for subject 7.

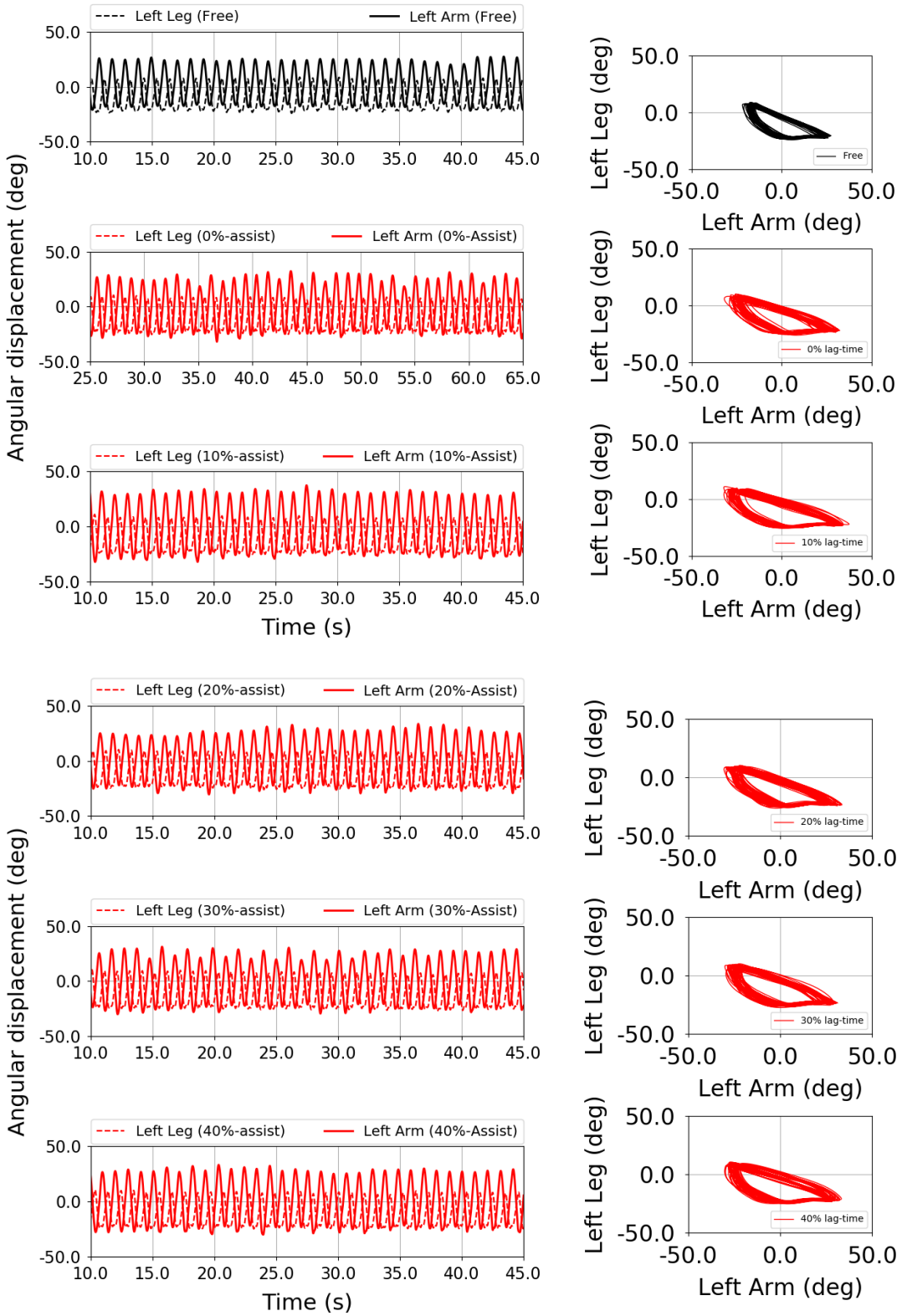

Fig 43. Phase diagram of the left arm- and hip-swing angular displacement for subject 8.

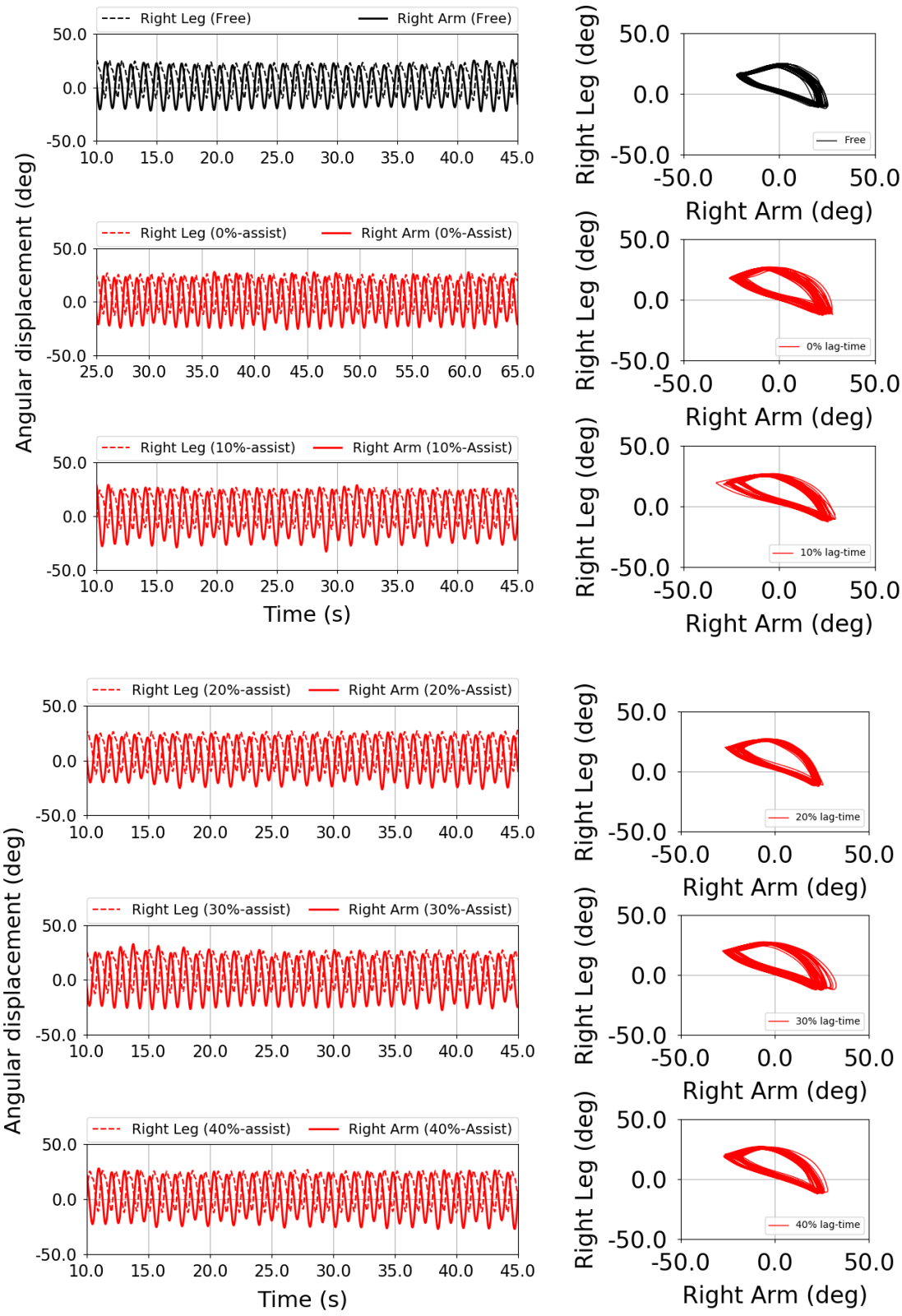

Fig 44. Phase diagram of the right arm- and hip-swing angular displacement for subject 8.

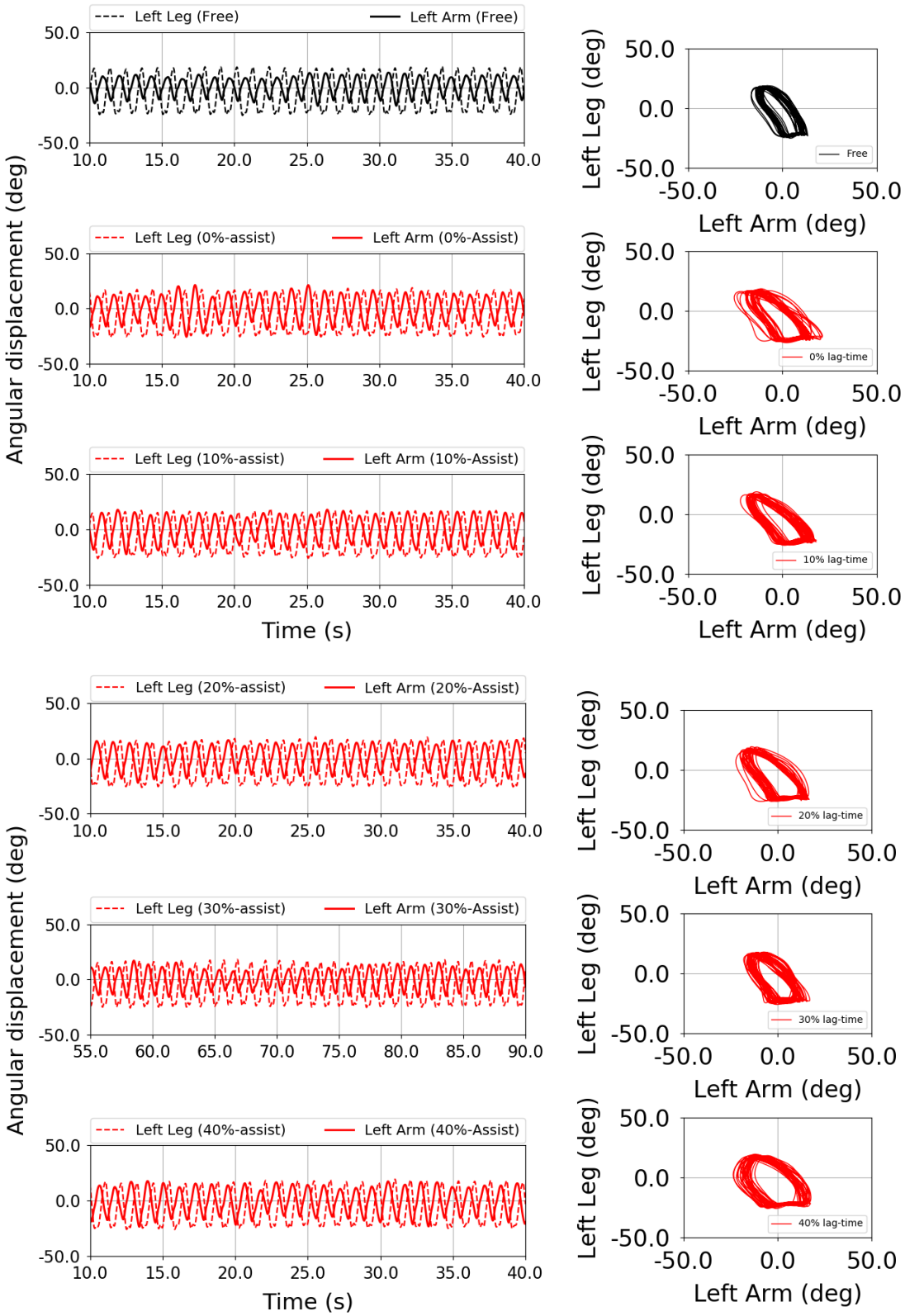

Fig 45. Phase diagram of the left arm- and hip-swing angular displacement for subject 9.

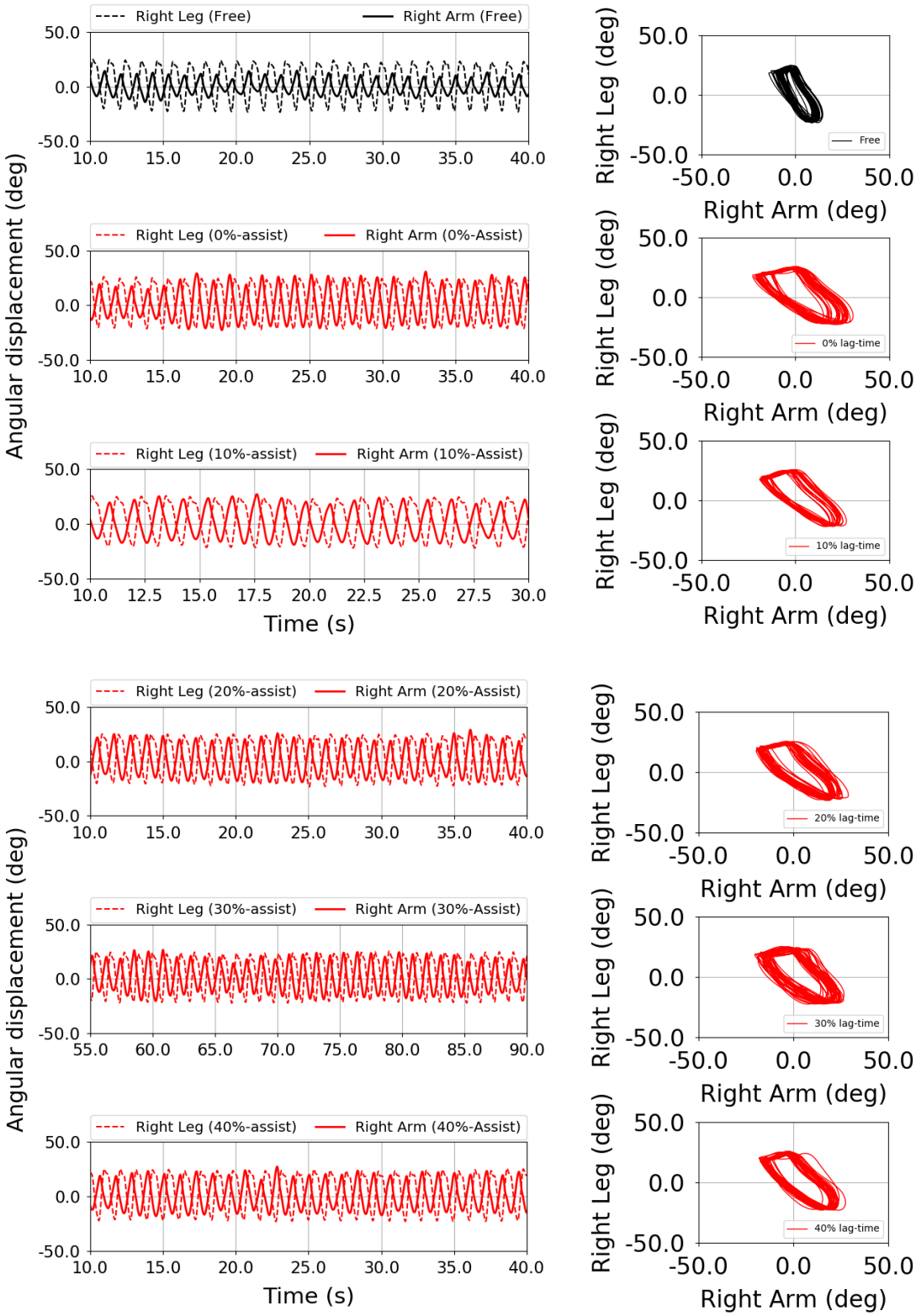

Fig 46. Phase diagram of the right arm- and hip-swing angular displacement for subject 9.

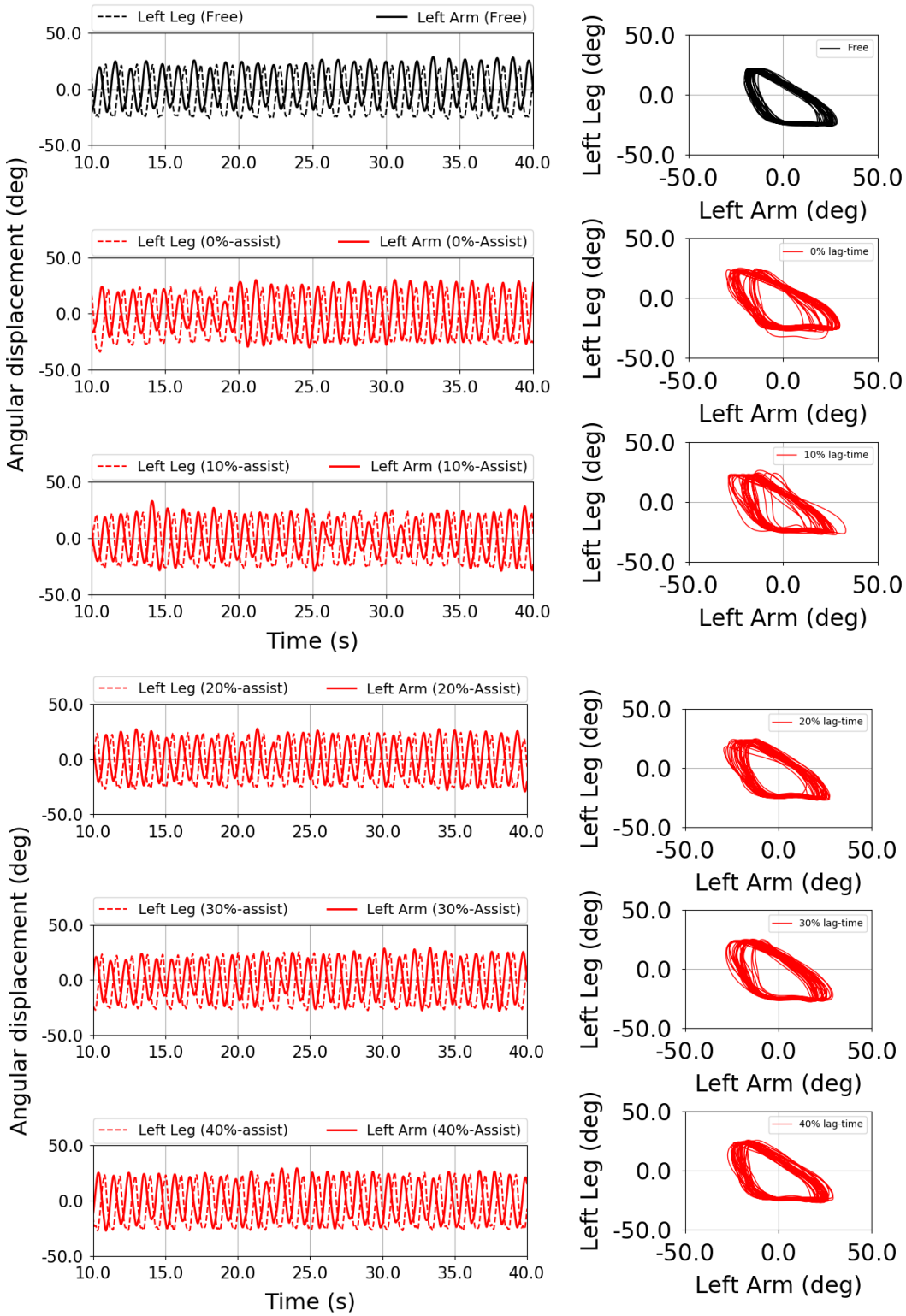

Fig 47. Phase diagram of the left arm- and hip-swing angular displacement for subject 10.

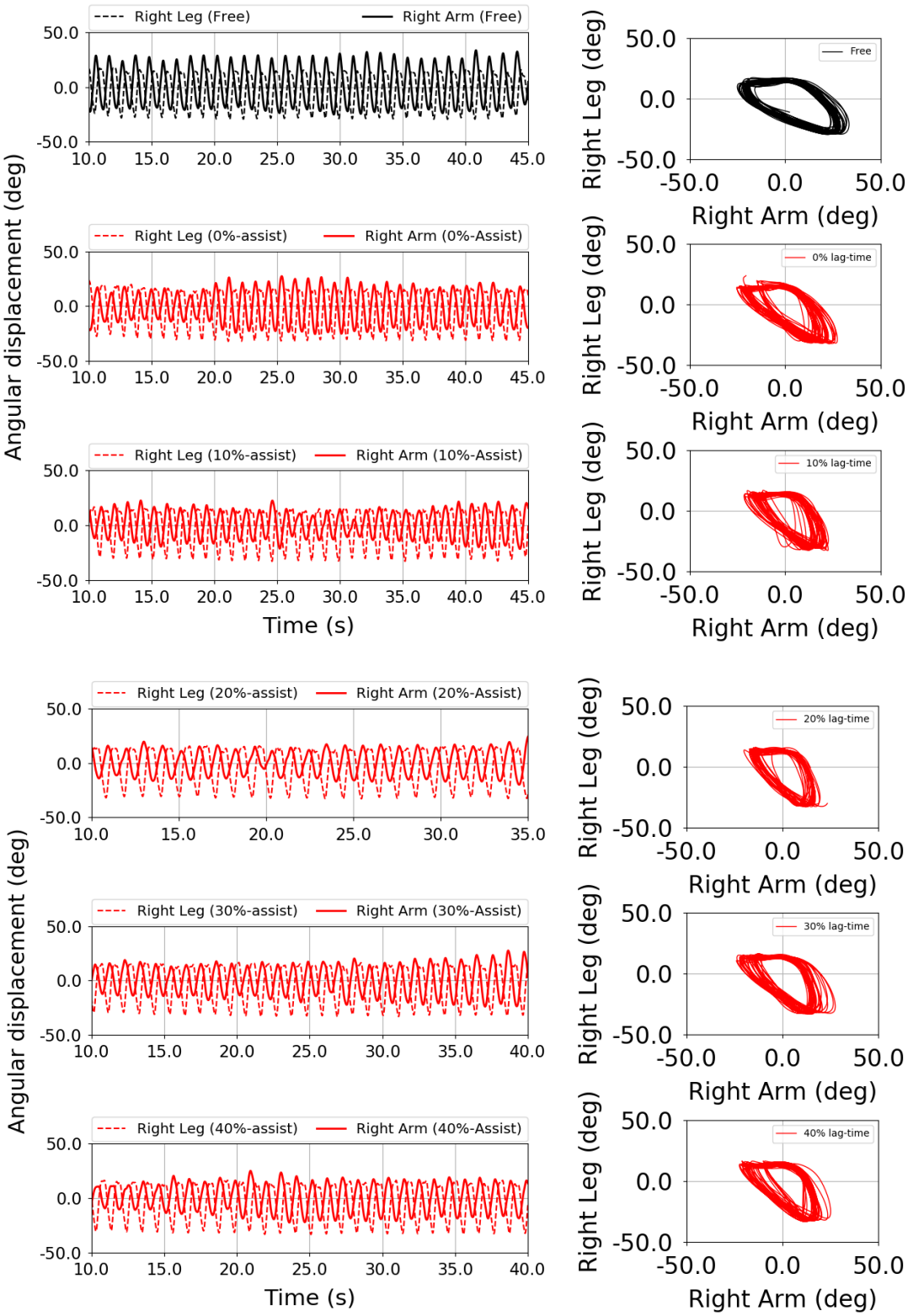

Fig 48. Phase diagram of the right arm- and hip-swing angular displacement for subject 10.

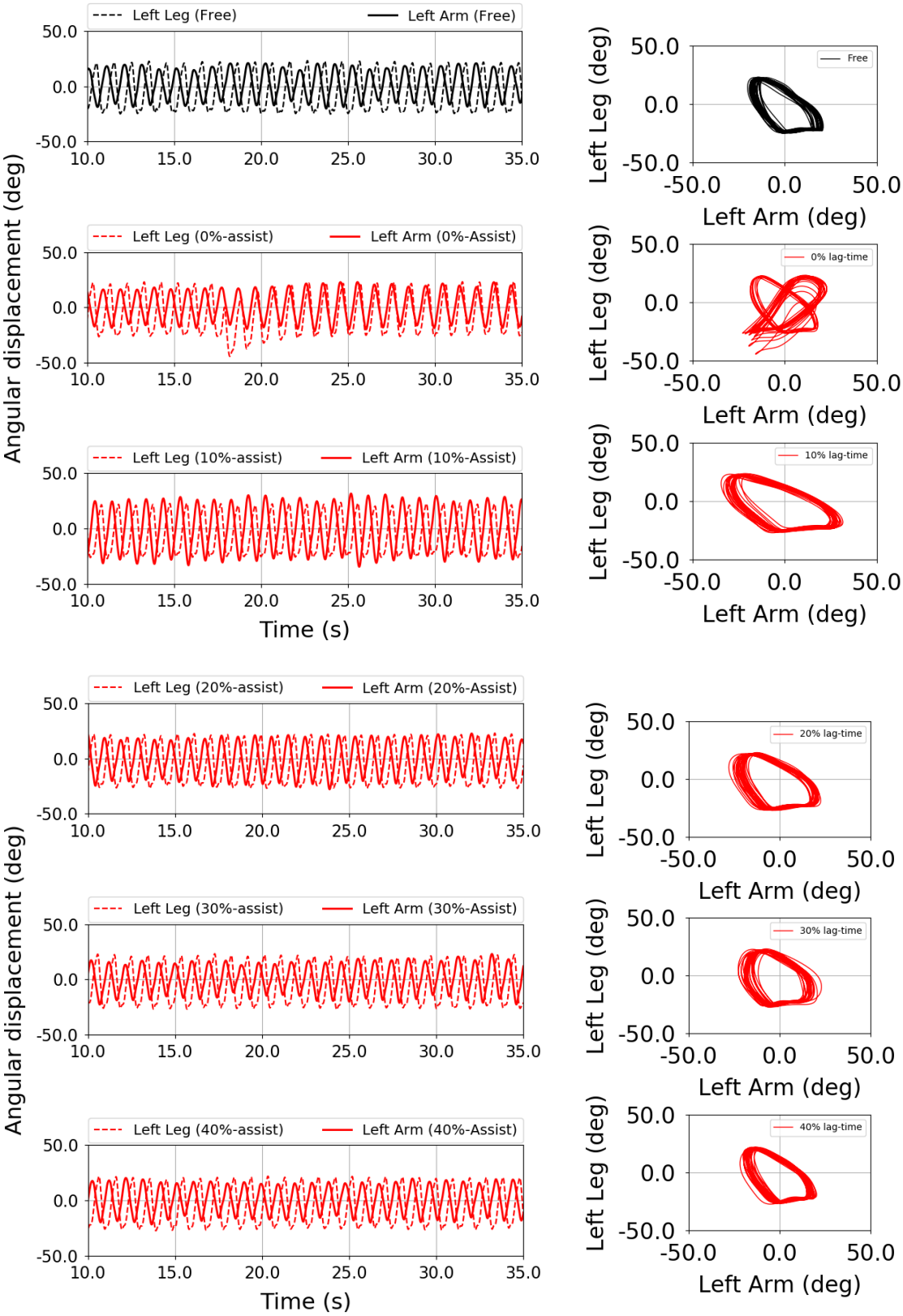

Fig 49. Phase diagram of the left arm- and hip-swing angular displacement for subject 11.

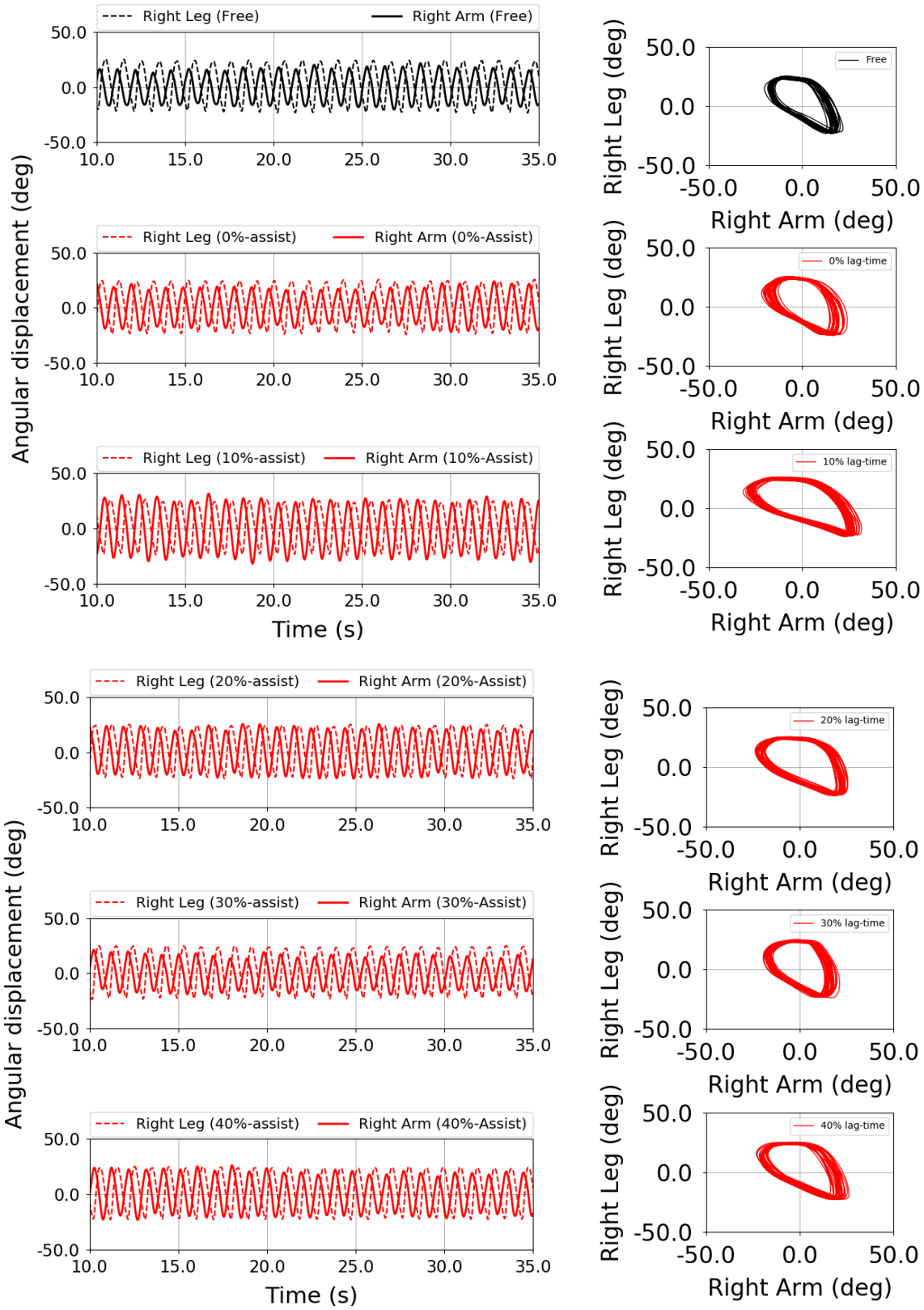

Fig 50. Phase diagram of the right arm- and hip-swing angular displacement for subject 11.

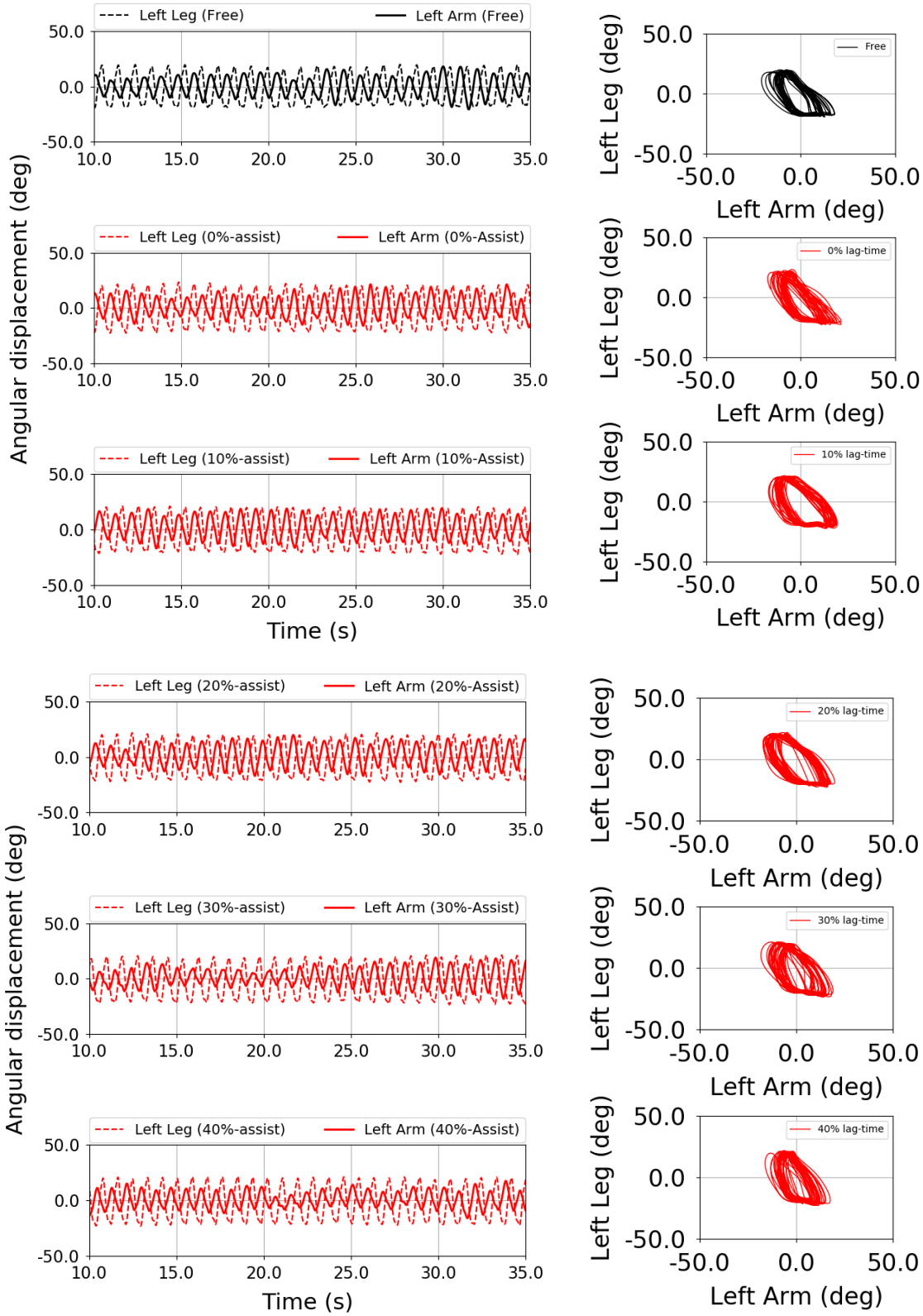

Fig 51. Phase diagram of the left arm- and hip-swing angular displacement for subject 12.

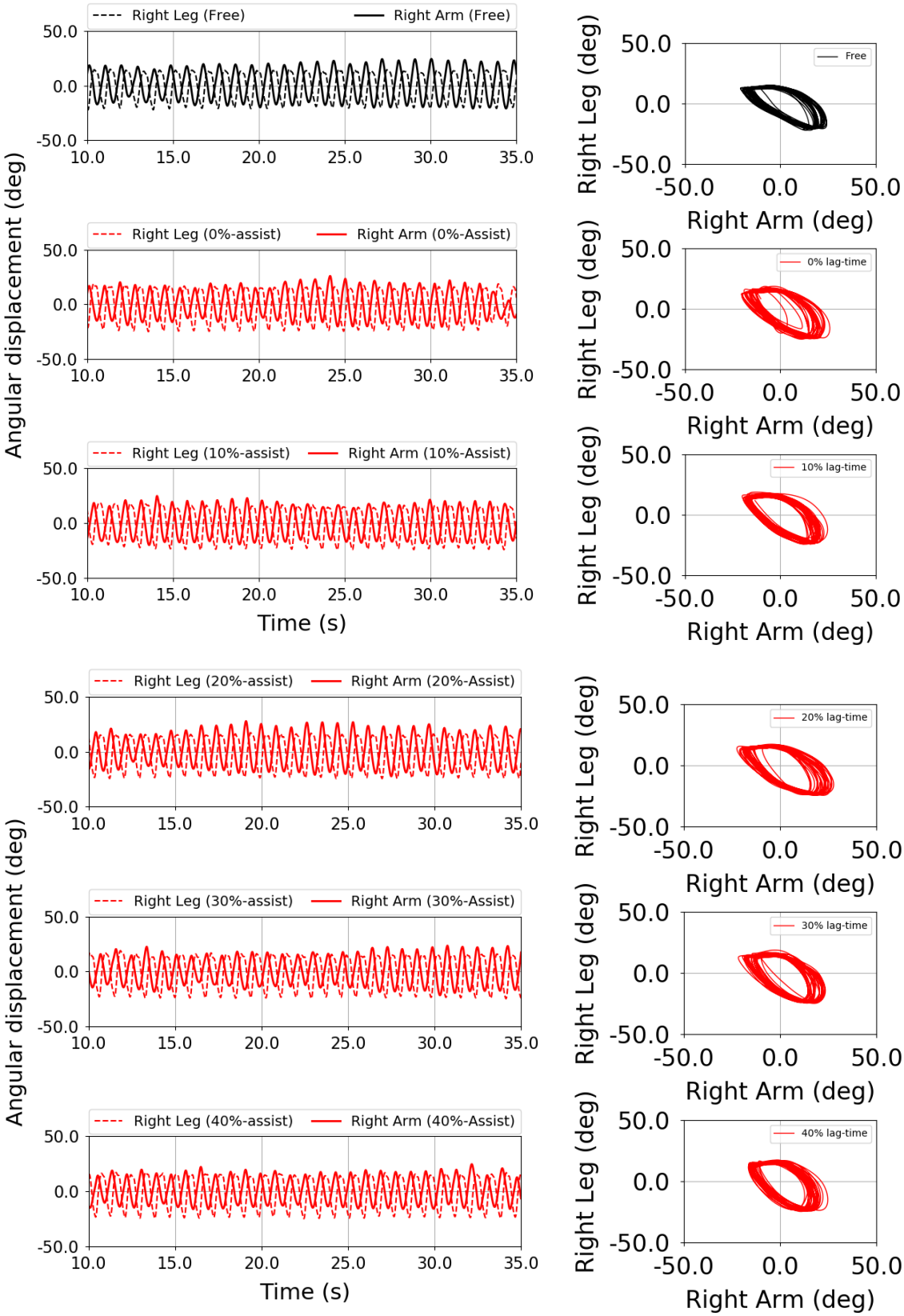

Fig 52. Phase diagram of the right arm- and hip-swing angular displacement for subject 12.

CHAPTER 8: PUBLICATION LIST

8.1 Peer-reviewed Journal

1. Yap, R.M.S., Nagashima, T., Hirobe, Y., Ogawa, K., Seki, M., Nakayama, M., Ichiryu, K., Miyake, Y. (2019). Gait assist wearable robot using interactive rhythmic stimulation to the upper limbs. *Frontier in Robotics & AI*, 6:25, 1–11.

8.2 Peer-reviewed International Conference

1. Yap, R.M.S., Qiao, L., Tani, K., Ogawa, K., Miyake, Y. (2016). Evaluation of a head motion synchronization system in the communicative process between human and robot. *Conf. Proc. of SICE 2016* (*SICE2016*), Tsukuba, Japan, 1514–1519.

2. Yap, R.M.S., Matsui, H., Nagashima, T., Hori, K., Hirobe, Y., Ogawa, K., Seki, M., Nakayama, M., Ichiryu, K., Miyake, Y. (2016). Development and evaluation of a gait assist wearable robot using motor rhythmic stimulation to the upper and lower limbs. *Conf. Proc. of the 10th Int. Conf. Complex Med. Engin.* (*CME2016*), Tochigi, Japan, 85.

3. Yap, R.M.S., Saruta, Y., Kono, D., Matsui, H., Ogawa, K., Seki, M., Ichiryu, K., Miyake, Y. (2015). Development of a power-assist wearable rehabilitation system using motor rhythmic stimulation to upper and lower limbs. *Conf. Proc. of SICE 2015* (*SICE2015*), Hangzhou, China, 1470–1475.

4. Yap, R.M.S., Inoue, Y., Miura, S., Kwon, J.H., Ogawa, K., Miyake, Y. (2015). Head motion synchrony in the process of consensus building: a comparison between native English and Japanese speakers. *Conf. Proc. of 9th Int. Conf. Complex Med. Engin. (CME2015*), Okayama, Japan, 31–36 (Best Paper Award).

8.3 Non-peer-reviewed Conference

1. Yap, R.M.S., Inoue, Y., Miura, S., Kwon, J.H., Ogawa, K., Miyake, Y. (2015) Embodied synchrony in the process of consensus building. 第27回自律分散システムシンポジウム, 1–6.